Aus dem Department für Augenheikunde Tübingen

Forschungsinstitut für Augenheilkunde

Sektion Experimentelle Vitreoretinale Chirurgie

Development of a rat choroidal neovascularization model by overexpressing VEGF with and without treatment

Thesis submitted as requirement to fulfill the degree

“Doctor of Philosophy” (Ph.D.)

at the

Faculty of Medicine

Eberhard Karls University

Tübingen

by

Liu, Shan

From

Shandong, China

2020

Dean：Professor Dr. I. B. Autenrieth

1. Reviewer: Professor Dr. U. Schraermeyer

2. Reviewer: Professor Dr. B. Sipos

Date of oral examination: 10.12.2019

Table of contents

List of figures

List of tables

List of abbreviations

AAV: adeno associated virus

AMD: age-related macular degeneration

Ang: angiopoietin

AOI: area of interest

BM: bruch's membrane

CC: choriocapillaris

Ch: choroid

CNV: choroidal neovascularization

EGFP: enhanced green fluorescent protein

EM: electron microscopy

FA: fundus fluorescein angiography

HIF-1: hypoxia-inducible factor 1

ICG: indocyanine green angiography

IHC: immunohistochemistry

ILM: inner limiting membrane

INL: inner nuclear layer

IV: intravitreal injection

LM: light microscopy

NG2: neural/glial antigen 2

OCT: optical coherence tomography

ONL: outer nuclear layer

OPL: outer plexiform layer

PDGF-B: platelet-derived growth factor-B

PIGF: placental growth factor

PR IS: photoreceptor inner segments

PR OS: photoreceptor outer segments.

RPE: retinal pigment epithelium

SLO: scanning laser ophthalmoscopy

SR: Subretinal injection

VEGF: vascular endothelial growth factor

VEGFR: vascular endothelial growth factor receptor

α-SMA: alpha-smooth muscle actin

1 Introduction

1.1 Characterisation of choroidal neovascularization

1.1.1 Causes and symptoms of choroidal neovascularization

Choroidal neovascularization (CNV) is the neovascularization in the choroid layer and subretinal space. A schematic diagram of a normal eye is shown in Figure 1. This study focused on retina-choroid interface (parts of the retina - retinal pigment epithelium (RPE) – Bruch's membrane (BM) – choriocapillaris (CC)). The newly formed blood vessels from the choroidal capillaries extend through the rupture of BM, as shown in the Figure 2. These abnormal blood vessels are between BM and RPE, or between the neural retina and RPE, or between RPE and choroid. Many eye diseases involving changes in the retina-choroid interface, such as wet age-related macular degeneration (AMD), can lead to the formation of CNV, also known as subretinal neovascularization (Bhutto and Lutty, 2012).

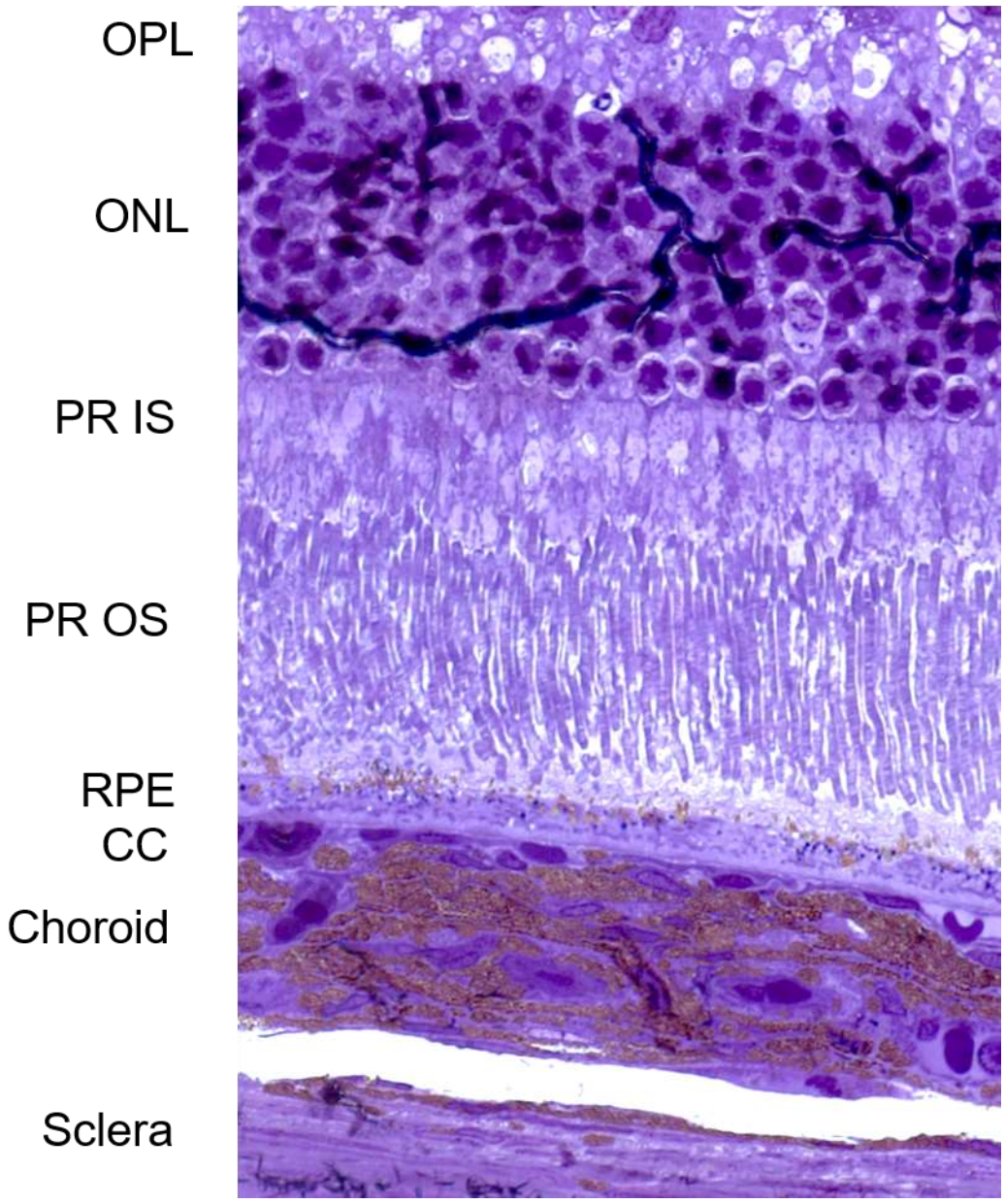

Figure 1: Healthy rat eye in light microscopy (semi-thin section stained with toluidine blue). Parts of retina, choroid and sclera are shown in this figure. OPL: outer plexiform layer; ONL: outer nuclear layer; PR IS: photoreceptor inner segments; PR OS: photoreceptor outer segments.

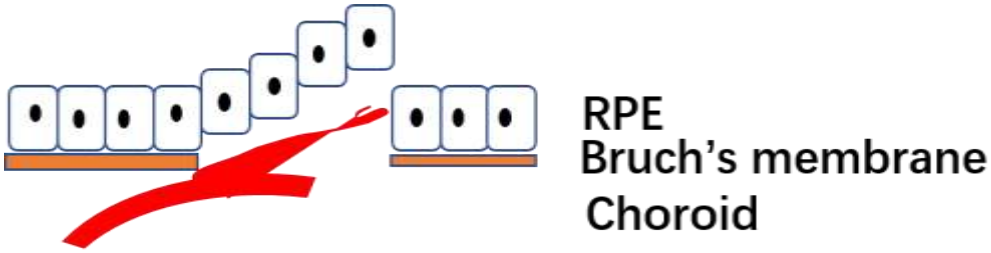

Figure 2: Schematic representation of CNV. CNV is the creation of blood vessels from the choroidal capillaries that extend through the rupture of BM. Figure from Xi Lei (with his kind permission).

1.1.2 Symptoms of CNV

There are no obvious symptoms in the early stages of CNV. With the progression of the disease, the leakages and bleeding from the newly formed abnormal blood vessels in CNV may lead to vision loss, visual distortion and colour disturbances. CNV most often occurs in the macula, thus damaging the central vision. If these symptoms repeated occurs, the macula can be damaged severely, resulting in permanent visual impairment. CNV has become one of the main causes of blindness in the developed countries, especially for those people over 60 years old (Wang et al., 2017).

1.1.3 Identification of CNV

The diagnose of CNV is based on symptoms and the results of FA/ICG/OCT (Farazdaghi and Ebrahimi, 2019).

1) Fundus fluorescein angiography (FA) is a very valuable method to detect CNV (Bindewald et al., 2005). In the early stage of FA, retinal vessels are visible and the retinal lesions starts to appear. A few lace-like or single-wheel shape hyper-fluorescent areas, or small hyper-fluorescent dots can be identified (Bindewald et al., 2005). In the middle phase, the retinal lesions become more obviously (Bindewald et al., 2005). In the late phase of FA, intravenous fluorescein fades, so the retinal vessels are no longer visible. The fluorescent

regions still can be identified, although they are less intense (Bindewald et al., 2005).

2) Indocyanine green angiography (ICG) is also a common examination method for the Identification of CNV. Table 1 shows the differences of FA and ICG. They used different fluorescent dye and different wavelengths. ICG has obvious advantages in choroidal vasculature imaging compared with FA, as shown in Table 1. Combined ICG images with FA images, retinal neovascularization can be excluded, and occult CNV can be better identified.

3) Optical coherence tomography (OCT) shows the retinal tissue structure and neovascularization (Hee et al., 1996).

Table 1: Comparison of FA and ICG. FA and ICG are common examination methods for the Identification of CNV.

Angiography	FA	ICG
Fluorescent dye	fluorescein-Na bound to about 60–80% (large) plasma proteins, fluorescein leak rapidly	indocyanine green bound to more than 98% plasma proteins, ICG diffuses very slowly
Wavelength	short wavelength: 488 nm, cannot penetrate RPE/choroid	long wavelength: 795 nm, pass through pigmented layers
Information shown in the images	provides the most detailed images of retinal capillaries	adds information about choroidal vessels, but shows less retinal vasculature details

1.2 Vascular endothelial growth factor

Vascular endothelial growth factor (VEGF), so called vascular permeability factor, is a highly specific vascular endothelial growth factor that promotes vascular permeability, extracellular matrix denaturation, vascular endothelial cell migration, proliferation and angiogenesis (Johnson and Wilgus, 2014).

1.2.1 Classification

VEGF is a family that includes VEGF-A, VEGF-B, VEGF-C, VEGF-D, VEGF-E, VEGF-F and placental growth factor (PlGF) (Christner, 2017). VEGF-A is the first to be discovered and the major regulator of neovascularization and vascular permeability (Chirco et al., 2017, Woolard et al., 2009). VEGF-B plays a role in non-neovascular angiogenesis. VEGF-A VEGF-B and PlGF are hemangiogenic VEGFs, while VEGF-C and VEGF-D are lymphangiogenic VEGFs which promote the formation of new blood vessels as well as lymphatic vessels in cancer tissues (Rauniyar et al., 2018). PlGF promotes pathological angiogenesis and increases vascular permeability, thus the blockade of PIGF has no effect on the healthy vasculature (Van Bergen et al., 2019). VEGF-A, VEGF-B, VEGF-C, VEGF-D and PlGF are VEGF isoforms in mammals. The VEGF-E is a potential angiogenic factor encoded by viruses, and VEGF-F is discovered in the snake venom.

VEGF-A is a dimeric glycoprotein which consists of 8 exons and 7 introns. The alternative splicing of mRNA from VEGF-A gene results in the several different subtypes of VEGF-A (see Figure 3). These are at least nine subtypes: VEGF121, VEGF145, VEGF148, VEGF162, VEGF165, VEGF165b, VEGF 183, VEGF189 and VEGF206, which are named according to the number of amino acids and their terminal exon (exon 8) splice site (proximal splice site (VEGFxxx) or distal splice site (VEGFxxxb)) (Bhisitkul, 2006). Among them, VEGF121, VEGF145 and VEGF165 are secreted soluble proteins, which can directly act on vascular endothelial cells to stimulate vascular endothelial cell proliferation and

neovascularization. VEGF165 is the most abundant subtypes of VEGF-A, followed by VEGF121 and VEGF189, while VEGF145 is only expressed in reproductive organs (Achen and Stacker, 1998, Chirco et al., 2017, Keyt et al., 1996).

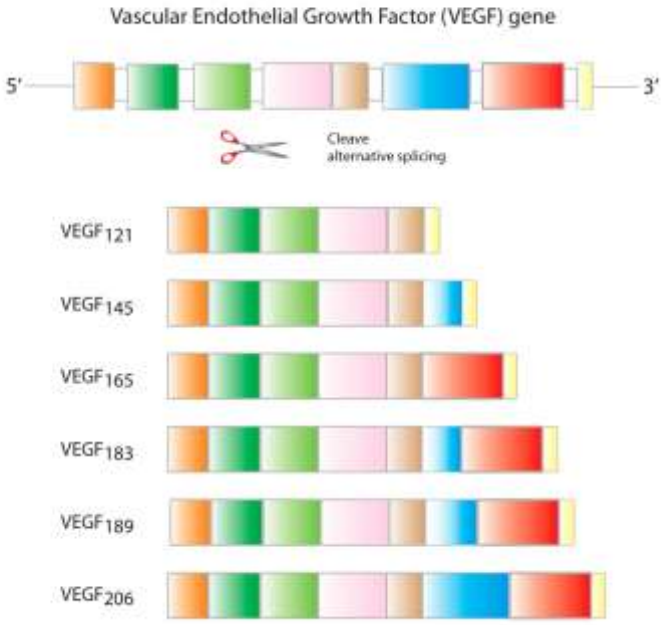

Figure 3: Schematic representation of the six different subtypes of human VEGF-A. A single VEGF-A gene consists of 8 exons which are marked with different colours. The alternative splicing of mRNA results in the several different subtypes of VEGF-A. Figure from the English language Wikipedia (https://commons.wikimedia.org/wiki/File:VEGF_isoforms.png).

1.2.2 VEGF receptors

A number of VEGF receptors (VEGFR) are distributed on the surface of human vascular endothelial cells (Shibuya, 2011). There are three VEGFRs: VEGFR-1, VEGFR-2 and VEGFR-3. Each of the VEGF family members (VEGF-A, VEGF-B, VEGF-C, VEGF-D, VEGF-E, VEGF-F and PlGF) combines specifically

with a certain subset of the VEGFRs. The VEGF that binds to all three VEGFRs do not exist naturally, but super-VEGFs interacting with all three VEGFRs has been created (Jeltsch et al., 2006). VEGF binds to the receptor, thereby activating the intracellular tyrosine kinase, triggering a downstream cellular signaling cascade that promotes the growth of new vessels (Abhinand et al., 2016). Only the hemangiogenic VEGFs (VEGF-A, PlGF, and VEGF-B) interact with VEGFR-1, while all the lymphangiogenic VEGFs (VEGF-C and VEGF-D) bind to VEGFR-3 that is lymphatic endothelial cells' primary mitogenic receptor (Rauniyar et al., 2018). A part of hemangiogenic and lymphangiogenic groups of VEGFs can combine with VEGFR-2, which is blood vascular endothelium's primary mitogenic receptor, thereby activating the proliferation and migration of blood vascular endothelial cells.

1.2.3 VEGF expression

Human RPE cells can not only produce and secret VEGF in vitro and in situ, but also express VEGFRs (VEGFR-1 and VEGFR-2) (Adamis et al., 1993). Overexpression of VEGF can also lead to the proliferation and migration of RPE cells, shown in both human and animal CNV (Adamis et al., 1993, Julien et al., 2008).

1.3 The cellular and molecular mechanism of CNV

The cellular and molecular mechanism of CNV are still ongoing investigation, however, VEGF has proved to be a key stimulator for CNV and its overexpression is observed in CNV with wet AMD patients and the laser model of CNV animal models (Hoerster et al., 2012, Mu et al., 2018, Ryan, 1982, Yi et al., 1997). Overexpression of VEGF can induce CNV in rabbits, rats and nonhuman primates (Baffi et al., 2000, Julien et al., 2008, Lebherz et al., 2005, Spilsbury et al., 2000, Wang et al., 2003).

Other factors like hypoxia-inducible factor 1 (HIF-1), angiopoietin-1 and angiopoietin-2 (Ang-1 and Ang-2) and platelet-derived growth factor-B (PDGF-B) are also involved in the process of neovascularization (Castro et al., 2018). HIF-1 can activate transcription of multiple target genes associated with angiogenesis, including VEGF, Ang-2 and PDGF-B (Campochiaro, 2013). Ang-2 is a growth factor for angiogenesis, promoting proliferation and migration of endothelial cells in collaboration with VEGF (Hackett et al., 2002). Ang-1 is an antagonist of Ang-2, inhibiting vascular permeability (Gale et al., 2002). In addition, PDGF-B play a role in blood vessel maturation, and its high retina-specific expression lead to retinal neovascularization (Mori et al., 2002).

A CNV vessel is forming based on the proliferation and migration of endothelial cells, regulating by proangiogenic factors and extracellular matrix (Neve et al., 2014). The CNV vessels are stabilized by pericyte recruitment which suppress endothelial cells proliferation (Castro et al., 2018). Macrophages also have an important role in CNV formation, especially the formation of fibrovascular scars, as they secrete a variety of growth factors (e.g. VEGF) (Grossniklaus et al., 2002, Oh et al., 1999, Tahiri et al., 2016).

At the cellular level, CNV seems to be a wound healing process including clotting, inflammation, angiogenesis and fibrosis (Kent and Sheridan, 2003, Schlingemann, 2004). Similar growth factors like VEGF and PDGF are involved in both CNV and skin wound healing (Schlingemann, 2004). RPE has a function to transport nutriment and oxygen by regulating the growth factors, however, the age-related changes in BM can block the transportation, resulting in the atrophy of CC and hypoxic neuroretina. The level of VEGF secreted by RPE increases, due to hypoxia, in contrast, the angiogenesis inhibitors expression decreases (Schlingemann, 2004). The imbalance of growth factors underlies the CNV formation.

1.4 Therapy of CNV

Intravitreal injections of anti-VEGF drugs (e.g. Lucentis® (ranibizumab, Genentech/Novartis), Avastin® (bevacizumab, Genentech/Roche), Eylea® (aflibercept, Regeneron/Bayer)) have been used in clinical trials for several years, showing benefits in visual acuity improvement and CNV regression in acute wet AMD and other CNV (e.g. myopic CNV) treatments (Gao et al., 2018, Schmid et al., 2015). Therefore, the common treatment for CNV is anti-VEGF therapy at present, and other approaches like photodynamic therapy, CNV surgery or laser treatment have been overcome. In this study, the effect of Avastin® was tested to check whether the CNV rat model is valid to study the effect of new drugs for CNV. The aim of Avastin® is to directly interact with VEGF extracellularly, thus avoiding the combination of VEGF and VEGFRs, inhibiting the progression of CNV. Although anti-VEGF therapy is the conventional treatment for CNV, there are still several adverse effects of anti-VEGF drugs, such as bleeding, increased blood pressure, cataract, photoreceptors loss, geographic atrophy and acute myocardial infarct. Thus, there is no optimal treatment for CNV, an efficient CNV animal model is needed for the investigate of new treatment options.

1.5 CNV animal models

The laser induced CNV rodent model is the most common CNV animal model. This model is easy to operate and is valid to induce several CNV lesions per eye in a short waiting time. However, it also has several disadvantages: the healthy retina is damaged due to the burn of laser before CNV formation starts, neovascularisation may origin from the retina (Semkova et al., 2003), and the CNV lesion induced by laser tends to self-healing, thus it is not suitable to teat long-term effect of treatments. The biggest disadvantage is that laser is not the natural cause of the disease, in contrast, laser can be used as the treatment for several ocular diseases in patients (e.g. retinal detachment), usually does not

induce neovascularisation. Therefore, the induction of CNV in the laser model does not mimic the progression of human CNV, it cannot be transferred to the root cause of human CNV, “VEGF”, which needed to be investigated.

There were also several CNV animal models induced by viral overexpression of VEGF (Kinnunen et al., 2006, Julien et al., 2008, Yu et al., 1999), but to my knowledge, none of them used on a routine basis thereafter, they did not yet receive the attention it deserves. In this study, the procedure of the CNV model was improved, e.g. chose the best vector to overexpress VEGF, confirm the best timepoint to test drugs.

1.6 Questions

1) How to develop an efficient CNV rat model by overexpressing VEGF?
    a) Which vector is the best?
    b) What are the differences between AAV-VEGF induced CNV and CNV transduced with Ad. VEGF?
    c) What are the advantages of AAV-VEGF induced CNV rat model compared with laser induced CNV model?
    d) What are the differences among AAV-VEGF induced CNV rat model compared with other CNV animal models?
    e) Does this model mimic human CNV?
2) Is this model valid to investigate the new treatment options for CNV?
    a) What is the best timepoint to test drugs?
    b) Does Avastin® reduce CNV in the CNV model?
3) Others:
    a) Why ICG always shows a rather spotty hyper-fluorescent pattern spreading around the CNV lesion?
    b) What are the early effects of VEGF overexpression?

2 Materials and Methods

2.1 Animals

Seven weeks old female Long Evans rats were purchased from Janvier Labs; Le Genest-Saint-Isle, France. Totally 118 eyes were used in this study (details see Table 2). The number of eyes with quantifiable data is less than that shown in Table 2, due to the death of the rats before the end of experiments, serious cataract and bleeding. The Avastin® treatment was performed 6 weeks after the VEGF vector injection, and the proposal is shown in Figure 4.

All the experiments were performed after approval by the Regierungspräsidium Tübingen (AK 09/14). All the rats were handled in conformity to the German Animal Welfare Act and were under the control of the animal protection agency and under supervision of veterinarians of the University of Tübingen.

Table 2: Number of the eyes injected with VEGF vectors, control vectors (EGFP, empty) and additional experiments using VEGF protein.

Injection reagent	Number of eyes								
	Duration of vector transduction (eyes without Avastin® treatment)				Avastin® treated eyes			Duration of VEGF protein/PBS expression	
					Duration of treatment				
	4w	6w	7w	9w	1w	3w	6w	1 h	24 h
HC Ad. VEGF vector	16								
AAV-VEGF vector	6	4	12	16	14	5	5		
HC Ad. EGFP vector	4								

AAV-EGFP vector	5			4					
AAV-empty vector	3								
VEGF protein								6	6
PBS								6	6
Total	118								

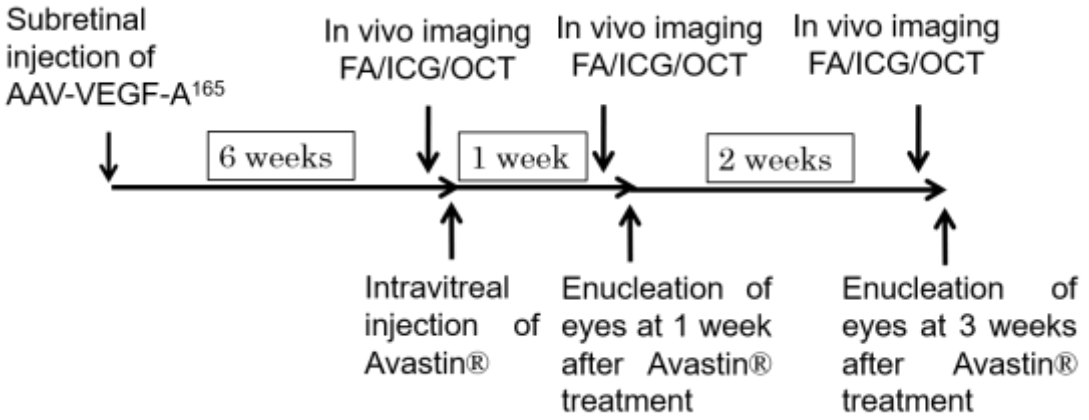

Figure 4: The proposal of Avastin® treatment test. The eyes were treated with Avastin® 6 weeks after VEGF vector injection.

2.2 Surgery

2.2.1 The suspension subretinal or intravitreal injected into the eyes

Table 3 summarized the volume and concentration of the suspension subretinal or intravitreal injected into the eyes. All the vectors were produced by Sirion Biotech Gmbh (Munich, Germany). In agreement with previous work (Julien et al., 2008), 2 µl of HC Ad. VEGF and HC Ad. EGFP vector suspensions **(**2µl PBS contain $1x10^7$ virus particles) were subretinal injected into the rat eye. $2x10^9$ virus particles of the AAV-VEGF-A165 vector in 2 µl PBS were subretinal injected into the eyes, while AAV-EGFP vector and AAV-empty vector were used to check the side effects of the AAV vector. To test if the AAV-vector can be

transduced by intravitreal injection, this surgery was performed in three AAV-EGFP transduced eyes. 100 ng VEGF-A165 (Sigma-Aldrich Chemie GmbH, Munich, Germany) in 2 µl PBS were subretinal or intravitreal injected into the eyes, thereby investigating the early effects of VEGF protein on choriocapillaris vasculature. PBS was used to check if the surgery itself was able to induce CNV. 19 eyes were intravitreal injected with 5 µl Avastin® (bevacizumab, Roche, Basel, Switzerland) 6 weeks after subretinal injection of AAV-VEGF-A vector in this study. 100 mg of Avastin® was diluted in 4 ml of vehicle solution (240 mg α, α trehalose 2 H_2O, 23.2 mg NaH_2PO_4 H_2O, 4.8 mg NaH_2PO_4 and 1.6 mg polysorbate 20). It was purchased and processed by the Pharmacy of University Hospital Tübingen.

AAV vector system uses the same VEGF cassette as in the Ad. vector studies. As shown in Figure 5, human VEGF-A165 cDNA, from the plasmid pBLAST49-hVEGF was inserted in a state of the art AAV2 vector (subtype 4) backbone. The different AAV vectors use the same backbone but have differing inserts according to the target gene. EGFP is inserted instead of human VEGF-A165 in AAV-EGFP vector (see Figure 6), and AAV empty-vector does not have expression cassette.

Table 3: The suspension subretinal or intravitreal injected into the eyes. SR: subretinal injection; IV: intravitreal injection.

Suspension	Volume and concentration	Injection methods
HC Ad. VEGF vector	2µl; $5x10^6$ virus particles/µl	SR
AAV-VEGF vector	2µl; $1x10^9$ virus particles/µl	SR
HC Ad. EGFP vector	2µl; $5x10^6$ virus particles/µl	SR

AAV-EGFP vector	$1x10^9$ virus particles/µl; SR: 2µl, IV: 2µl (n=2 eyes) or 5µl (n=1 eye)	SR: n=6 eyes, IV: n=3 eyes
AAV-empty vector	2µl; $1x10^9$ virus particles/µl (n=2 eyes) / $2x10^9$ virus particles/µl (n=1 eye)	SR
VEGF protein	2 µl; 50 ng VEGF-A165/µl	SR: n=6 eyes, IV: n=6 eyes
PBS	2µl	SR: n=6 eyes, IV: n=6 eyes
Avastin®	5 µl; 25 mg/ml	IV

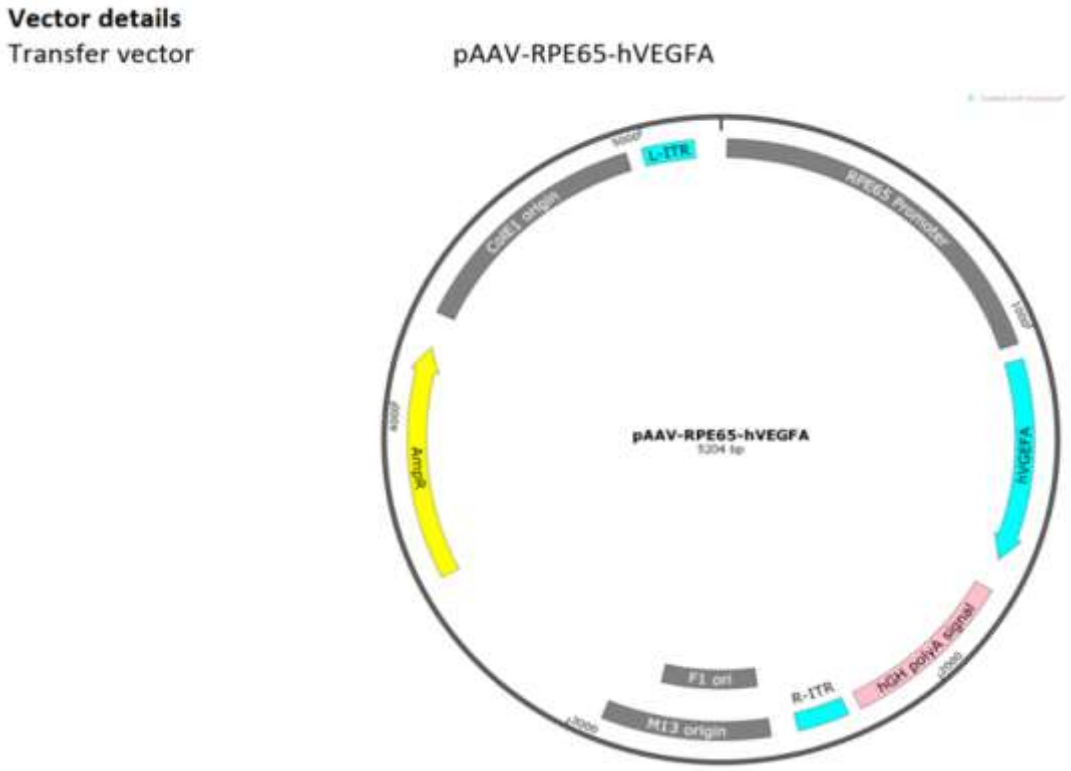

Figure 5: Vector map of AAV-hVEGF-A165 vector. The AAV vector contains an RPE specific RPE65 promotor instead of the unspecific CMV promotor used in Ad. Vector.

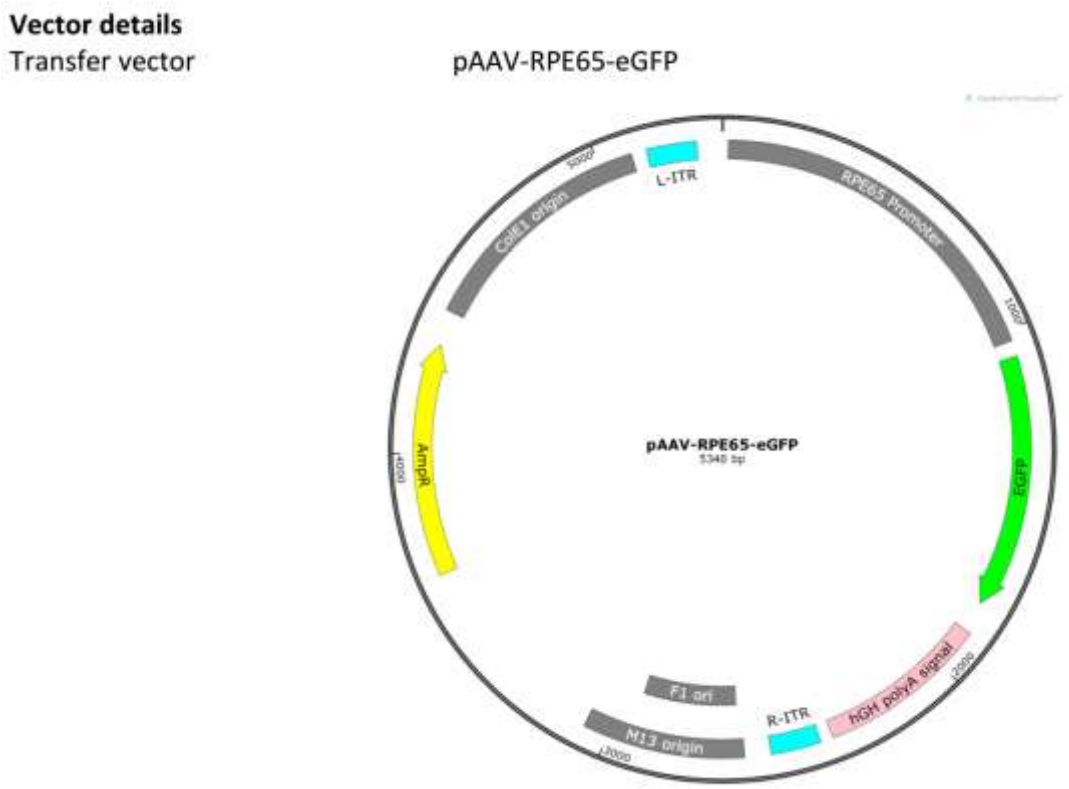

Figure 6: Vector map of AAV-EGFP vector. AAV-EGFP vector has the same backbone with AAV-hVEGF-A165 vector, but EGFP is inserted instead of human VEGF-A.

2.2.2 Subretinal injection

First weighed the rats, and then three component narcosis (0.005 mg fentanyl, 2 mg midazolam and 0.15 mg of medetomidine/kg body weight) was intraperitoneal injected into the rats. Their pupils were dilated with 1 to 2 drops of medriaticum drops (pharmacy of the University of Tübingen, Germany) and a drop of topical Novesine (Omni Vision, Puchheim, Germany). A surgical microscope was needed for the following injection. The sclera was first opened with a 25 G needle close to the limbus, then 2 µl of vector suspension were injected into the subretinal space of the eye by using 10 µl NanoFil syringe with a NanoFil 34 G blunt needle (World Precision instruments). Figure 7 shows the route of subretinal and intravitreal injection. As shown in Figure 7(A), subretinal injection is a method to delivers the vector suspension into the subretinal space

between RPE and the neuroretina. After the injection, topical antibiotic eye drops Gentamicin-POS® (Ursapharm, Saarbrüken, Germany) were applied on the eye. An antidote (0.12 mg nalaxon, 0.2 mg flumazenil, 0.75 mg atipamezole/kg body weight) was subcutaneous injected into the rat to neutralize the anaesthesia.

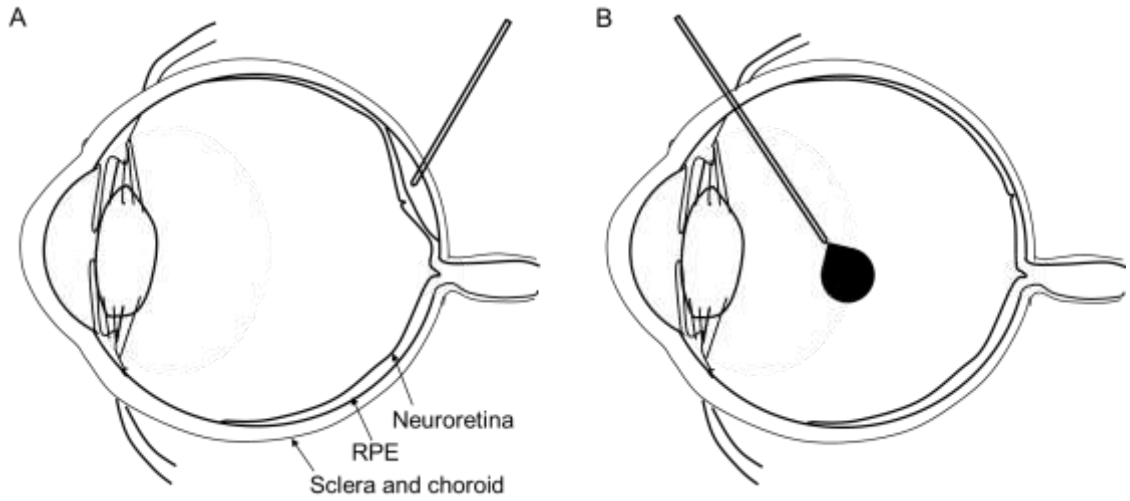

Figure 7: Subretinal injection (A) and intravitreal injection (B). (A) The vector solution is delivered by the needle into the subretinal space between RPE and the neuroretina. (B) Intravitreal injection uses the pars plana access to deliver vector solution (in black) into the vitreous cavity.

2.2.3 Intravitreal injection

As shown in Figure 7 (B), the solution is delivered through the pars plana into the vitreous cavity by using a 10 µl NanoFil 34-gauge bevelled needle. The whole process is performed under a surgical microscope. To reduce reflux, the needle was kept inside the eye for an additional 3-4 seconds after the injection.

2.3 In vivo imaging (SLO/OCT, angiography)

CNV-like hyper-fluorescence can be observed in angiography starting from 2 weeks after VEGF vector injection, based on the study of the other VEGF induced CNV animal models (Julien et al., 2008, Wang et al., 2003). Therefore, in this study, scanning laser ophthalmoscopy (SLO), OCT, FA and ICG were

performed starting at 2 weeks after VEGF vector injection. To confirm the best time point for the investigation of the treatments, in vivo imaging examinations were performed at different time points after VEGF vector injection (2, 3, 4, 6, 7, 9 weeks) by using a Spectralis^{TM} HRA+OCT (Heidelberg Engineering, Heidelberg, Germany, see Figure 8) device modified for the use with rats based on the protocols from (Huber et al., 2009, Fischer et al., 2009).

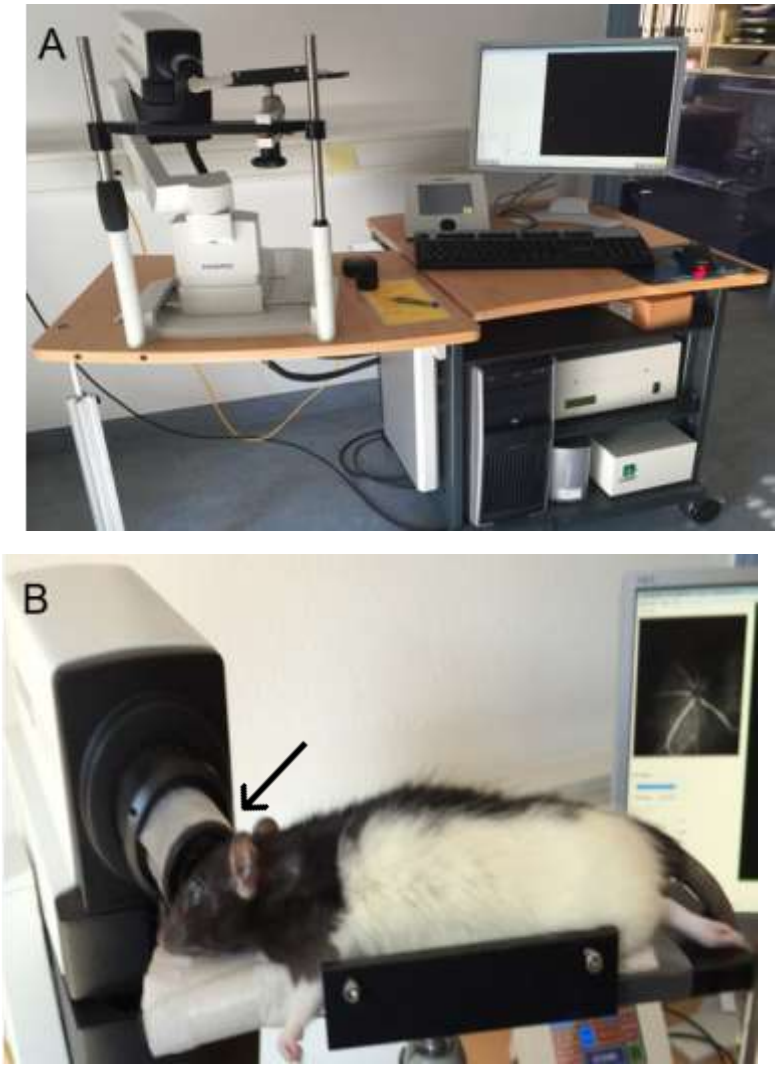

Figure 8: SpectralisTM HRA+OCT device (Heidelberg Engineering, Heidelberg, Germany) modified for the use with rats (A) and a rat is being performed in vivo imaging (B). A 78 dpt double aspheric lens (marked with black arrow) was placed directly to the outlet of the device.

A 78 dpt double aspheric lens (Volk Optical, Inc., Mentor, OH 44060, U.S.A.) was placed to the outlet of the SLO/OCT machine (Figure 8 (B)), and an additional custom-made +3.5 dpt contact lens was directly on the eyes of the rats. The contact lens is essential to avoid drying of the eyes and to obtain proper image quality. After anaesthesia, the pupils dilated and treated with Methocel to prevent eye dryness and better adherent to the +3.5 dpt lens. The cloudy cornea due to eye dryness can degrade the resolution of images, especially for OCT images. FA and ICG dyes (42 µl fluorescein (Alcon 10%), 208 µl 0.9 % NaCl, 250 µl indocyanine green (ICG, 5 mg/ml, Diagnostic Green) were injected in the tail vein and in vivo imaging was performed immediately to obtain the early phase FA and ICG angiograms, and the late phase angiograms were performed after at least 20 minutes. The GFP protein can be visualized by autofluorescence imaging in the FA mode.

It takes much longer time to perform angiography in rats than in patients, as the rat should be replaced in front of the machine according to the position of the eye in the anaesthetic rat. Therefore, the early phase angiograms of the second eye are usually delayed and performed in a time frame of 3-10 minutes after dye injection, and the late phase angiograms of the same eye were obtained 10 minutes later. The rats were sacrificed immediately after completing the last in vivo imaging.

The ‘‘automatic real time’’ (ART) mode of the SLO/OCT machine is used to obtain a high-quality image based on up to 100 consecutive images in real time (Charbel Issa et al., 2013).

As the SLO/OCT machine is designed for human patients, the dimension in x and y axis are not calibrated for the animal experiments, in contrast, the dimensions in z axis in OCT images is displayed properly. Therefore, the data of retinal thickness and CNV lesion thickness in OCT images is correct. Garrido et al. (Garcia Garrido et al., 2015) provided data to correct the distortion-related

problems in the analysis of OCT images caused by the unequal X and Y scales in mouse. However, this image calibration cannot be used for rats due to the size differences between mouse and rats. Thus, the measurements of CNV hyper-fluorescent areas in FA/ICG angiographs are displayed in arbitrary units (au) in this study instead of µm using in the included software in the Heidelberg SLO/OCT machine. The retinal thickness and CNV lesion thickness in OCT images are presented in µm.

2.4 Light/electron microscopy

After the enucleation of the eyes, the whole eyes were fixed in 5 % glutaraldehyde in 0.1 M cacodylate buffer over night at 4 °C. The CNV area in the eye was cut according to the angiographs by the assistance of a microscope and finally embedded in EPON (SPI-Pon™812 Epoxy Embedding Kit, SPI supplies, West Chester, PA). The rest of the eyeball was also embedded for internal control of healthy tissue. The protocol (chemicals purchased from Fluka, Germany) of the embedding was listed in Table 4.

Table 4: The protocol of the fixation and embedding for electron microscopy.

Processes	Chemical solution	Time
Fixation	5 % glutaraldehyde in 0.1 M cacodylate buffer (pH 7.4)	Overnight at 4°C
Washing	Three times 0.1 M cacodylate buffer	10 minutes each
Postfixation	0.1% osmium tetroxide: 0.1 M cacodylate buffer 1:1	2 h
Washing	Three times 0.1 M cacodylate buffer	10 minutes each

Dehydration	Ethanol 30-50-70%	15 minutes each
Block staining	Saturated uranyl acetate in 70% Ethanol	Overnight at 4°C
Dehydration	Ethanol 70-80-95%	15 minutes each
	Two times absolute Ethanol	20 minutes each
Intermedium	Two times Propylenoxid	20 minutes each
Resin	Propylenoxid : Epon 1:1	2 h
	Epon	2 h
	Epon	1 h
Polymerisation	60°C	48 h

Semithin sections were cut, stained with toluidine blue and observed under light microscopy (LM). Ultrathin sections were placed on formvar coated copper grids (Plano, Germany), stained with lead citrate and examined by electron microscopy (EM) with a Zeiss 900 TEM (Zeiss Axioplan2 imaging, Zeiss, Jena, Germany, see Figure 9).

The embedded tissues were cut by using Reichert-Jung Ultracut E Ultramicrotome (Leica, Nussloch, Germany) (see Figure 10). There are several diamond knifes, some are used to cut semithin section (0.7 µm) for LM, and the others are used for EM (ultrathin section 0.05 µm).

Figure 9: Transmission Electron microscope (Zeiss EM 902a with Digital camera MegaView III)

Figure 10: Reichert-Jung Ultracut E Ultramicrotome used for sectioning the embedded tissues.

2.5 Immunohistochemistry

After the enucleation of the eyes, the whole eyes were fixed in 4.5 % formalin (Roti Histofix, Carl Roth, Karlsruhe, Germany) and embedded in paraffin for the histologic study. The position of the CNV area can be confirmed according to the angiographs. A thread through the tissue outsides the sclera was used to mark the position of the CNV area, to increase efficiency to obtain sections with CNV. 4 µm thick sections were cut and stained with hematoxylin-eosin (HE) or respective antibodies according to standard procedures. The slides were first deparaffinized, then cooked in citrate buffer, pH 6.0 or Tris-EDTA buffer, pH 9.0 for 2 minutes to retrieve the antigens. Primary antibodies used in this study were listed in the Table 5. HE staining was performed to locate the CNV area. For most experiments, the “DAKO REALTM Detection System, Alkaline Phosphatase/RED, Rabbit/Mouse” kit was used as a secondary antibody. A Cy3 mouse secondary antibody was used as the secondary antibody for the

anti-RPE65 antibody staining and a Cy3 goat secondary antibody was used for the anti-Iba1 staining (secondary antibodies were bought from jackson immunoresearch, ELY, UK). A Zeiss Axioplan2 imaging microscope (Zeiss, Jena, Germany) cover-slipped with FluorSave (Calbiochem, La Jolla, CA, USA) was used to investigate the fluorescence staining of the samples.

Table 5: List of primary antibodies.

Target protein/cell type	Host/Company	Dilution
Pericytes:		
- α-SMA (alpha-smooth muscle actin)	From mouse, Sigma	1:800
- humanNG2[LHM2] (neural/glial antigen 2)	From rabbit, Abcam	1:50
RPE:		
- RPE65	From goat, Santa Cruz	1:100
Macrophages/activated microglia:		
- Iba1	From rabbit, Wako	1:1000
Growth/Transcription factors:		
- VEGF (rat, human)	From mouse, GeneTex/Biozol	1:300
Leakage:		
- albumin	From rabbit, Abcam	1:100

Additionally, Masson trichrome staining was performed according to the protocol from (Jayes et al., 2019). The sections were deparaffinized and stained with celestinblue, Meyer's hemalaun, acid fuchsine, phosphomolybdic acid 1%, methylene blue and acedic acid 1% in EtOH for each 5 minutes with washing

steps in between, respectively. For Masson trichrome staining, fibrin, elastin and collagen in the sections can be presented differentially. Fibrin is stained in dark red, collagen in blue and elastin in light red.

2.6 Quantifications in eyes transduced with VEGF vector

2.6.1 Detection and quantification of hyper-fluorescent CNV lesion areas in angiography data sets

As the area of hyper-fluorescent region in the angiogram is corresponding to the area of CNV lesion (Lu and Adelman, 2009), it was measured and analyzed in FA and ICG angiographs, shown in Figure 11. The area can be measured automatically after contouring the CNV lesion by using the included software in the Heidelberg SLO/OCT machine.

Additionally, FA and ICG angiographs of the same eye can be displayed and imaged simultaneously, allowing the simultaneous comparison of the area of the CNV lesion in FA and ICG angiographs (see Figure 11).

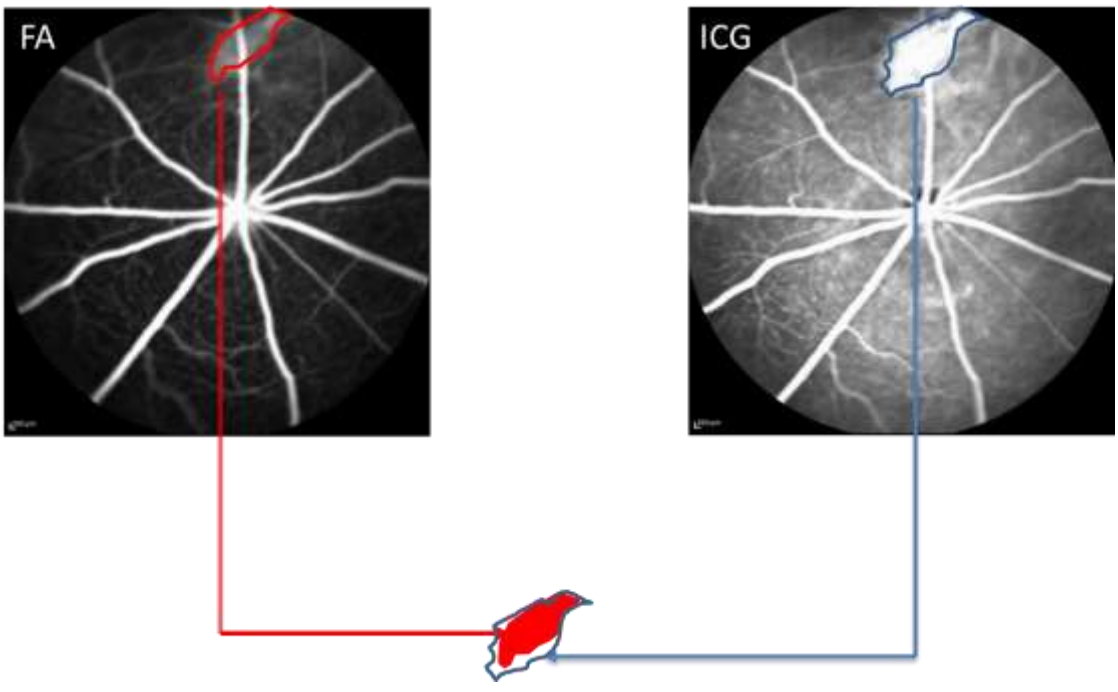

Figure 11: Measurement and comparison of the area of CNV lesions in FA and ICG in the eye 4 weeks after VEGF transduction. FA and ICG angiographs of this eye were imaged simultaneously. The contour of CNV area is red in FA and blue in ICG. ICG shows an obvious larger CNV area than FA in this eye.

2.6.2 Quantitative analyses of the maximal thickness of the CNV lesion and the retina in OCT data sets

The SLO/OCT machine has a function to scan and obtain a series of OCT images in a specified region, thus a series of OCT images in the whole CNV lesion area were collected for each eye in this study. Figure 12 is an example of a series of OCT images in the whole CNV lesion region. The CNV lesion in each OCT image is corresponding to the hyper-fluorescent region in the FA angiograph (left image of Figure 12).

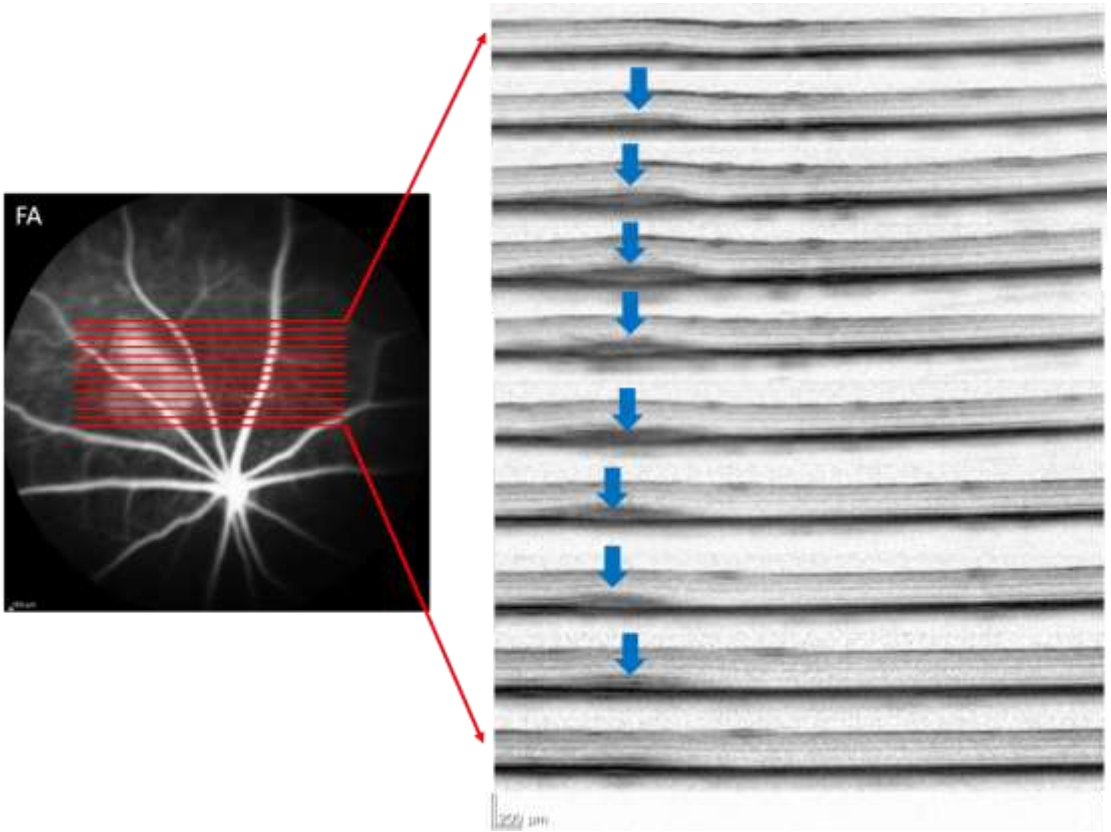

Figure 12: A series of OCT images in the whole CNV lesion region in one CNV eye. The CNV lesion in each OCT image is marked with blue arrows, corresponding to the

hyper-fluorescent region in the FA image. There are no obvious changes shown in the topmost and lowest OCT images, representing the top and bottom edges of the hyper-fluorescent area in FA.

The retinal and the CNV lesion thickness were measured in each OCT image of each eye by using the measure methods in Figure 13, and the maximal data of each eye was used for statistical analysis. In addition, retinal thickness in the adjoining area without lesion was measured as controls and termed as “normal retinal thickness”.

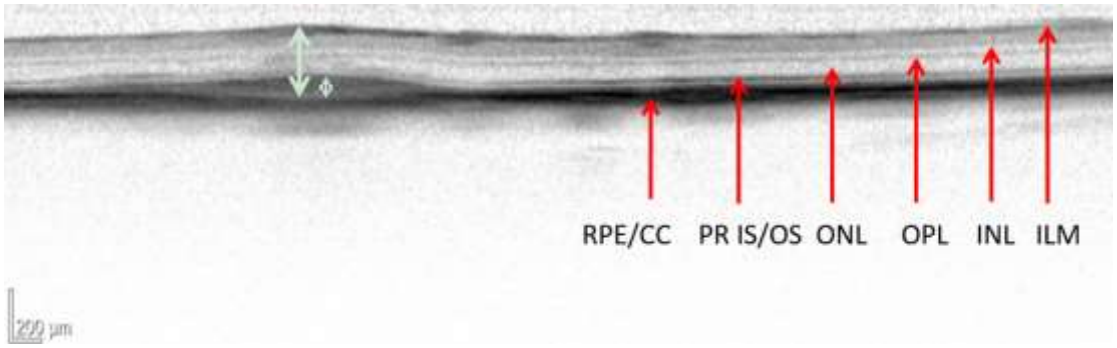

Figure 13: Measurement of the thickness of the retina (between ILM (internal limiting membrane) and choroid) and CNV lesion (marked with white double-headed arrows). Different layers of the retina were marked with red arrows, respectively. INL: Inner nuclear layer.

2.6.3 Quantification of choriocapillaris loss and RPE loss with CNV

The quantification of choriocapillaris loss and the RPE loss with CNV were analysed in this study. The area of CC in per length of BM and the length of RPE in per length of BM were measured in a series of images of whole semithin sections of several different CNV rats according to the protocol from (Biesemeier et al., 2014).

2.6.4 Quantification of VEGF expression by IHC

The quantification of human VEGF staining in the CNV eyes was performed by using ImagePro Plus 6.0. The percentage of VEGF positive staining area in the total CNV area was calculated following the method shown in Figure 14, to test Avastin® treatment effect.

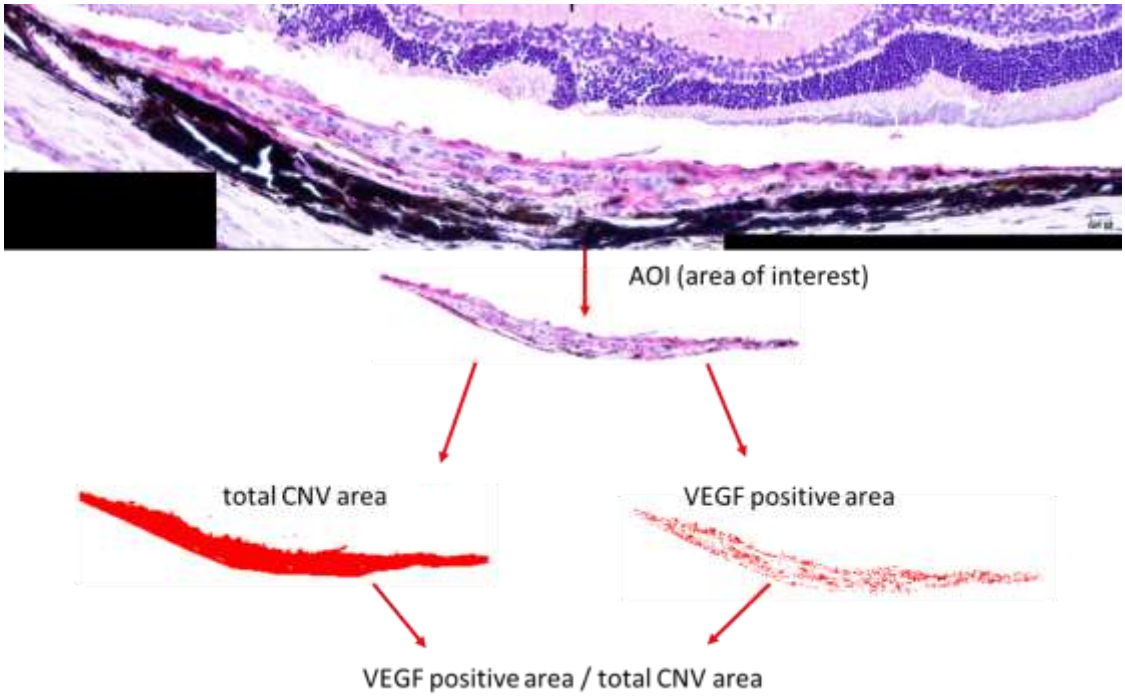

Figure 14: Quantification of VEGF expression in CNV eyes. First, the AOI is obtained from the original staining image. Then the total CNV area and the VEGF positive area can be measure by using ImagePro Plus 6.0. Finally, the percentage of VEGF positive area of the total CNV area is calculated.

2.7 Description of CNV from human eyes

Five human CNV samples removed from the sub-macular surgery were analysed by LM/EM and IHC (the same samples used in (Schraermeyer et al., 2015)). VEGF and NG2 primary antibodies used for the rat CNV models were also used for human CNV samples. The morphological features of human CNV were compared with rat CNV induced by VEGF transduction.

2.8 Statistics

All the statistical analysis used IBM SPSS Statistics 25 software. Student's t-test was performed to compare the results of two groups and ANOVA (analysis of variance) was used for the multiple comparisons of the different groups in angiography and OCT analyses. The significance level is P=0.05. The mean value and standard deviation are shown in the box figures.

3 Results

3.1 Control experiments

The following controls were applied during this project, as shown in Table 6, and the details will be presented in the respective chapters below.

Table 6: Number of eyes with CNV detected by in vivo imaging and histology in the controls applied in this study.

Number of eyes with CNV / Number of eyes used for controls	PBS controls	EGFP vector controls		AAV-empty vector controls
		HC Ad. EGFP vector	AAV-EGFP vector	
In vivo imaging	0/12	0/4	1/9	0/3
Histology	0/12	Retinal degeneration was observed in all the eyes	1/9	0/3

3.1.1 Investigation of PBS controls after subretinal and intravitreal injection

As shown in Table 6, subretinal and intravitreal PBS injection did not lead to any pathological changes in histologic examinations, except for minor traumata due to the injection procedure. Hyper-fluorescence indicative for vascular changes

was not observed in FA/ICG angiography in all the eyes. The subretinal bleb was observed in OCT in all the eyes subretinal injected (shown in Figure 15). The direct effect of the injection procedure was observed: bleeding in 2 eyes after subretinal injection, minor bleeding in 3 eyes and 1 eye with retinal puncture after intravitreal injection.

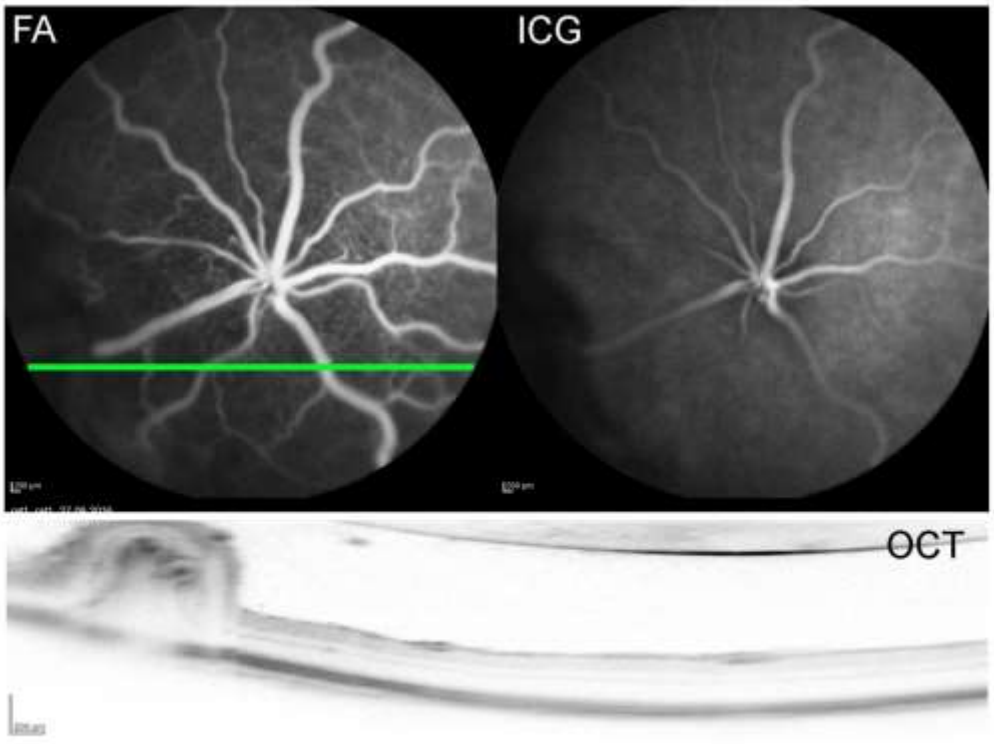

Figure 15: FA/ICG angiography and OCT of a PBS control eye 24h after subretinal injection. Hyper-fluorescence cannot be observed in FA/ICG. The position of the subretinal bleb observed in the OCT image is corresponding to the lower temporal periphery of the eye (the position of the green line in the FA image).

3.1.2 Investigation of the AAV-EGFP vector controls after subretinal and intravitreal injection

The autofluorescence of GFP can be observed in the FA mode till 9 weeks after subretinal injection of EGFP vector. However, the two eyes intravitreal injected

with 2 µl AAV-EGFP vector did not show obvious GFP autofluorescence, only the eye intravitreal injected with a higher volume of 5 µl AAV-EGFP vector expressed GFP up to 6 weeks.

Apart from one eye, the rest eyes transduced with EGFP vectors did not showed any CNV-like lesions in FA and ICG angiography (Table 6 and Figure 16 (a)-(c)). Traumata caused by the injection procedure disappeared 2 weeks after the vector injection. In conformity with the PBS control, a subretinal bleb was observed in OCT after subretinal injection of a 2 µl volume of vector suspension (Figure 17).

All the eyes transduced with HC Ad. EGFP vectors showed retinal degeneration after histological evaluation, including EM (Figure 18). The CNV lesions induced by HC Ad.VEGF vector showed retinal damage (e.g. completely loss of photoreceptors and rosette-like retinal changes) frequently, thus the high retinal toxicity caused by the Ad. vector was confirmed. Except for one eye, retinal degeneration or CNV was not observed by LM and EM in the eyes injected with AAV-EGFP vector (Figure 16).

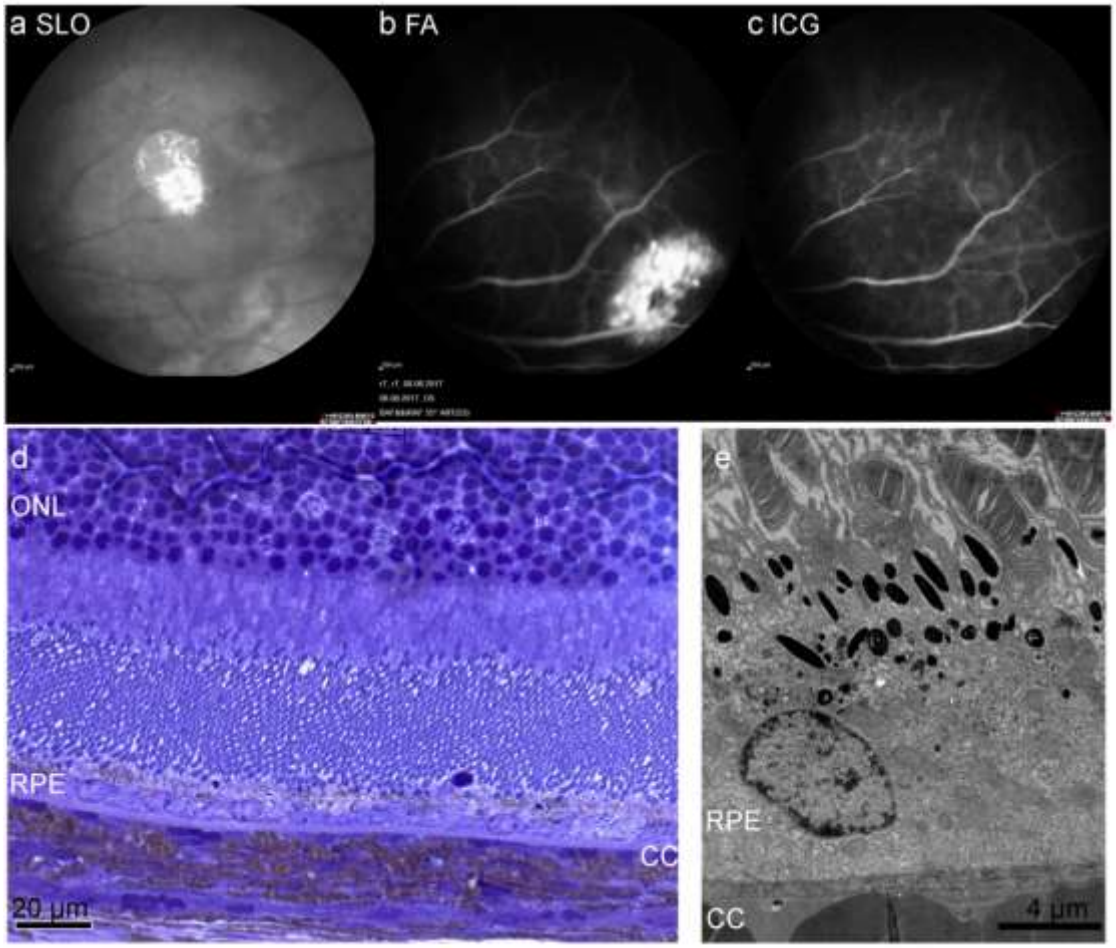

Figure 16: Investigation of an eye transduced with AAV-EGFP vector: (a) SLO, (b) combined GFP autofluorescence and FA angiography, (c) ICG angiograph, (d) LM, (e) EM. As ICG angiography (c) do not show any pathological hyper-fluorescence, the ring-like shape hyper-fluorescence in (b) is GFP autofluorescence. The spotty appearance of the fluorescence could be due to transduction of individual RPE cells. LM and EM do not show any histological changes. The tissue shown in (d) and (e) is corresponding to position of GFP autofluorescence in (b). The vector toxicity or CNV formation are not observed in this control eye.

Figure 17: OCT image, 12 hours after subretinal injection of a 2 µl volume into a rat's eye.

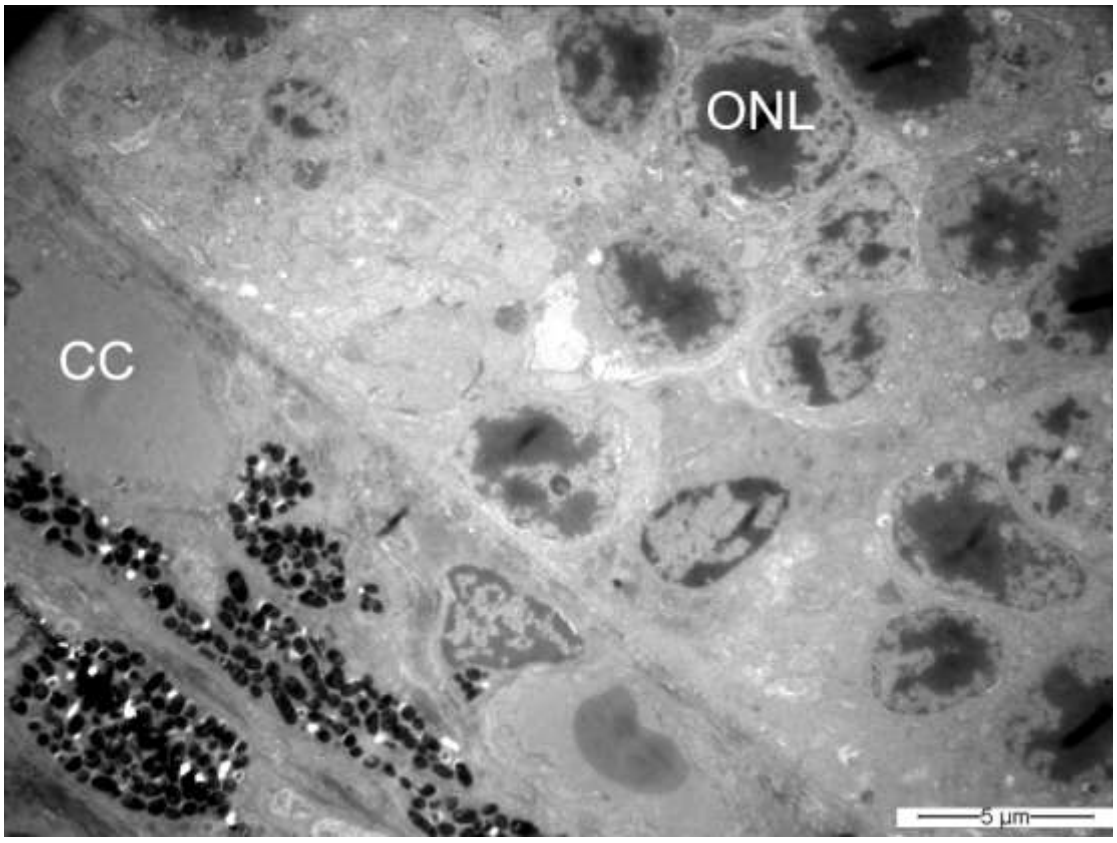

Figure 18: Electron micrograph of the eye transduced with HC Ad. EGFP vector. The cells between ONL and CC (e.g. photoreceptors and RPE cells) cannot be observed, indicating the retinal toxicity of the Ad. vectors.

3.1.3 Investigation of the AAV-Empty vector after subretinal injection

No CNV-like lesion or retinal toxicity was shown in angiography and microscopic analysis (LM/EM) in any eyes after subretinal injection of AAV-Empty vector, including the eye with double dose compared with AAV-VEGF vector (Figure 19).

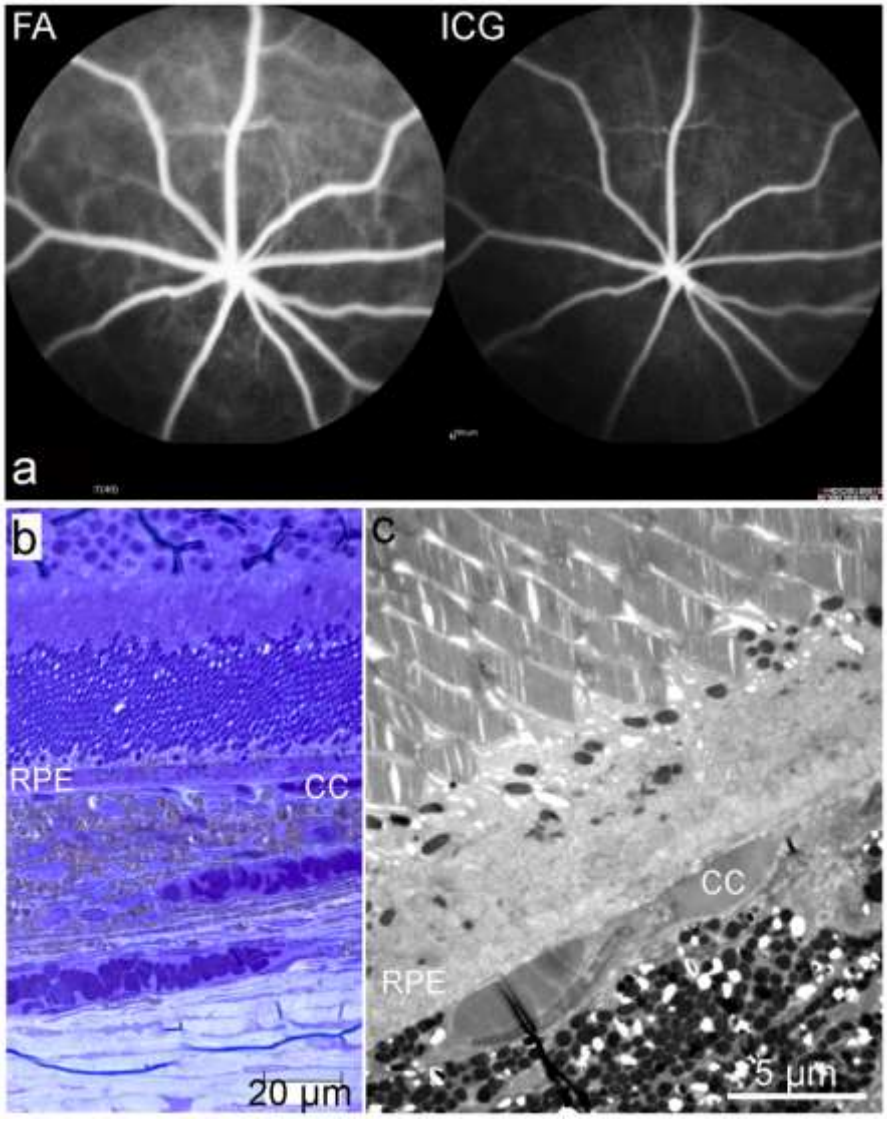

Figure 19: Angiography (a) and histological (b, c) evaluation of eyes after subretinal injection of AAV-Empty vector. FA and ICG angiographs do not show any vascular changes. Light micrograph (b) and electron micrograph (c) do not show any toxicity or CNV-like changes in the retina-choroid interface. four weeks after AAV-Empty vector injection.

3.2 Characterisation of CNV induced by overexpression of VEGF in rat eyes

All the eyes transduced with VEGF vectors were performed in vivo imaging several times, and then after enucleation, further histological analyses like LM/EM were performed. A summarizing figure panel is shown in Figure 20, and the details of the findings are presented in the respective chapters below. The eyes successfully transduced with VEGF vector and showing CNV-like signs in FA/ICG/OCT will be termed “CNV eyes” in the following. In addition, the CNV-like lesion and the hyper-fluorescent area shown in FA/ICG will be termed as “CNV lesion” and “CNV area”, respectively.

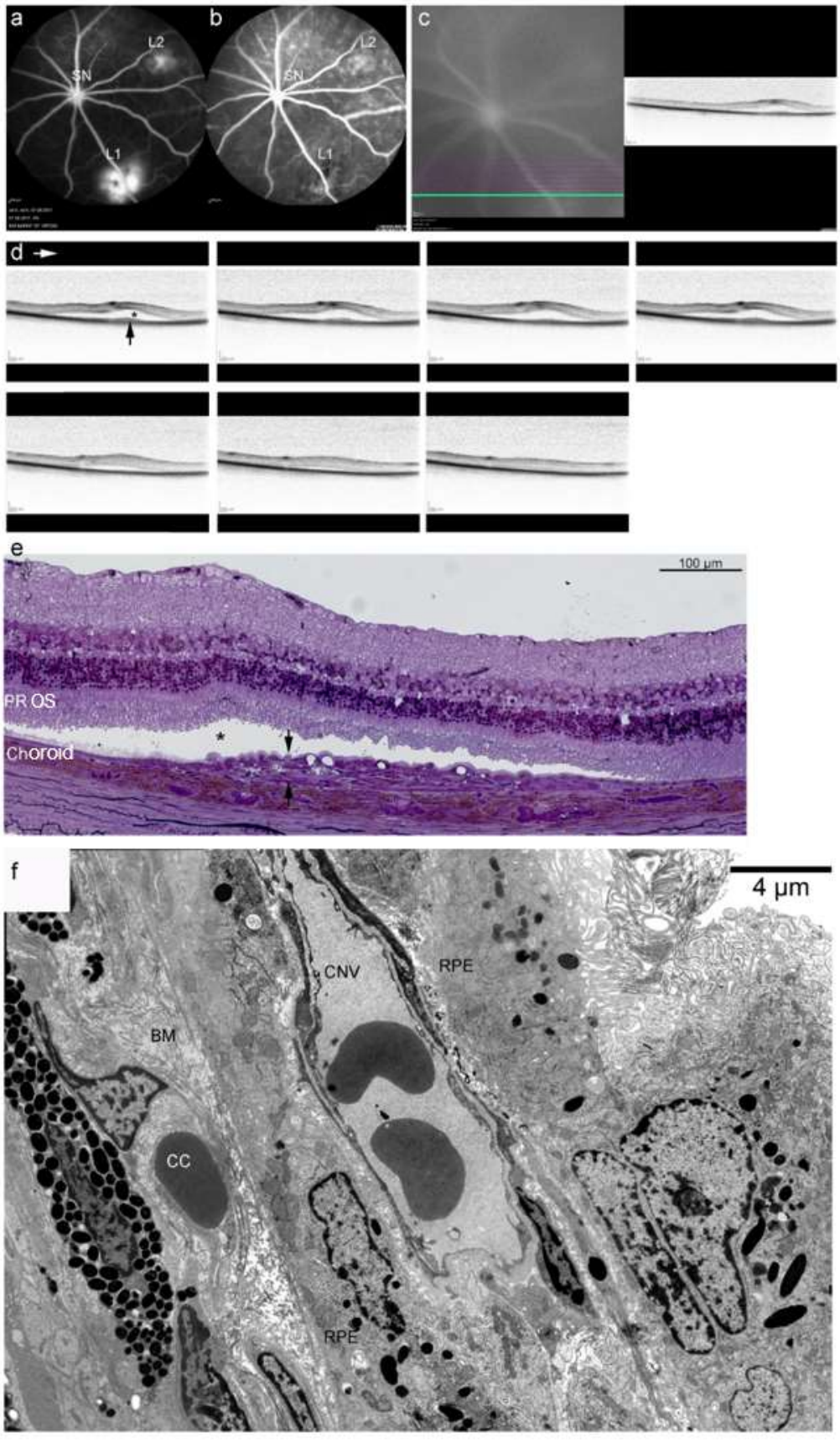
a
b
c
L2
SN
L1
d
e
100 µm
PR OS
Choroid
f
4 µm
CNV
RPE
BM
CC
RPE

Figure 20: Summary of CNV features evaluated by FA/ICG angiography, SLO-OCT and LM/EM of the same eye, 4 weeks after VEGF transduction: (a) FA and (b) ICG, lesion 1 and 2 (L1, L2). Normally, each CNV eye shows only one CNV lesion, however, a few CNV eyes shows more than one lesion due to the diffusion of the vector suspension during and after the subretinal injection. (c) OCT of L1: green line in the left ICG image corresponds to the right OCT image. Pink lines in the ICG image correspond to the series of OCT images in (d). The lesion as hill-like structure labelled with black arrow in the first OCT image in (d) is corresponding to the CNV area in (e) and (f). Subretinal space is marked with *. (e) Light microscopical image of L1. The black arrows label the CNV area below the subretinal space (*). (f) Electron microscopical image of L1. A newly formed blood vessel can be observed between multi-layered RPE (CNV).

3.2.1 Angiography of CNV eyes

The CNV eyes detected by in vivo imaging were summarized in Table 7. 81% of the eyes transduced by HC Ad. VEGF vector showed the signs of CNV 4 weeks after the vector injection. Due to the high toxicity of the HC Ad. vector shown by retinal degeneration in the GFP controls (Table 6 and Figure 18), an AAV vector system was used to develop the model further (AAV-VEGF model). 50% of the eyes transduced with AAV-VEGF showed CNV after 4 weeks' duration in FA/ICG, in contrast 91% of the eyes showed CNV after 6 weeks' duration. In addition, all the eyes used to test the effect of Avastin® showed CNV at 6 weeks after AAV-VEGF transduction.

Table 7: Number of eyes with CNV detected by in vivo imaging.

Injection reagent	Number of eyes with CNV detected by in vivo imaging/Number of eyes used for model			
	Duration of vector transduction (eyes without Avastin® treatment)		Avastin® treated eyes	
			Duration of treatment	
	4w	6w-9w	1w	3w
HC Ad. VEGF vector	13/16 (81.25%)			
AAV-VEGF vector	3/6 (50%)	29/32 (91%)	14/14 (100%)	5/5 (100%)

As the newly formed blood vessels (CNV) from CC extend through the rupture of BM into the retina, the vascular changes in the choroid should be shown in ICG and the changes in the retina lead to hyper-fluorescence in both FA and ICG. As shown in Figure 21 and 25, the ICG signal always showed a spotty pattern stretched over a larger area than the FA signal. In addition, a few eyes showed additional hyperfluorescent areas in ICG, possibly caused by alterations and leakage of the choriocapillaris which were features of CNV (Figure 22).

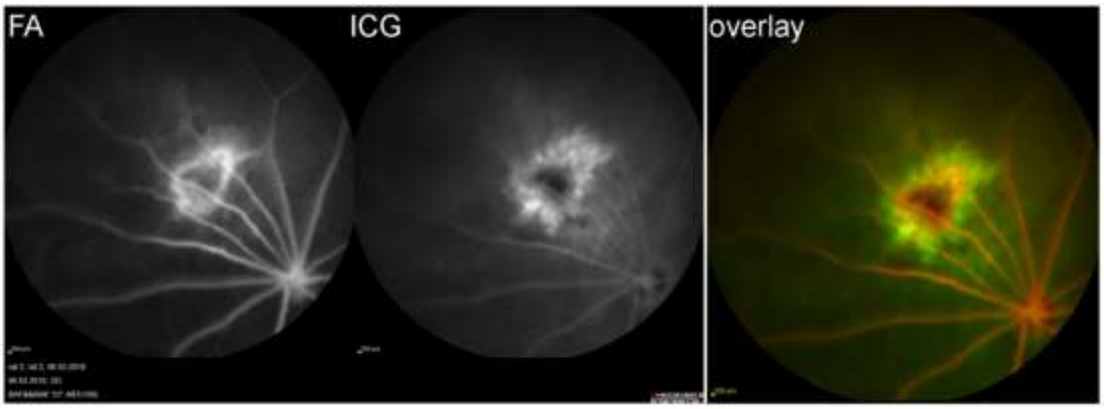

Figure 21: Comparison of the CNV area in FA and ICG in an eye 6 weeks after

transduction with AAV-VEGF. The right image showed the overlay of FA and ICG (FA signal: red colour; ICG signal: green colour; Overlay: yellow colour). The overlay areas contain the retinal vessels and CNV area in the retina. The ICG signal shows spotty pattern stretched over a larger area than the FA signal.

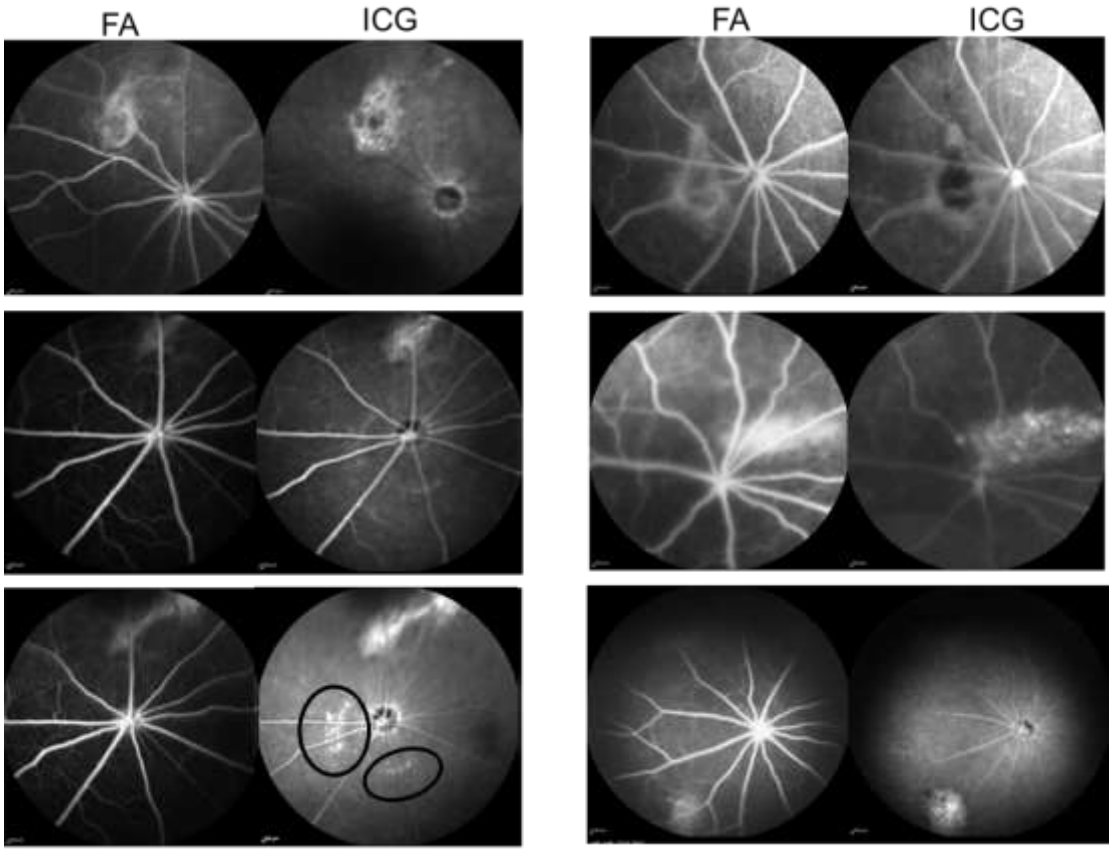

Figure 22: Angiography of six CNV eyes. The left image of each angiograph is FA, the right is ICG. ICG shows a larger CNV area than FA in each eye. One eye shows additional ICG hyper-fluorescent areas which are not observed in FA.

The early phase angiograms of the rat eye are usually delayed, because the SLO/OCT machine is designed for human. Thus, it is rare to observe a leakage in the animal models. However, the leakages were observed in a few CNV eyes in this study. As shown in Figure 23, the CNV lesion (marked in red) become more obviously in the late phase of ICG compared with the early phase. This is a

leakage from the choriocapillaris, a main feature of CNV.

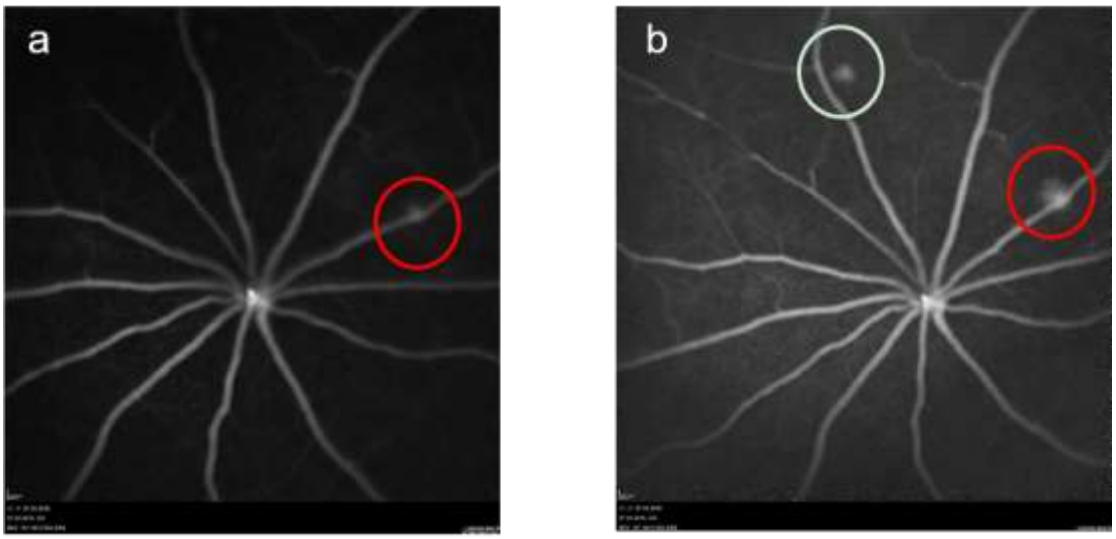

Figure 23: ICG angiographs of the early phase (a) and late phase (b). The CNV lesion marked in white is not visible due to its peripheral position. The lesion marked in red is a leakage.

The ring-shaped hyper-fluorescent area with a dark area in the middle is always observed in FA and ICG, correlating well with the OCT images showing obvious subretinal lesions in the hyperreflective areas (Figure 24). Two small CNV lesions in Figure 24 (b) is corresponding to the central hyper-fluorescent area in FA (Figure 24 (a)). The retinal thickness decreased in the dark area compared with the surrounding hyperfluorescent area in FA.

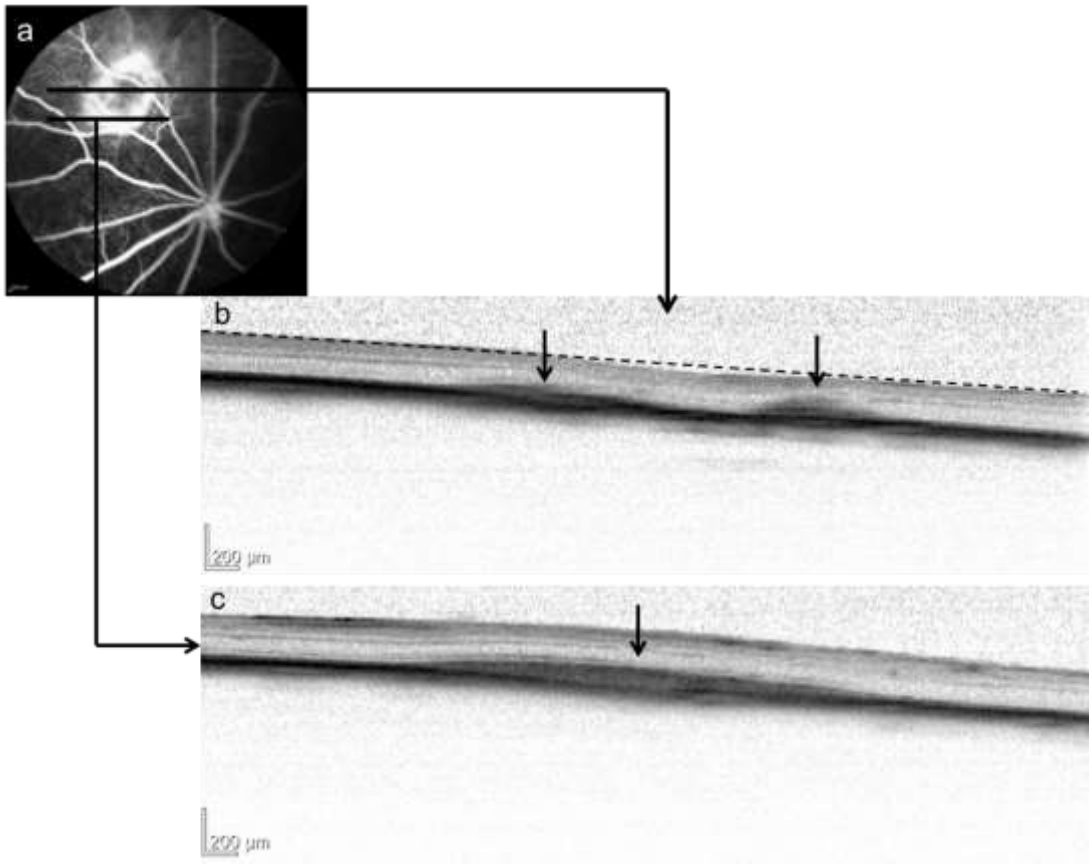

Figure 24: A FA angiograph (a) and corresponding OCT images (b and c) cutting the ring-shaped hyper-fluorescent area centrally (red) and at the outer rim (black). OCT lesions reflect the hyper-fluorescent area in FA. The dashed line in (b) shows the decrease of the retinal thickness between the two small CNV lesions marked with black arrows. A large CNV lesion marked with black arrow is shown in (c), corresponding to the outer rim of the ring-shaped hyper-fluorescent area in FA.

In contrast to FA, ICG showed a rather spotty pattern around the CNV lesion and usually spreads over time (see Figure 25). This leads to a larger hyperfluorscent field that can cover the whole background of the eye at the late time point (shown in 7 and 9 weeks ICG angiographs in Figure 25). However, after additional ICG dye injections, these spotty patterns do not change significantly within a time frame of 20 minutes. CNV lesion sizes in ICG is hard to be

quantified, as the CNV lesion and the migrating ICG labelled cells are difficult to be distinguished.

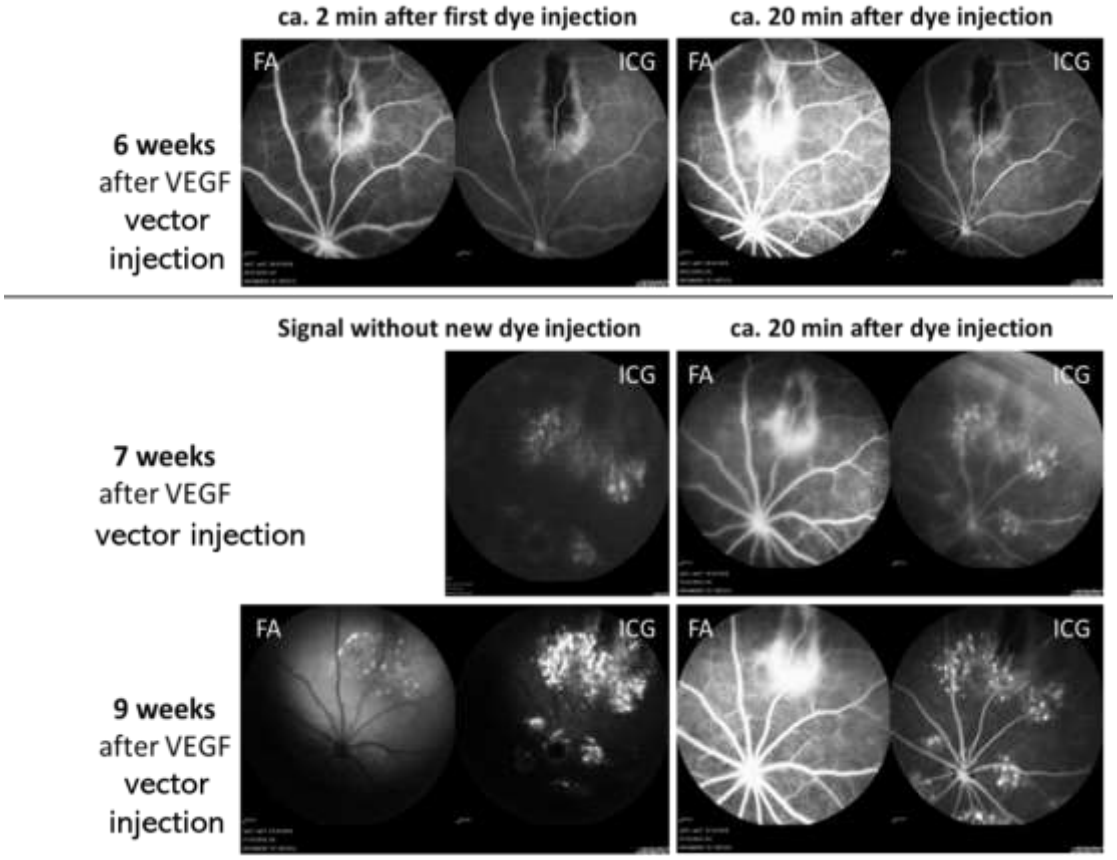

Figure 25: Peculiarities in FA and ICG angiography 6, 7 and 9 weeks after AAV-VEGF injection. At 6 weeks after AAV-VEGF vector injection, a ring-shaped hyper-fluorescent area was shown in both early phase (about 2 minutes after dye injection) and late phase (about 20 minutes later) FA/ICG. The ICG fluorescent can be observed one and two weeks later without new dye injection and shows a rather spotty pattern spreading over the whole background of the eye. The spotty patterns, however, do not change dramatically after additional dye injections within a time frame of 20 minutes, at 7 and 9 weeks after VEGF vector injection, respectively. These ICG angiographs show both the ring-shaped lesion as well as the spread hyper-fluorescent spots. The FA signal, presented before new dye injection, is probably due to autofluorescence caused by photoreceptor damage.

3.2.2 Light and electron microscopical evaluations of CNV (ultra)structure

CNV induced by VEGF-overexpressing in rats was characterized by newly formed blood vessels with fenestrations between BM and RPE or between multi-layered RPE cells, multi-layered RPE, loss of photoreceptors and concomitant extracellular matrix formation (mainly collagen type I) (Figures 30-33).

RPE

Proliferation of pigmented RPE-like cells leads to the thickening of the RPE layer towards the retina. Large vacuolar structures (see Figure 28) and extreme elongation of the microvilli (see Figure 27 (a)) were often shown in the RPE layer surrounding the CNV lesion.

CNV vessels

The newly formed blood vessels with fenestrations originate from CC, as fenestration is a feature of choroidal capillaries (Figure 27 and 33). The invading of CNV vessels from the choroidal capillaries through the rupture of BM and into the subretinal space was found in few cases (Figure 29). Multi-layered basal lamina (Figure 27), collagen accumulation (Figure 26-33) and perivascular supporter cells (Figure 26 and 33; confirmed by α-SMA and NG2 staining, histology section) were observed in the surrounding of many CNV vessels. Rare CNV vessels lost fenestration and pericytes and became leaky in the CNV rats, while these irregular vessels were frequently seen in late stages of wet AMD.

Endothelial cells of CNV vessels

The endothelium in CNV vessels often showed many transcytotic vesicles and an activated endoplasmic reticulum system suggesting high cellular activity

(Figure 27 and 33). As shown in Figure 29 (c), a small vascular lumen was formed by the bifurcations of endothelium in the CNV vessel. It is a source of leakage in neovascular choroidal vessels, if the outer endothelial wall closes incompletely (Schraermeyer et al., 2015).

Bruch's membrane

Rebuilding of the extracellular matrix in BM lead to disorder of RPE cellular function. Thin cells (unidentified thin, elongated undifferentiated cells) were observed in CNV area and between CC and BM, which might be an early feature for endothelial proliferation (see Figure 27 (b)). These cells are also observed frequently in CNV areas of human eyes. The integrity of the elastic layer in BM was often lower in CNV areas. Same finding has been described in human patients, elastic layer loss integrity and become obvious thinner with the progression of AMD (Chong et al., 2005). Collagen bundles with different thickness appeared disorganized between choriocapillaris and BM.

In many cases, a new BM was formed between two well-developed basal laminas with an elastin- and collagen-like material in between (see Figure 27). Thus, a new "CC-BM-RPE" interface on top of the CNV facing the viable retina was probably formed, suggesting a transformation of viable CNV tissue into a retinal scar.

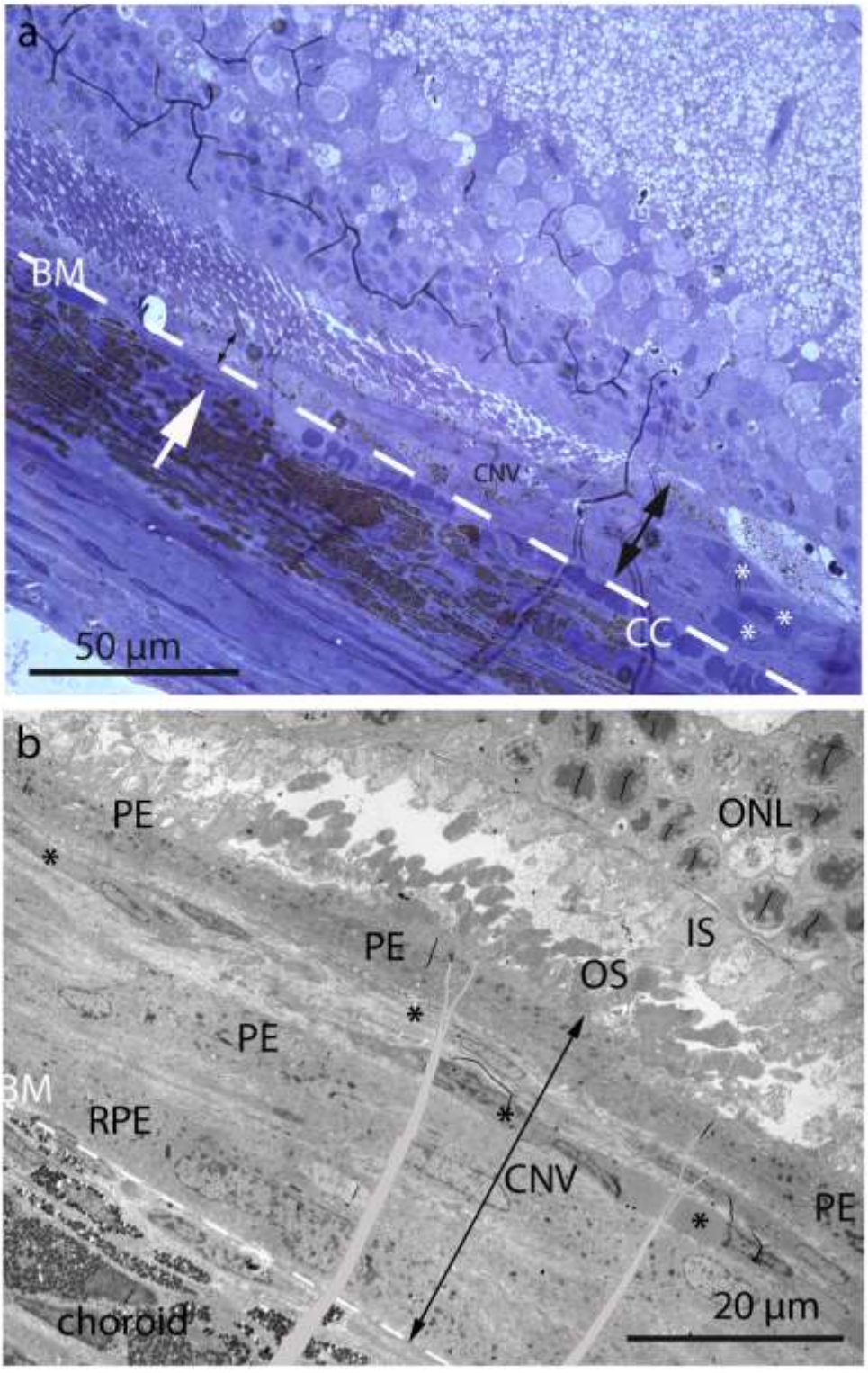

Figure 26: Representative LM (a) and EM (b) images of CNV structure: both images show the CNV area (double arrows) with CNV vessels (*), multi-layered pigmented RPE

cells (small double arrow in **a**, PE in b) and extracellular matrix deposition. (a) CNV is associated with CC loss at the border region (white arrow) and advanced retinal degeneration (e.g. photoreceptors loss). (b) A new “CC-BM-RPE” interface on top of the CNV facing the retina that seems to be functional as shown by survival of photoreceptors (with outer segments, inner segments and ONL). BM marked with dotted line.

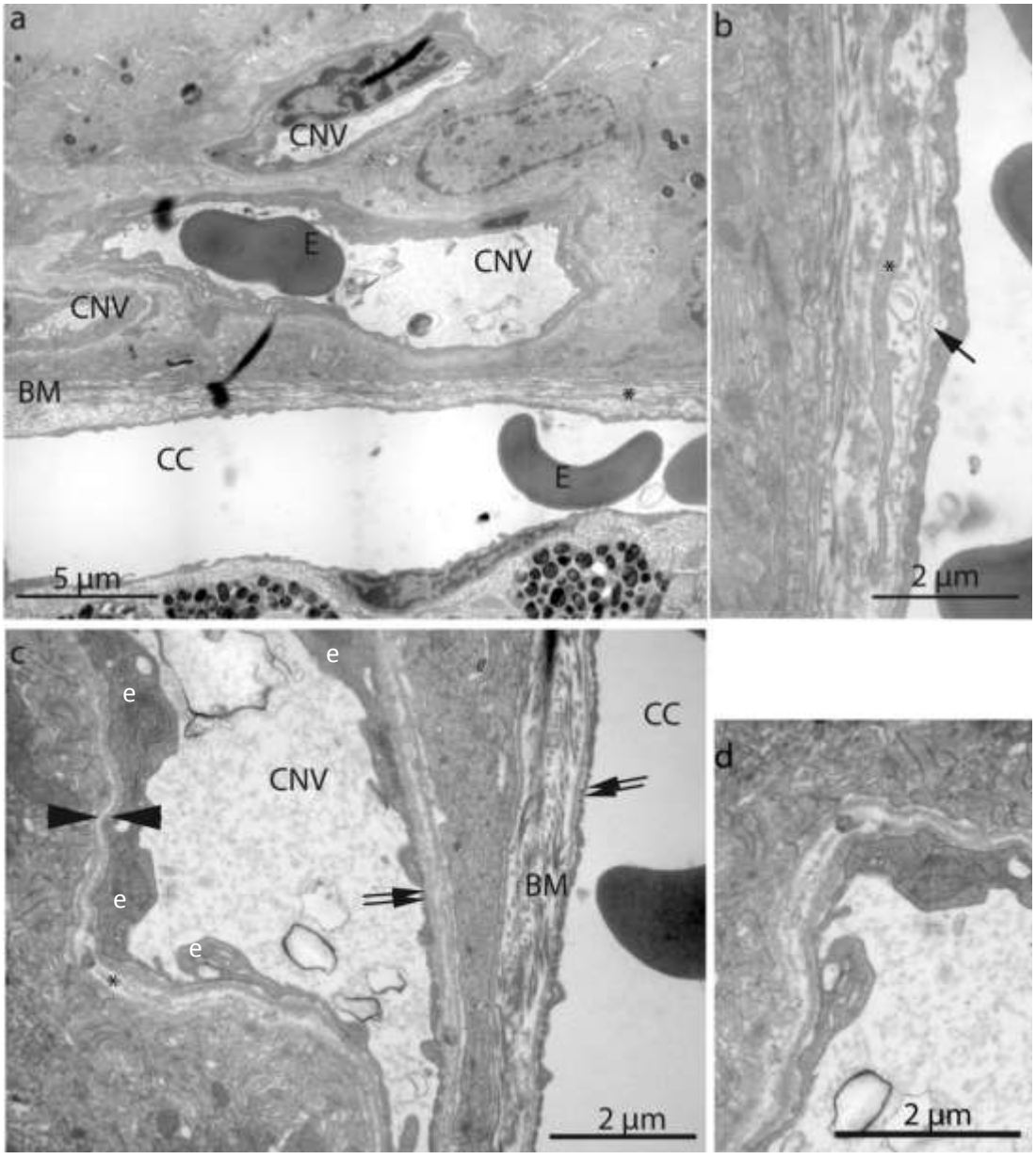

Figure 27: Ultrastructure of CNV: (a) Several newly formed blood vessels surrounded by the microvilli of melanized RPE cells can be seen. The vessels appear functional as they contain erythrocytes (E) and are surrounded by perivascular cells. A thin cell of unknown origin can be observed (*, magnified in b). (b) Magnification of the thin cell in a. It is clearly localised between the elastic layer of BM (on its left) and CC (on its right). Additionally, multi-layered basal membranes of the choroidal capillary can be observed (arrow). (c) A multi-layered basal lamina around the CNV vessel (two arrow heads, magnification of the neighbouring area (*) in d and irregular endothelial cells (e) with many vesicles can be observed. The CNV vessel with fenestrations (arrows) originates from CC. Microparticles can be observed in the vessel lumen. (d) Magnification of the area labelled with an asterisk in c. Irregular endothelium with several vacuoles, activated endoplasmic reticulum, fenestrations and a well-developed basal lamina can be observed. In this area, it looks like a new BM is forming as between the two basal laminas an elastin- and collagen-like material together with vesicular structures are accumulating.

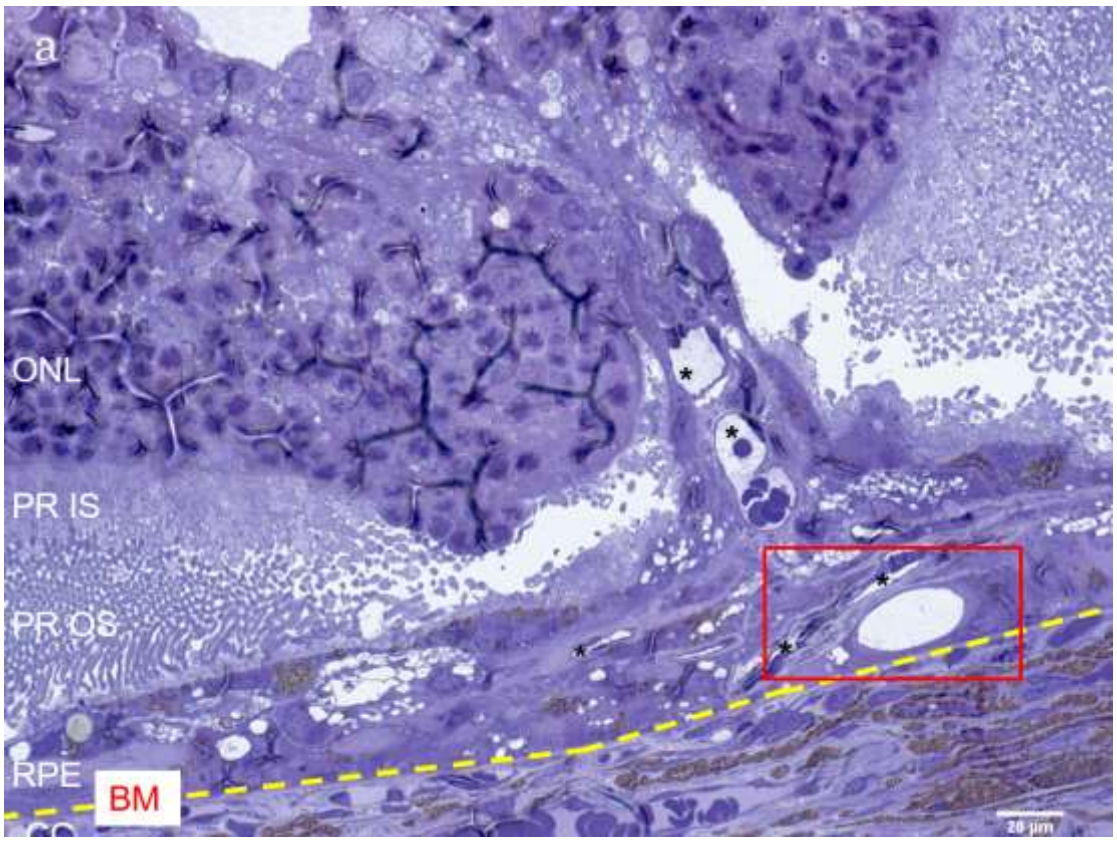

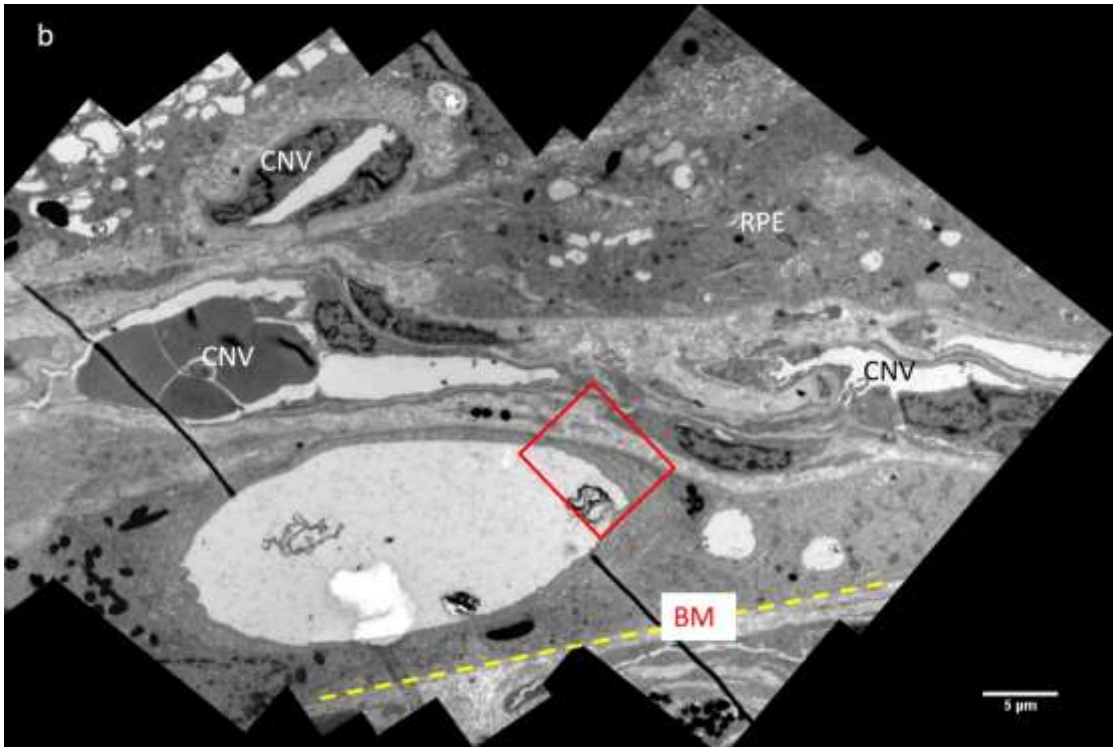

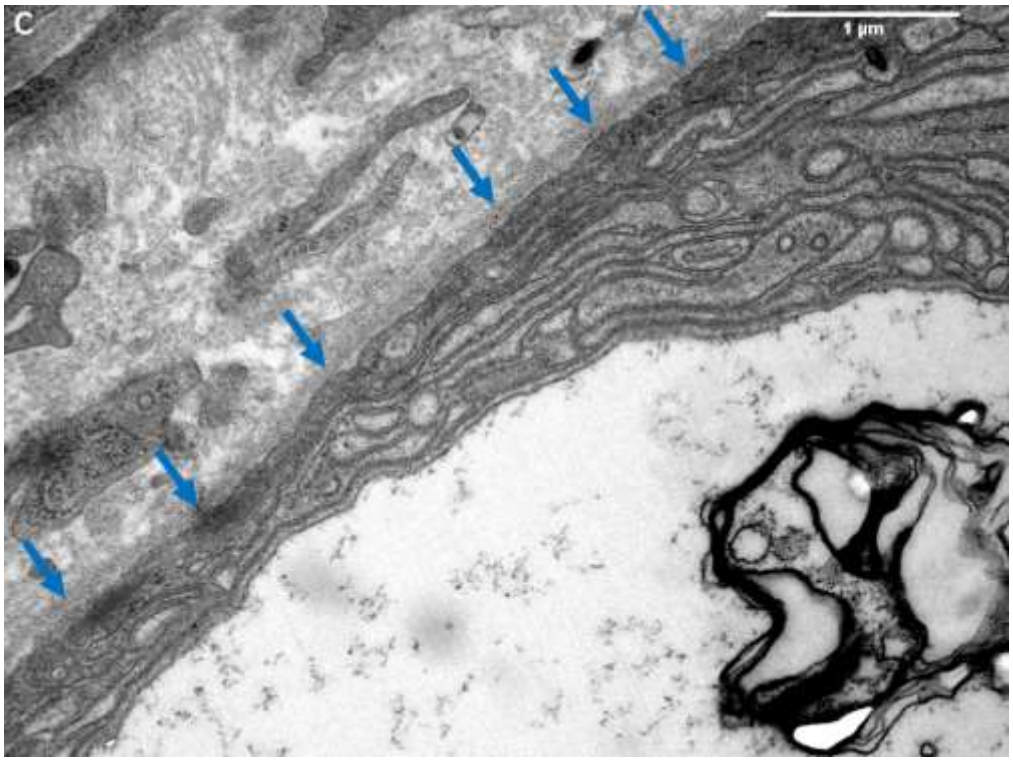

Figure 28: Large vacuolar structures in the RPE layer shown in LM (a) and EM (b and c). (a) Several CNV vessels (*) interwoven with melanized RPE cells and loss of photoreceptors can be observed. Many large vacuolar structures can be seen in the

multi-layered RPE, especially a specific large vacuolar structure is located between CNV vessels and BM (labelled with red rectangle, shown in b). BM is marked with yellow dotted line in both a and b. (b) EM of the area labelled with red rectangle in a. Above BM, many vacuoles can be observed. It likes the CNV vessels is locating between two melanized RPE cells that contain many vacuoles. The density of microparticles in the large vacuoles are higher than that in the lumen of CNV vessels. (c) Magnification of the area labelled with red rectangle in b. The large vacuole is surrounded by RPE microvilli and contains a specific substance. The high density of microparticles in the vacuole might due to edema or leakage from CNV. The space between the vacuole and CNV vessels is filled with collagen and many debris, some of which contains melanin, a feature of RPE cells. A well-developed basal lamina marked with blue arrows can be observed outside the RPE microvilli.

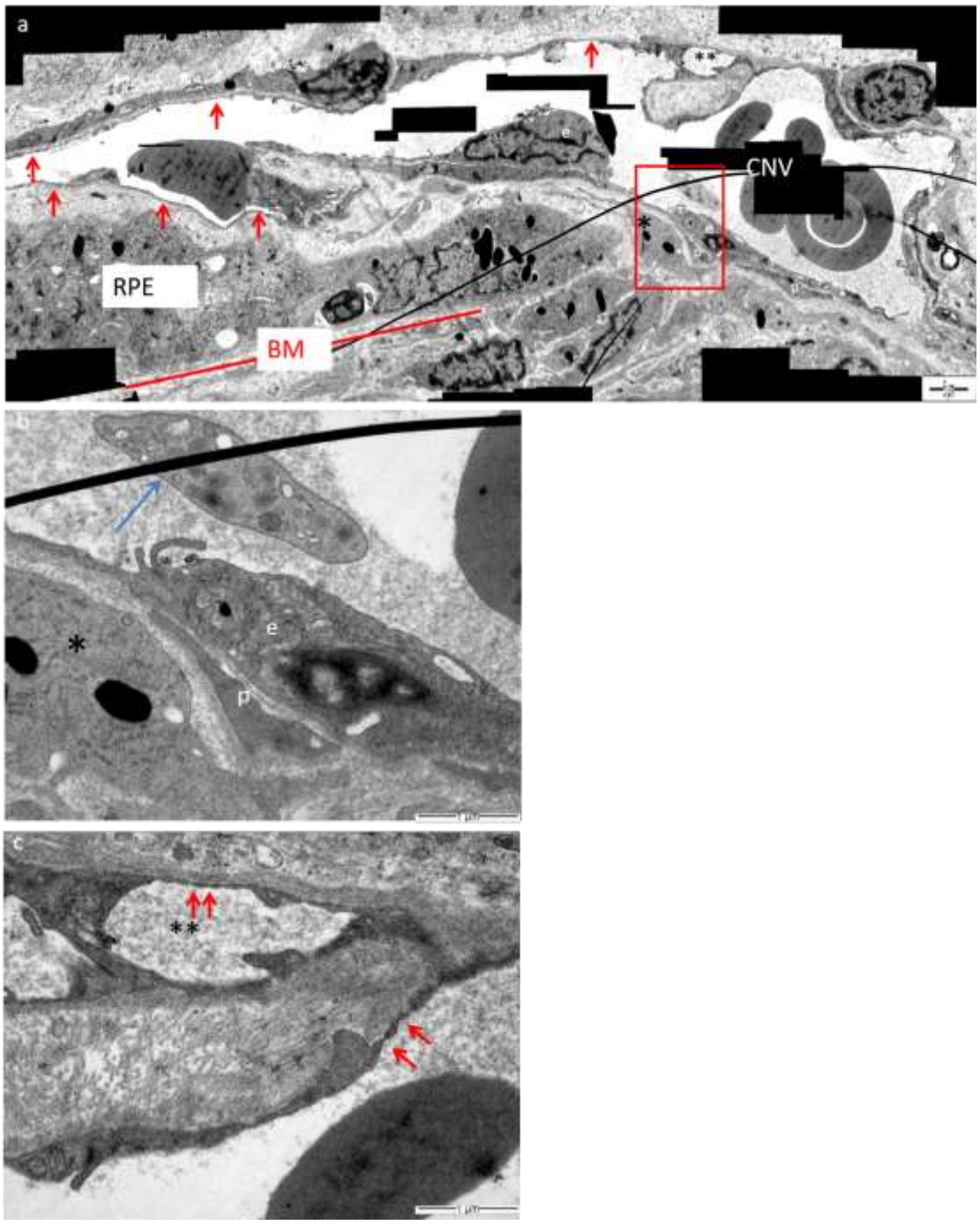

Figure 29: EM of a typical CNV. (a) The breakthrough of an individual choriocapillaris vessel through BM and into the RPE is shown in this figure. The vessel consists of endothelial cells (e) with varying thickness and is associated with pericytes (p). The spaces between the RPE cells and CNV vessels are filled with extracellular matrix, mainly collagen. A thrombocyte in the lumen of the CNV vessel and debris of unknown origin can be observed (*), the surrounding area labelled with red rectangle is magnified

in b. In addition, a small vascular lumen (**) formed by the irregular endothelium is magnified in c. BM is marked with red line and fenestration is marked with red arrows. (b) Magnification of the red rectangle area in a. The thrombocyte is marked with blue arrow, aiming to stop the leakage. An endothelial cell with several vesicles and a pericyte surrounded by basal membrane can be observed. The spaces between the endothelial cell and debris (*) were filled with extracellular matrix, mainly collagen. The debris is likely from original melanized RPE cell layer. (c) Magnification of the area labelled with two asterisks in a. The deposition of extracellular matrix (mainly collagen) towards the lumen of the vessel results in the formation of the small vascular lumen marked with **. It is enclosed by the endothelial cell walls of CNV vessels and filled with plasma. If its outer wall closes incompletely, the leakage in neovascular choroidal vessels will occur. Fenestration is marked with red arrows.

3.2.3 (Immuno)histochemistry of CNV eyes

Immunohistochemistry (IHC) experiments were focused on the transduction of VEGF, RPE proliferation, the main component of the deposit of extracellular matrix in the CNV lesions and the occurrence of leakage.

VEGF expression in CNV eyes

The CNV eyes were stained with anti-VEGF antibodies (anti-human and anti-rat antibodies) to confirm the expression of VEGF. Both of two antibodies were stained positively in CNV areas, here only anti-human antibody staining was shown to demonstrate the viral transduction with human VEGF vector. Although VEGF expression is ubiquitous in the retina and choroid, it is significantly increased in CNV areas, especially in the RPE cells within and close to the CNV lesions (Figure 30 (a)). The eyes of human AMD patients were stained as positive control and the eyes with AAV-EGFP were used for negative control.

The RPE cells were stronger stained in the human AMD samples compared with the AAV-EGFP transduced eye (Figure 30 (b) and (c)).

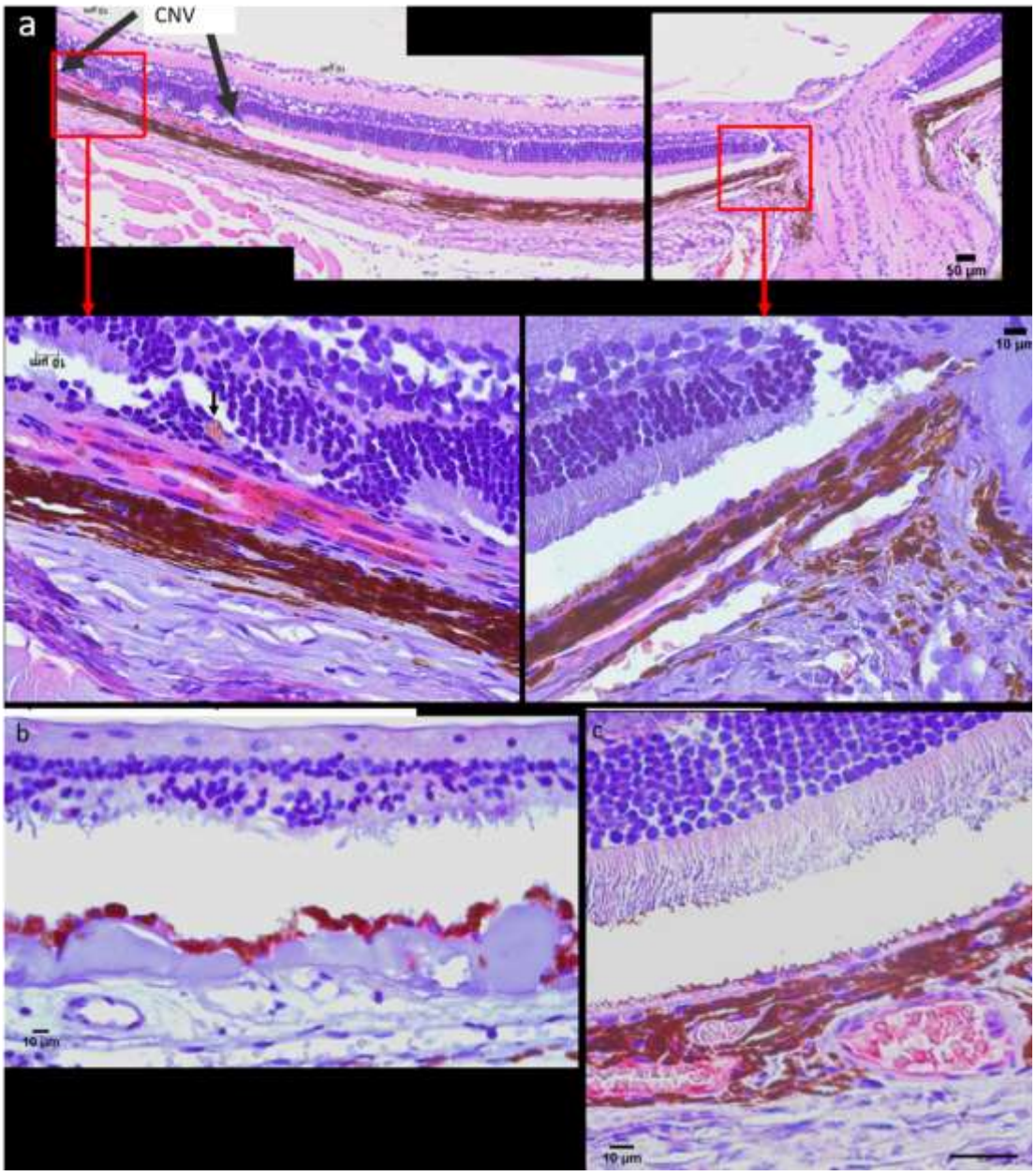

Figure 30: Exemplary image of human VEGF staining in a CNV rat eye (a), a human AMD eye (b) and an AAV-EGFP eye (c). (a): VEGF staining significantly increased in the RPE cells within and close to the CNV lesions. A single pigmented cell without VEGF positive stained (marked with black arrow in lower left image) can be

observed above CNV lesion in the subretinal space, which might be disconnected RPE cell or microphage. (b) and (c): The RPE cells were significantly stained in the human AMD eye as compared with AAV-EGFP eye.

Verification of RPE proliferation in CNV

The CNV eyes showed multi-layered RPE65 positive staining, indicating that multi-layered pigmented cells in the CNV lesion were truly RPE cells (Figure 31).

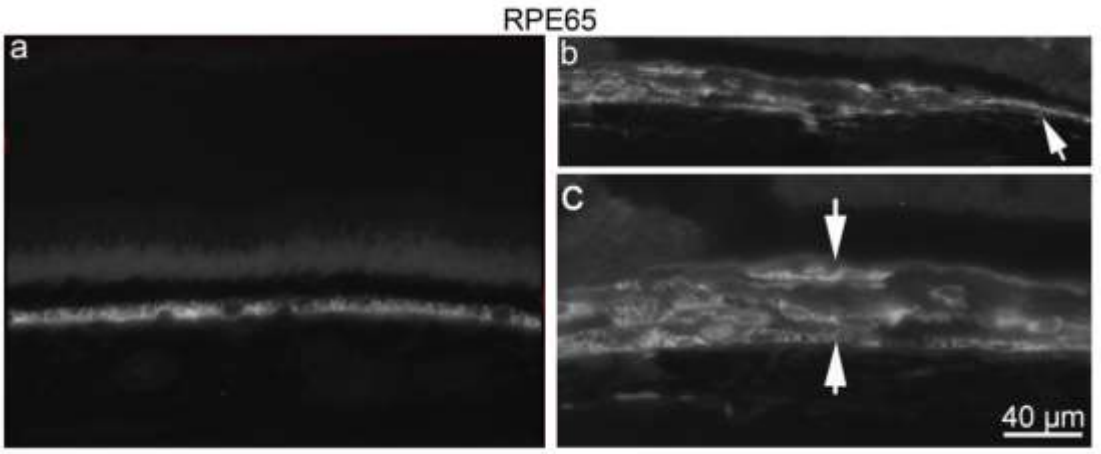

Figure 31: Identification of RPE cells in CNV eyes: (a) RPE65 staining in controls: the single layer RPE can be observed. (b) The CNV eyes show multi-layered RPE positive for RPE65. The arrow in b shows the point where the single RPE layer switches to multilayers with CNV. (c) Magnification of b: multi-layered pigmented RPE65 positive cells can be observed in the CNV area, corresponding to the pattern of RPE-like pigmented cells in light and electron micrographs.

Extracellular matrix components deposition

The components of extracellular matrix can be presented in different colors in Masson trichrome staining (collagen: blue, fibrin: deep red and elastin: light red). The accumulation of collagen was observed significantly in the CNV areas of the eyes (Figure 32). The CNV area did not show a large field of fibrin and elastin. In addition, several single pigmented cells were observed in the subretinal space

(between CNV lesion and ONL), which might be disconnected RPE cells or microphages.

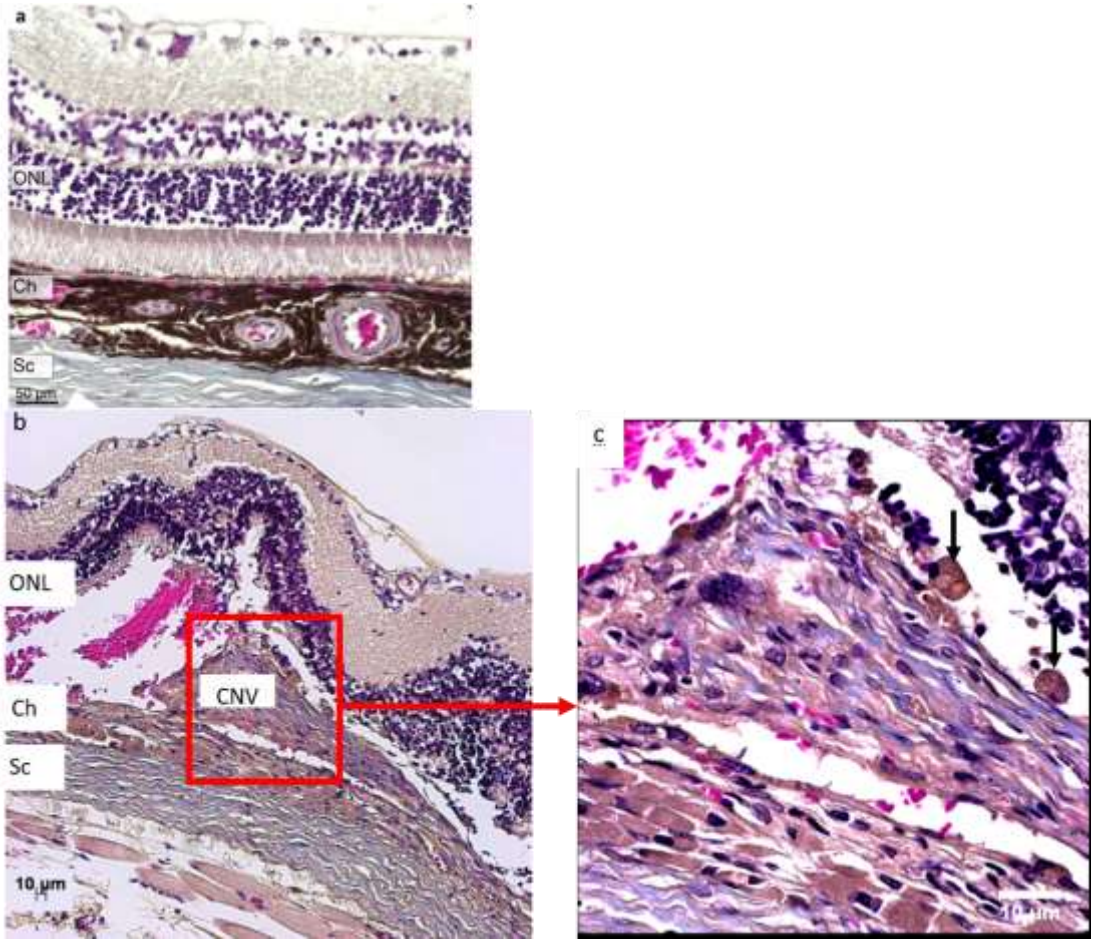

Figure 32: Masson trichrome staining of a control eye (a) and a CNV eye (b and c). (a) Control eye: Collagen (blue) can be seen in the sclera and BM. The choroidal and retinal vessels are identified, as erythrocytes in the vessels are stained in bright red. (b) The CNV vessels, accumulation of collagen, photoreceptor loss and bleeding in the subretinal space can be observed. (c) Magnification of the CNV area within the red box in b. The fibrosis in the CNV area is significant. Few pigmented cells (marked with black arrows) between the CNV area and ONL might be detached RPE cells or microphages. Ch choroid, sc sclera.

Identification of pericytes in CNV

The CNV vessels associated with perivascular cells can be observed in EM in the CNV eyes. Several antibodies were used to verify if these perivascular cells are truly pericytes, e.g. α-SMA and NG2. α-SMA positive staining was observed in all the blood vessels in the retina and choroid, especially the newly formed vessels in the CNV area (Figure 33). NG2 stained pigmented RPE cells and the endothelia of vessels in the CNV area and the choroid (Figure 33).

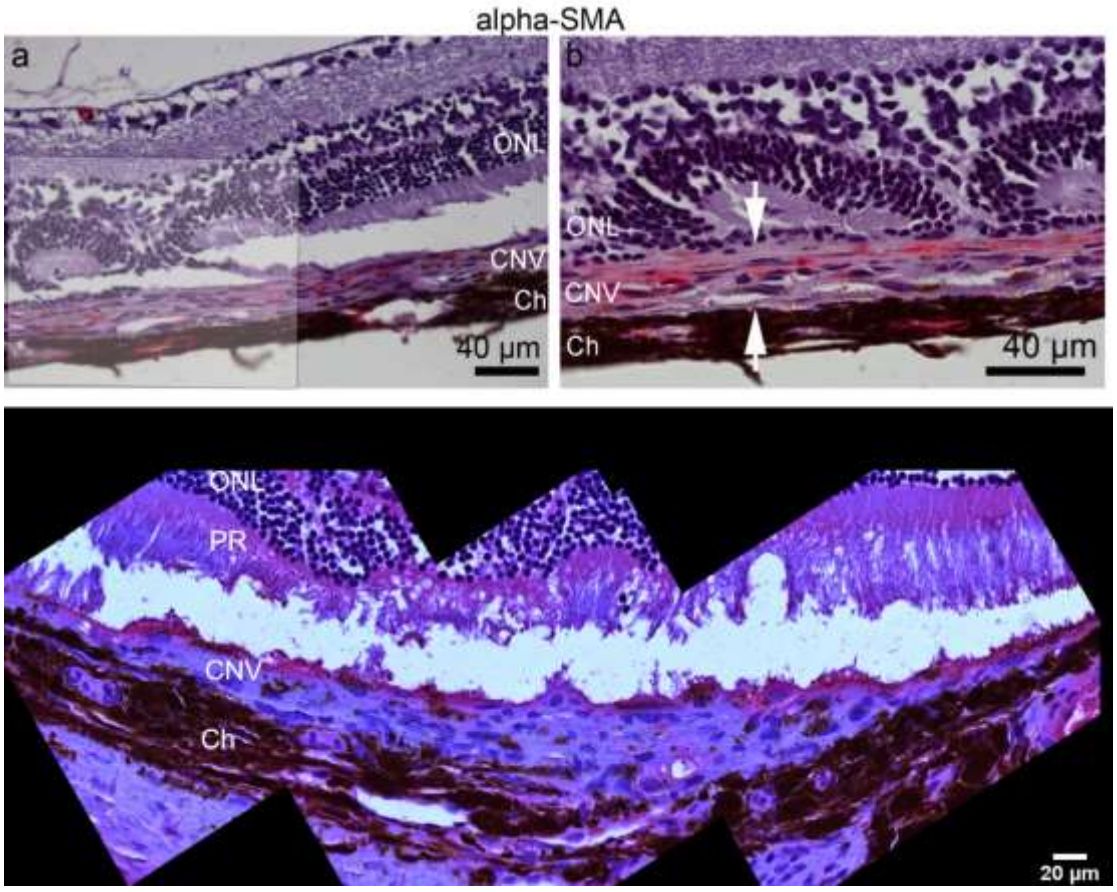

Figure 33: Exemplary images of α-SMA and NG2 staining in the CNV eye. All the blood vessels (particularly the smooth muscle cells and pericytes) in the retina, choroid and CNV are stained. NG2 also shows a positive staining in the “original” RPE layer and the endothelia of vessels in the CNV area and choroid. Ch choroid.

Identification of macrophages / activated microglia in CNV

As shown in Figure 34, Iba1 staining shows that macrophages/ activated microglia deposit in the CNV area as well as in the subretinal space. A larger amount of macrophages/ activated microglia can be observed in the choroid and neural retina as compared with the controls.

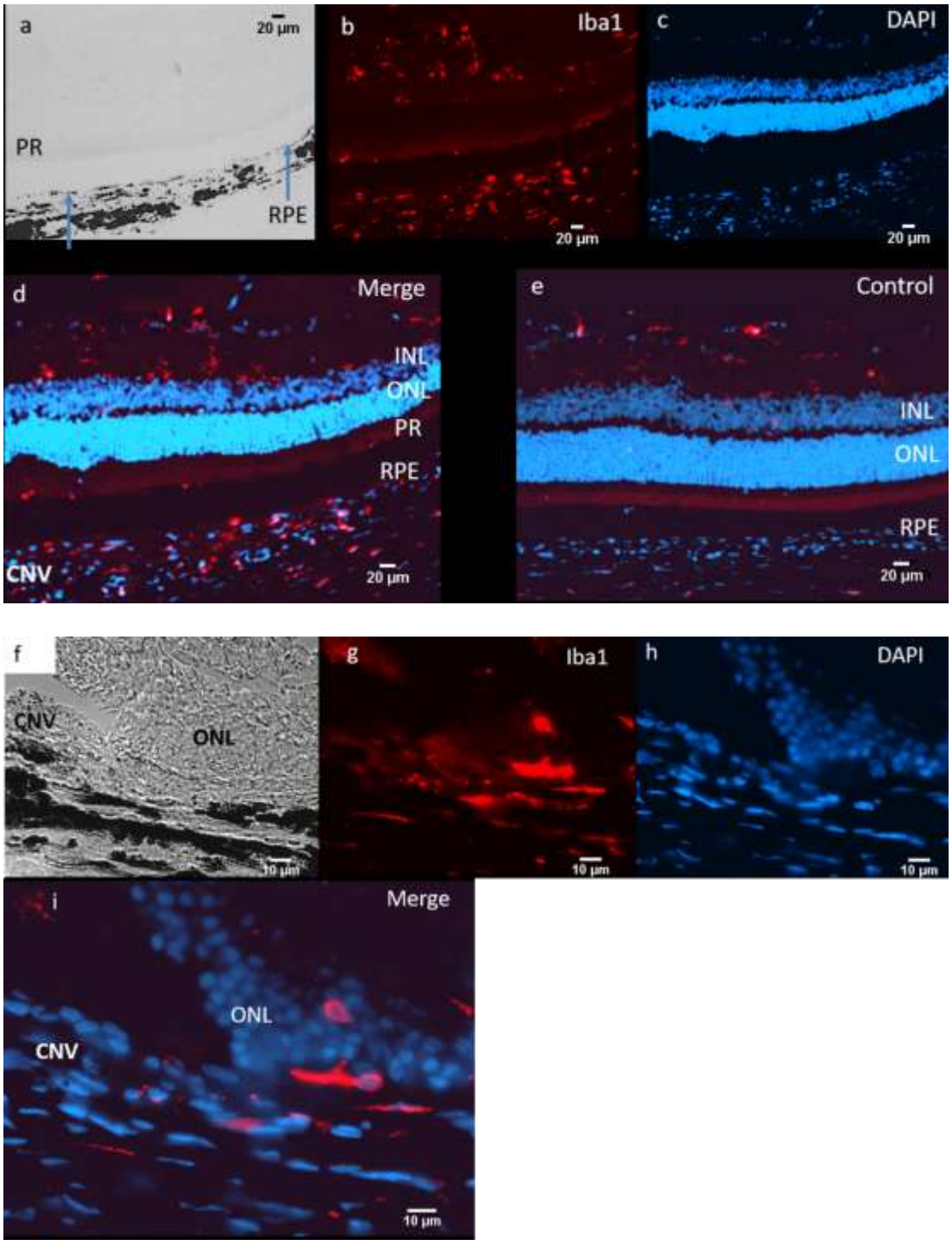

Figure 34: Exemplary images of Iba1staining (with DAPI) of the CNV eyes (a-d and f-l) and AAV-EGFP control eye (e). For the control eye, no macrophages or activated microglia in RPE layer, photoreceptors (PR) and ONL are observed. The CNV eye (a-d) shows macrophages/ activated microglia deposit in the CNV area and heavily infiltrated the retina. In addition, the deposit is also observed in the subretinal space in the other CNV eye (f-i).

Marker for vascular leakage

Albumin staining in the CNV eye showed staining of several individual cells and vessels in the CNV (Figure 35). Large vacuoles observed in multi-layered RPE did not show a distinct albumin staining.

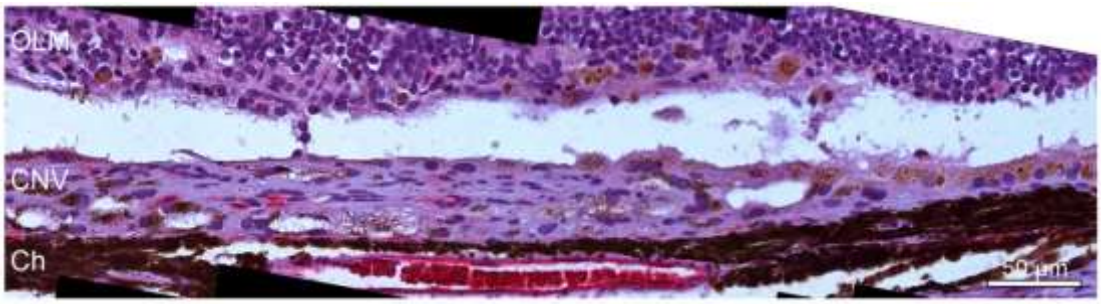

Figure 35: Exemplary image of albumin staining in the CNV eye. Individual cells and blood vessels, especially in the CNV have a positive albumin staining.

3.2.4 Detection and quantification of hyper-fluorescent CNV lesion areas in angiography data sets

The CNV areas in FA angiography increased significantly after 6 weeks compared with earlier time points (Figure 36, 2 weeks: 5.4±9.3 au, 3 weeks: 3.3±3.7 au, 4 weeks: 4.7±5.7 au, 6 weeks: 19.4±9.8 au, 7 weeks: 19.4±9.3 au, 9 weeks: 17.9±10.0 au; ANOVA, $p < 0.05$). However, there is no significant growth or regression of CNV areas among 6 weeks and 9 weeks after the VEGF vector injection. A fully grown CNV can be obtained after 6 weeks' duration of VEGF overexpression.

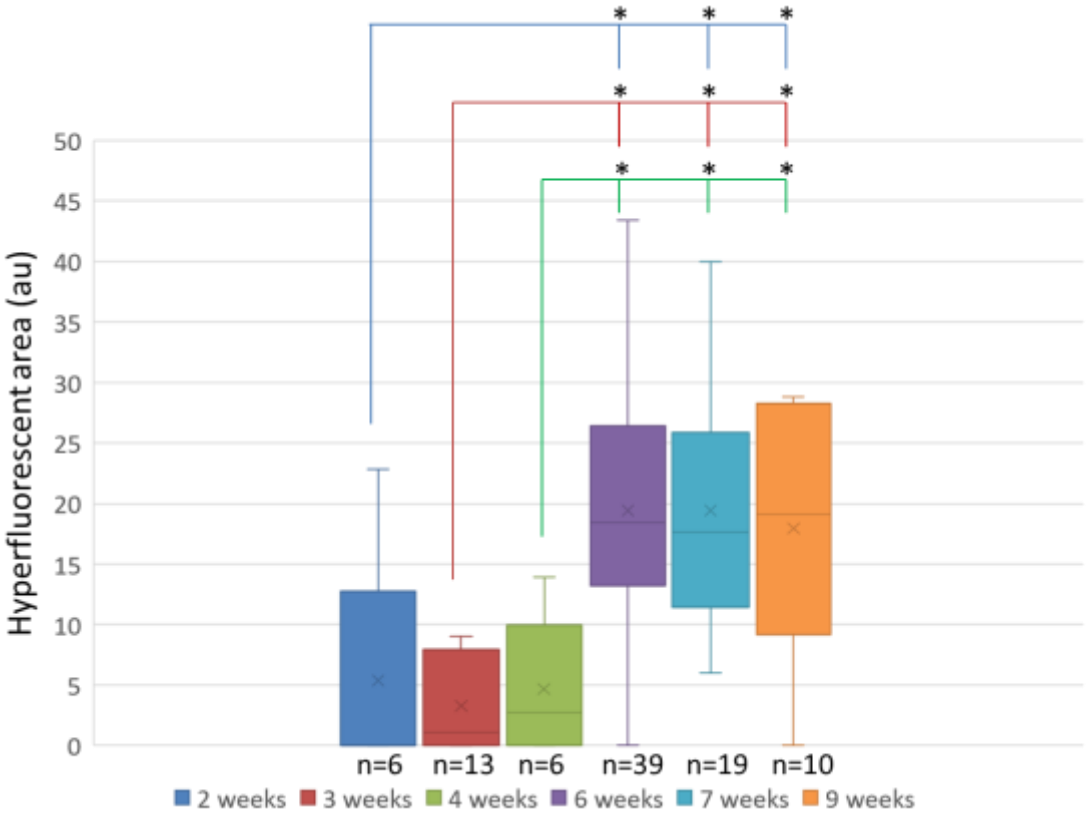

Figure 36: Comparison of the hyper-fluorescent areas in late phase FA among 2-9 weeks after VEGF overexpression. The hyper-fluorescent areas increase significantly after 6 weeks compared with earlier time points (ANOVA, * $p < 0.05$). Hyper-fluorescent areas in FA reach a stable size after 6 weeks. Mean values ± standard deviations are shown. au= arbitrary units.

3.2.5 Quantitative analyses of the maximal thickness of the CNV lesion and the retina in OCT data sets

The maximum retinal thickness of each eye and the retinal thickness in the adjoining area without lesion in the same OCT image were quantified. The retinal thickness at the CNV lesion site increased significantly with time (Figure 37, normal: 218.6±11.4µm, 6 weeks: 289.6±26.0µm, 7 weeks: 305.9±24.0µm, 9 weeks: 315.5±11.0µm; ANOVA: $p < 0.05$). Especially, the CNV lesion was

thickening with time and showed a significant difference if compared between 6 and 9 weeks after VEGF transduction (Figure 38, 6 weeks: 99.8±19.8µm, 7 weeks: 109.9±19.6µm, 9 weeks: 120.2±21.9µm; ANOVA: $p < 0.05$).

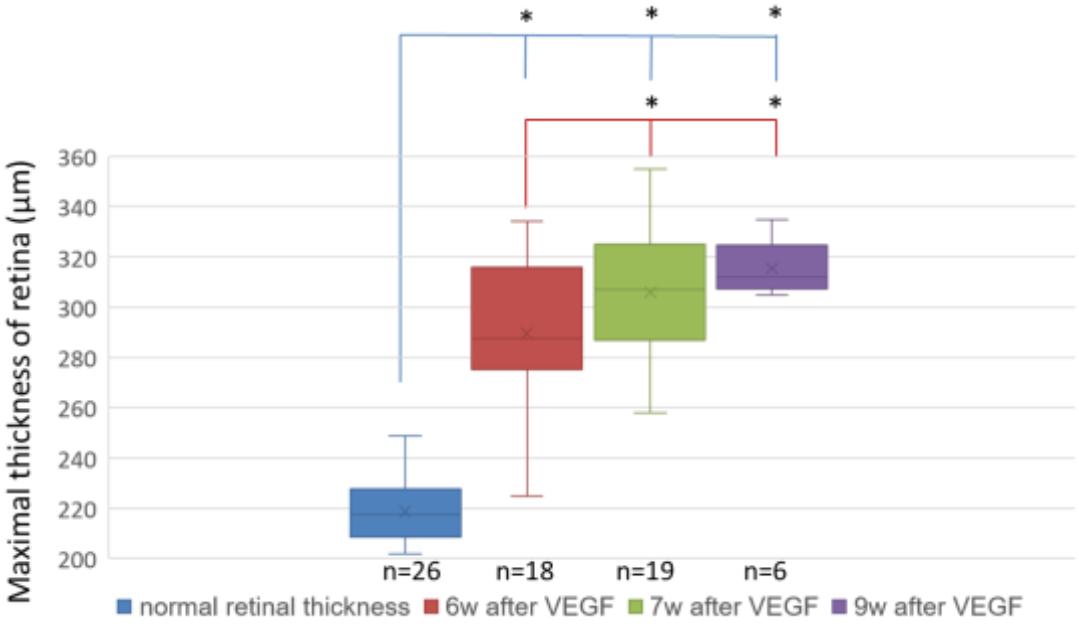

Figure 37: Quantification of the maximal retinal thickness in CNV rat eyes. The maximum retinal thickness of each eye and the retinal thickness in the adjoining area without lesion in the same OCT image were used for the box figure. All groups were of significantly differences to each other (ANOVA, * $p < 0.05$).

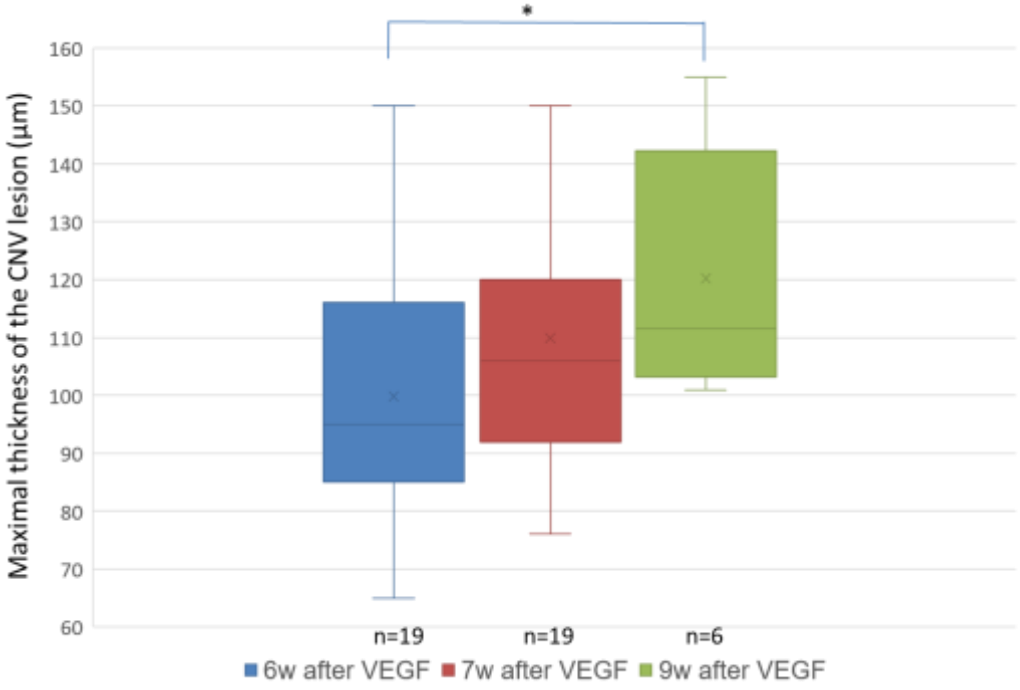

Figure 38: Quantification of the maximal CNV lesion thickness in CNV rat eyes. The thickness of CNV lesion increased significantly between 6 and 9 weeks after VEGF transduction (ANOVA, * $p<0.05$).

3.2.6 Quantification of choriocapillaris loss and RPE loss with CNV

Loss of CC and RPE in CNV eyes compared with controls were quantified in this study. As shown in Figure 39 and 45, the area of CC in per length of BM significant decreases in the CNV eyes compared with controls (t-test, $P<0.05$) and 87.38% BM was covered by RPE cells in the CNV areas.

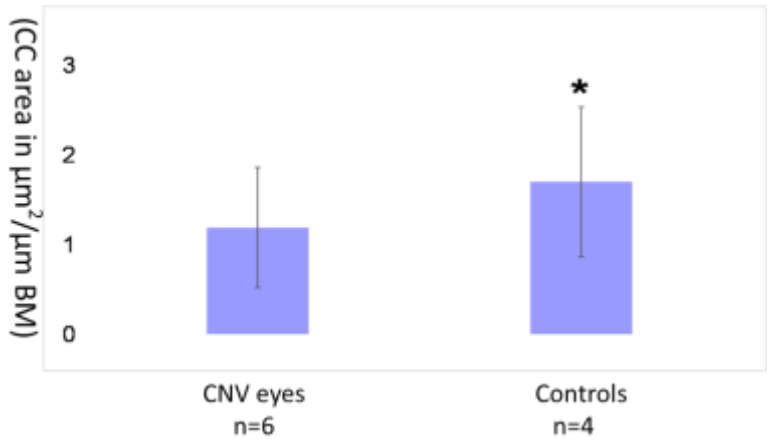

Figure 39: The comparison of choriocapillaris loss between CNV eyes (n=6) and controls (n=4). The area of CC in per length of BM decreases significantly in the CNV eyes compared with controls (t-test, P<0.05).

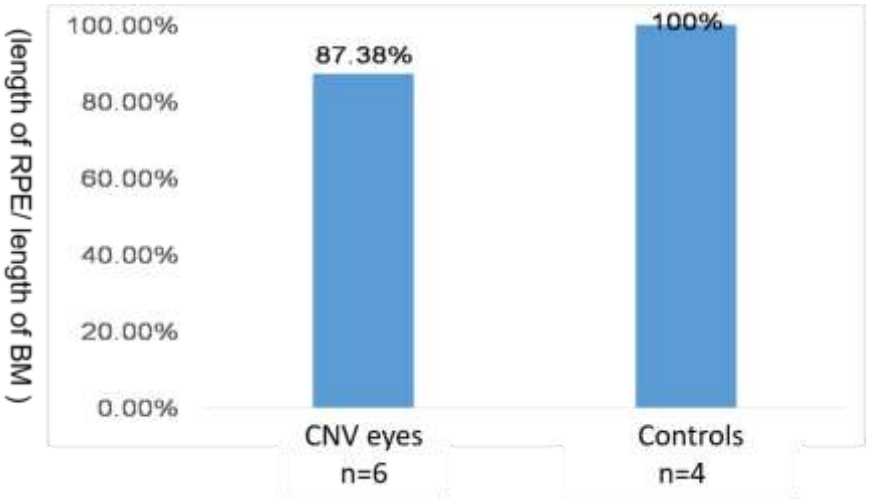

Figure 40: The comparison of RPE loss between CNV eyes (n=6) and controls (n=4). No RPE loss is shown in control eyes, in contrast, the average length of RPE per length of BM in CNV eyes is 87.38%.

3.3 Treatment of the VEGF driven CNV with Avastin®

The proposal of Avastin® treatment test is shown in Figure 4. FA/ICG did not show statistically significant differences of hyper-fluorescence area in the CNV eyes over time either after Avastin® treatment or without treatment. Avastin® did not show clear effect at 6 weeks after Avastin® treatment. The retinal and the CNV lesion thicknesses of the Avastin® treated eyes were measured at 1 and 3 weeks after Avastin® treatment (Figure 41). Additionally, the human VEGF staining areas were also quantified (Figure 42).

3.3.1 Quantitative analyses of the maximal thickness of the CNV lesion and the retina in OCT data sets in Avastin® treated eyes

In the Avastin® treated CNV eyes, a decrease in the changes of the maximal retinal thickness (-7.6±20.8μm) and the maximal CNV lesion thickness (-7.9±16.6μm) in the Avastin® treated CNV eyes was detected one week after Avastin® treatment. In contrast, an increase in the changes of the maximal retinal thickness (14.2±17.2μm) and the maximal CNV lesion thickness (10.1±7.0μm) in the untreated CNV eyes was detected at the same time point. The thickness of the retina and the CNV lesion decreased significantly one week after Avastin® treatment compared with untreated CNV eyes (Figure 41, t-test, $P<0.05$). The decrease was no longer significant at 3 weeks after treatment, but Avastin® still has a tendency to reduce the growth of CNV.

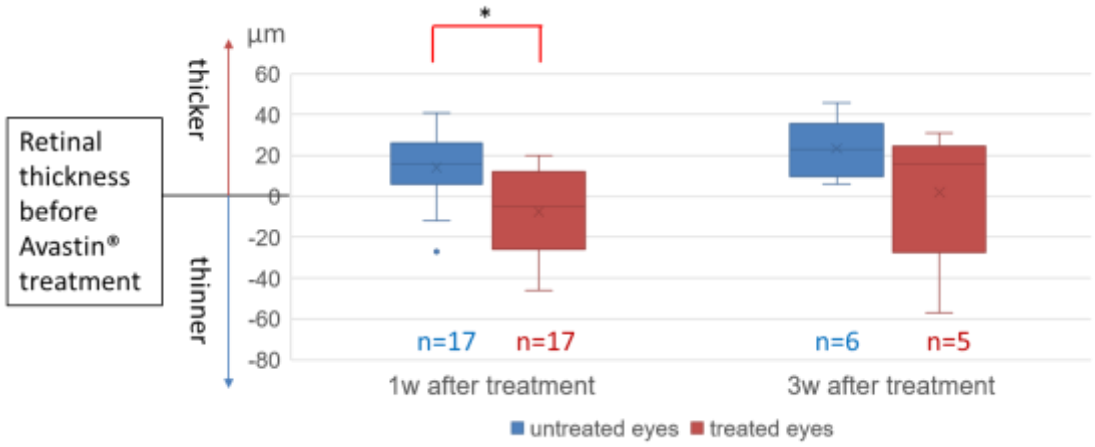

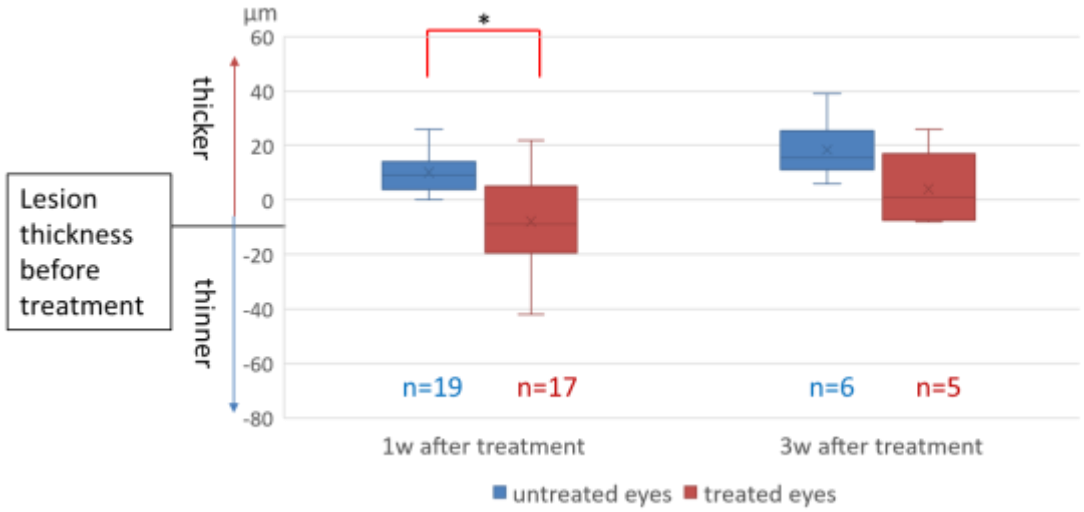

Figure 41: Changes of the maximal retinal and CNV lesion thickness between pre-treatment and 1 week/3 weeks after Avastin® treatment. Avastin® can reduce the retinal and CNV lesion thickness significantly one week after treatment (t-test, $P<0.05$), and it still tends to reduce the thicknesses 3 weeks after treatment.

3.3.2 Quantification of VEGF expression by IHC

As CNV in this rat model was induced by overexpressing VEGF, the comparison of VEGF overexpression between Avastin® treated eyes and untreated eyes were performed to further evaluate the treatment effect. The quantification of human VEGF expression was measured following the method shown in Figure 14. Figure 42 shows that the expression of VEGF in the treated group has a slight but not significant reduction up to 3 weeks after the treatment (mean value of the percentage of VEGF positive staining area in the total CNV area: untreated group: 24%; treated group: 19%).

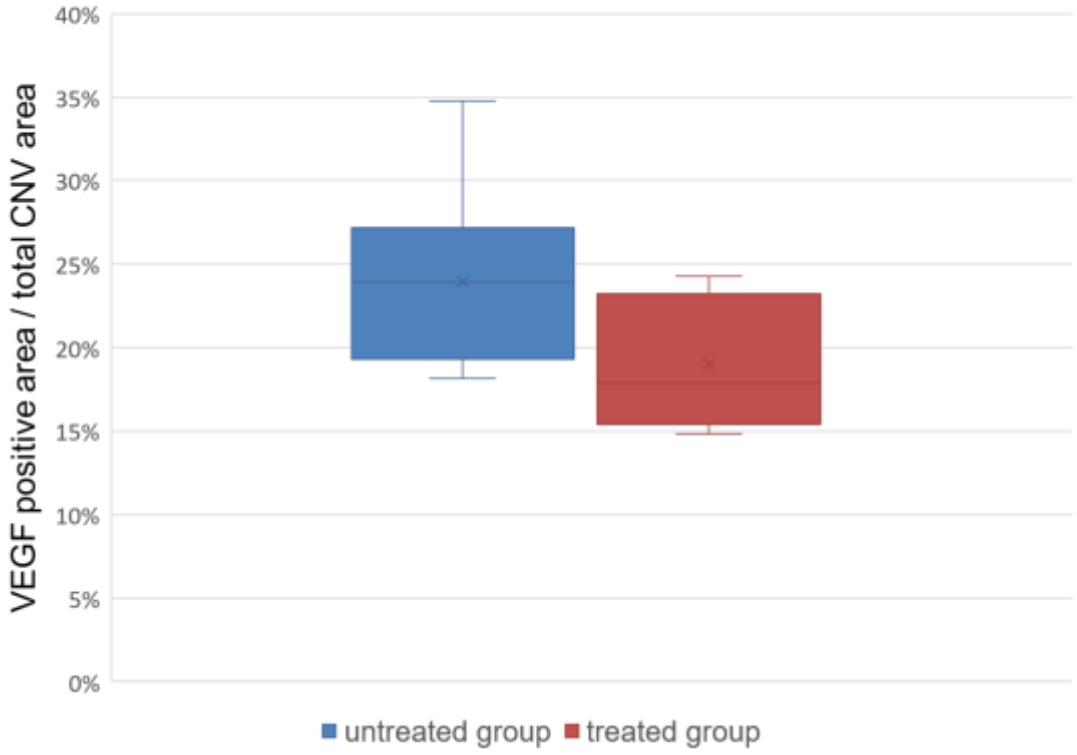

Figure 42: Quantification of VEGF expression in Avastin® treated eyes (n=5) and untreated eyes (n=9). The treated eyes did not show a significant decrease of VEGF expression up to 3 weeks after the treatment.

3.4 Changes in the choroid-RPE interface after subretinal VEGF protein injection within the first 24 h

The aim of this side project was to investigate the early effects of VEGF in the choroid-RPE interface in the rat. Human VEGF protein was injected subretinally or intravitreally into the rat eye. 1 h and 24 h after injections, in vivo imaging and LM/EM analyses were performed.

No direct effects of the VEGF protein injection were observed, except for a diffuse hyper-fluorescence in FA in few eyes, as shown in Figure 43. The subretinal bleb was observed in OCT in the eyes injected subretinally (Figure 43).

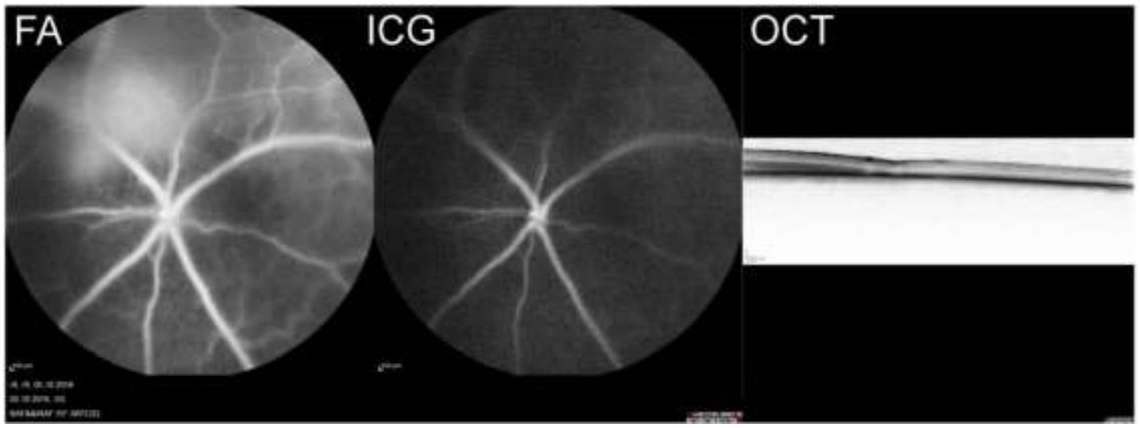

Figure 43: Exemplary angiography and OCT images, 1 h after subretinal injection of 2 µl VEGF suspension. Only FA shows hyper-fluorescence, and no trauma observes in the eye. OCT on the right shows a subretinal bleb contains the residual of VEGF suspension.

Changes in the choroid-RPE interface were observed as early as 1h after VEGF protein subretinal injection in the electron micrographs (Figure 44). Activation of RPE with elongated cellular processes like labyrinth end feet and microvilli was observed. Endothelial cells also showed elongated cellular processes, of which pointed into the vessel lumen (see Figure 44 (d)) or sprouted into BM. Especially, the endothelial cell walls were becoming leaky as judged by the increase of transcytosis vesicles and the appearance of open cell connections. In addition, thickening BM with incomplete absent elastic layer was regularly observed. Similar effects can be seen in the eyes with VEGF intravitreal injection but less pronounced. All the eyes did not show any significant changes of retinal blood vessels after VEGF protein injection.

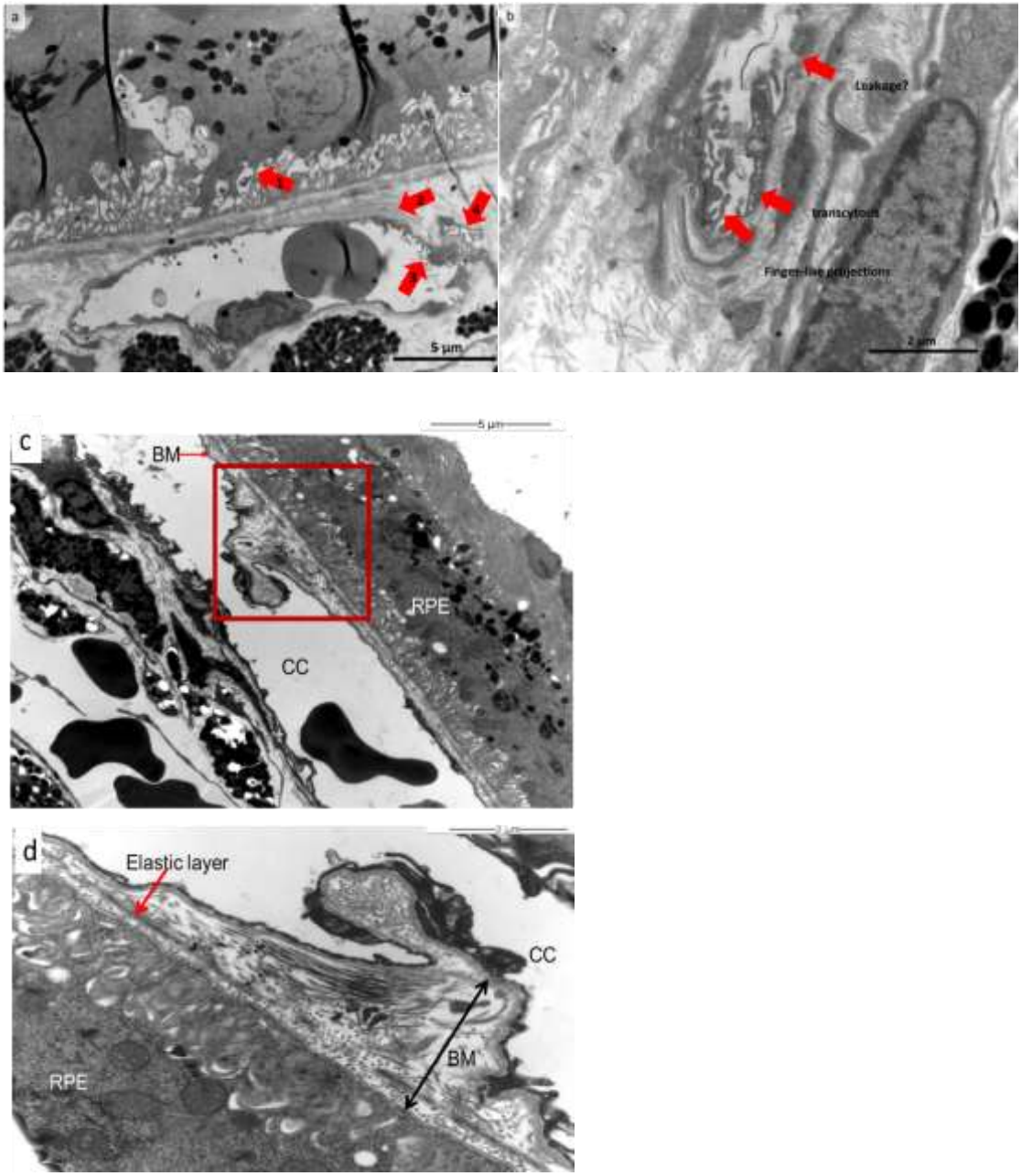

Figure 44: Ultrastructural changes 1h after VEGF protein injection: (a) Changes observed in the choroid-RPE interface: activation of RPE (arrow 1), collagen formation around CC vessels (arrow 2), finger-like processes in the vessel lumen (arrow 3, also shown in (b)) and endothelial cell sprouts into BM (arrow 4). (b) Open endothelial cell connections (a feature of leakage) and transcytosis vesicles can be observed. (c) Extracellular matrix deposit from BM towards the CC vessel. (d) Magnification of the red box area in (c). Deposit of extracellular matrix, mainly collagen leads to the elongated

cellular processes of endothelial cells towards the lumen of the CC vessel. The thickness of BM is 2.6µm (normal eye BM: 0.5–1.5 µm thick (Leeson and Leeson, 1967)). The thickening BM with incomplete absent elastic layer can be observed regularly.

3.5 Findings in human CNV

The human CNV samples were observed by LM and EM. The original RPE cell layer was separated from the choroid by the CNV vessels and the increased extracellular matrix, as shown in Figure 45. Figure 46 shows the CNV vessels with varying thicknesses of endothelial cells in human CNV samples. The endothelia often contained a large number of vesicles, which were an indication of leakage (Hofman et al., 2000). Accumulation of collagen and fibrin were observed frequently in the human CNV samples. The labyrinth capillaries were also observed frequently in human CNV, which was responsible for leakage in human wet AMD patients (Schraermeyer et al., 2015). These capillaries originated from CC, as they had many fenestrations. In addition, degenerating CNV vessels with incomplete lumen, loss of endothelial cells and irregular thrombocytes were often seen in human CNV.

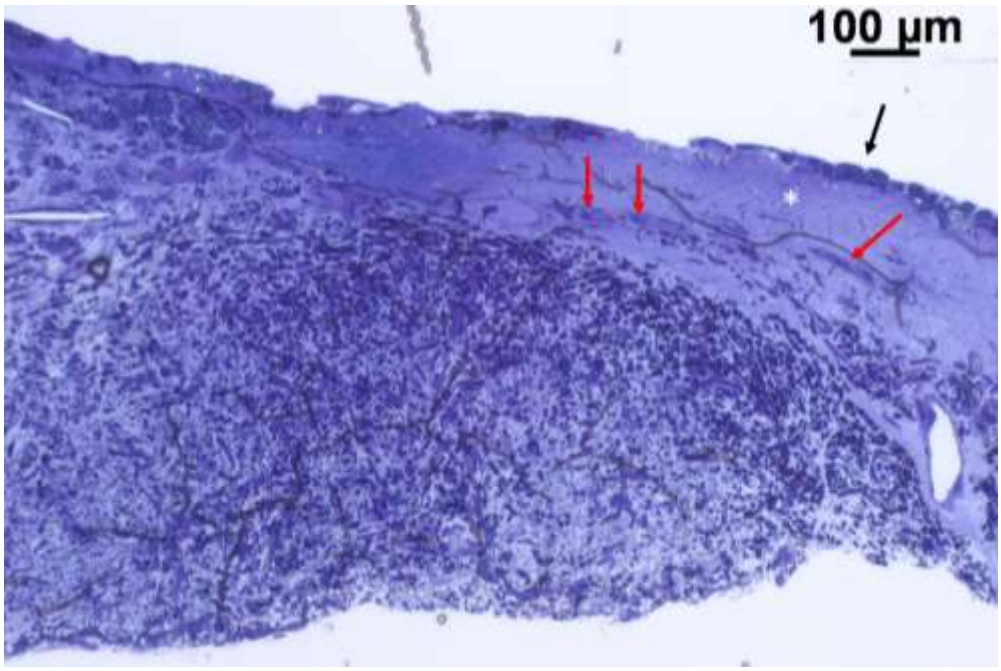

Figure 45: Light micrograph of a human CNV sample. The original RPE layer is labelled with a black arrow. The space (asterisk) between the RPE layer and the choroid is filled with increased extracellular matrix, and it is more than 100µm thick. The CNV vessels are marked with the red arrows.

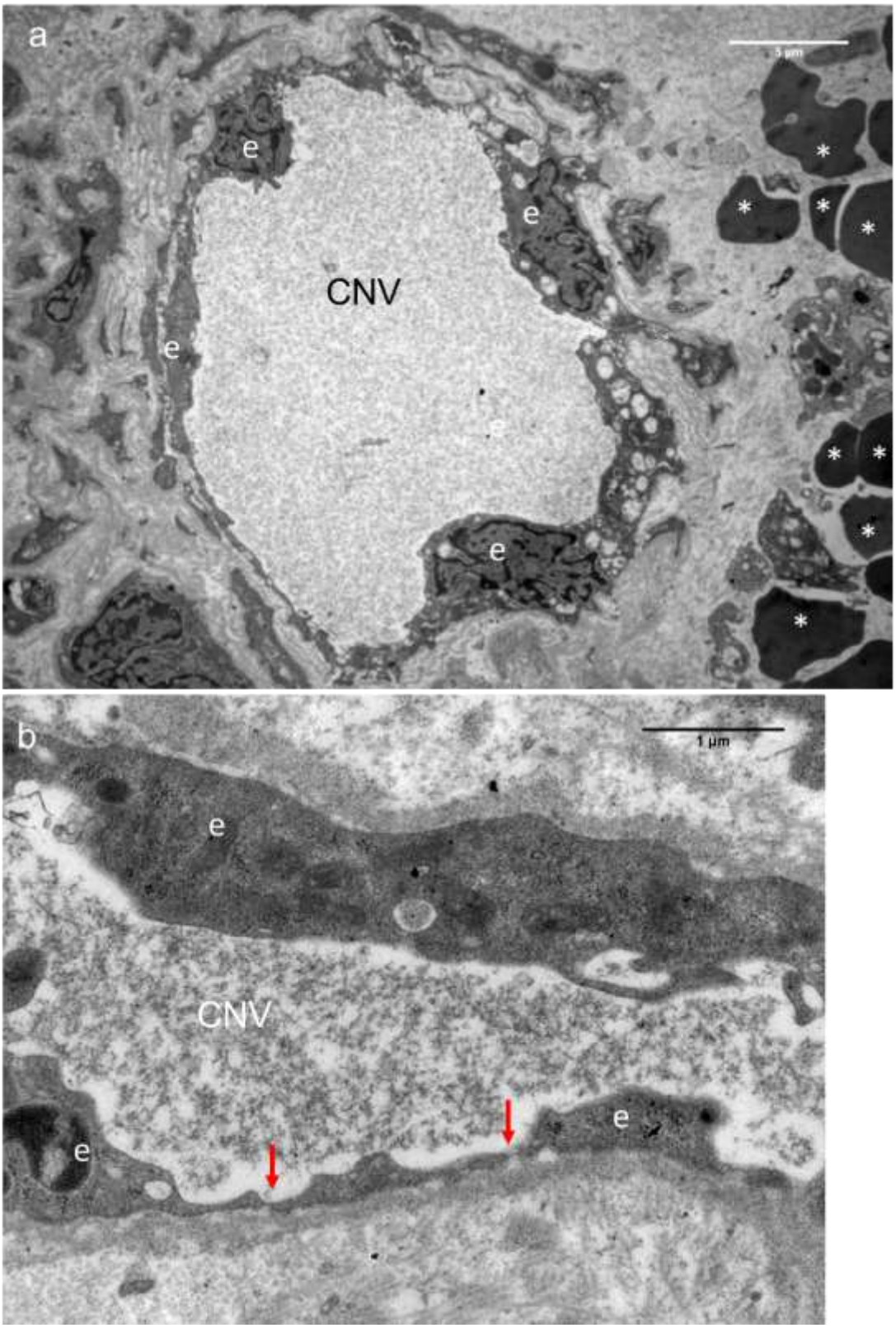
a
5 µm
e
e
e
CNV
e
e
b
1 µm
e
CNV
e
e

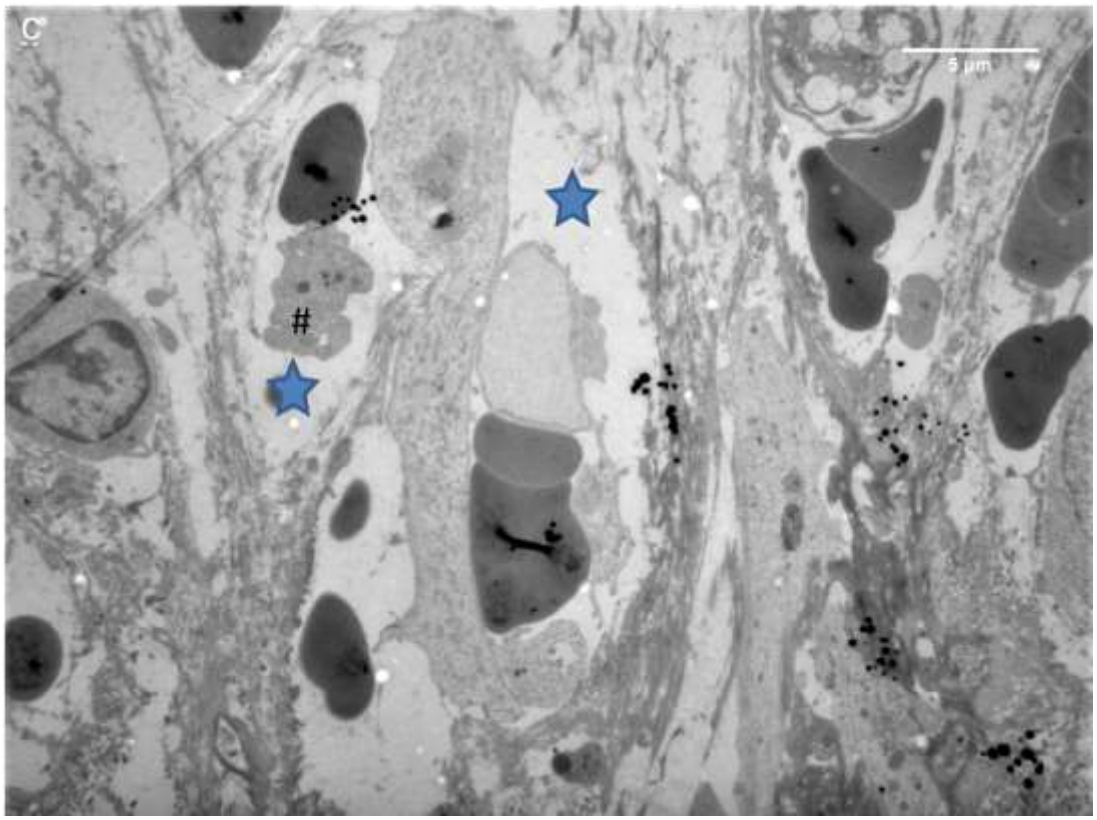
c
5 µm
#

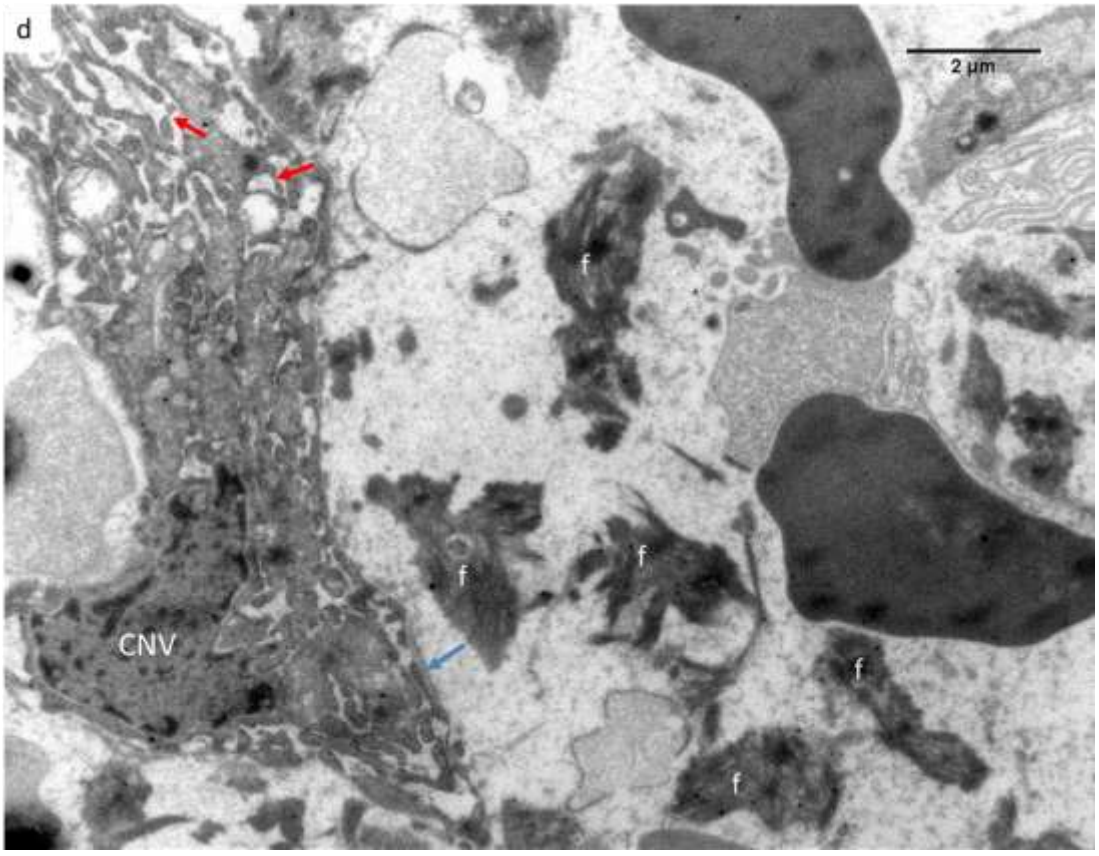
d
2 µm
f
f
f
f
CNV
f
f

Figure 46: Ultrastructure of human CNV: (a) A CNV vessel with varying thicknesses of endothelial cells and pericytes is surrounded by extravascular erythrocytes (*). Many vesicles can be observed in the endothelia. (b) Magnification of a CNV vessel. The vessel has fenestrations (black arrows) and contains microparticles. The accumulation of collagen can be seen around the vessel. (c) Degenerating CNV vessels (marked with blue stars) with incomplete lumen, loss of endothelial cells, loss of pericytes and irregular thrombocyte (#) can be seen. (d) A labyrinth capillary with fenestrations (red arrows) and basal lamina (blue arrow) can be observed. Accumulation of fibrin (marked with f) can also be seen around the CNV vessel.

4 Discussion

4.1 The AAV vector system

In the last decade, different viral vector systems were used for ocular overexpression of proteins in a lot of studies (Campochiaro, 2011). Campochiaro and Zhang et al. mentioned that the adenovirus vector system was active with a high immunogenicity for only about 1 month, leading to retinal toxicity (Campochiaro, 2011, Zhang et al., 2012). All the eyes transduced with HC Ad. vectors showed retinal damage after histological evaluation in this study, indicating the high retinal toxicity of the Ad. vector. As discussed in (Lambert et al., 2016), lentiviral and AAV viral constructs are safer and more effective. Even for human patients, subretinal AAV2 vectors have proven to be safe and effective to treat a several disorders for up to 3.5 years, e.g. (Roy et al., 2010, Zhang et al., 2012), and their treatments for AMD are also under investigation (Moore et al., 2017). Therefore, this vector system was used to develop a CNV rat model in this study, as it has already proved effective for ocular gene therapy.

In this study, the AAV control eyes did not show any signs of toxicity at any time point after subretinal and intravitreal vector injections (including AAV empty vector and AAV-EGFP vector), and the eyes subretinal injected with 2 µl EGFP vector showed protein expression in a time frame of 2 weeks till at least 9 weeks. CNV induced by AAV-VEGF vector subretinal injection was still valid at 9 weeks after vector injection, allowing long-term studies of the new treatments in the CNV rat model. The protein expression can even valid for several months to years, according to Rolling (Rolling et al., 2006). The AAV vector construct itself cannot induce CNV in the eyes, as no AAV-empty transduced eyes showed CNV.

As the intravitreal injection is less invasive compared with subretinal injection, AAV-EGFP vector was intravitreal injected into three eyes to investigate whether this surgery can lead to proper transduction of the vector. However, the two eyes intravitreal injected with 2 µl vector did not show obvious GFP autofluorescence, only the eye injected with a higher volume of 5 µl expressed GFP up to 6 weeks. The transduction efficacy of intravitreal injection is less than that in the subretinal route.

In the study of (Wang et al., 2003), 95% of the AAV-VEGF transduced eyes (23 CNV eyes/ 25 total eyes) showed CNV and no spontaneous regression of the CNV was observed within 20 months after the vector injection. This indicated that the CNV induced by the AAV-VEGF vector could exist for a long-term. Similar in this study, 91% of VEGF transduced eyes presented with a fully grown CNV observable by angiography after 6 weeks' duration of VEGF overexpression. No CNV eye showed spontaneous regression within 9 weeks after AAV-VEGF vector injection. The eyes transduced with HC Ad. VEGF vector, used in the early experiments of this project, showed CNV-like lesions in 81.25% % of injected rat eyes 4 weeks post injection. Therefore, the eyes transduced with AAV VEGF vector show better transduction efficacies compared

with those achieved by the Ad. VEGF vector, that is only to be used for 4 weeks after the vector injection.

4.2 Correlation of the AAV-VEGF transduced CNV rat model to the HC Ad. VEGF transduced CNV rat model

The characteristics of the HC Ad. VEGF transduced CNV rat model and the AAV-VEGF transduced CNV rat model were summarized in Table 8.

Table 8: Comparison of the two different CNV rat models. The changes observed in the eyes are labelled with "√", and "-" refers to the changes not found yet.

	CNV rat eyes transduced with AAV-VEGF vector	CNV rat eyes transduced with HC Ad. VEGF vector
Angiography and OCT (percentage of eyes with CNV)	4 weeks: 50%; 6 weeks: 91% (100% in the 38 eyes used for the test of Avastin®)	4 weeks: 81%
Microscopic changes		
multi-layered RPE	√	√
complete RPE loss		√
retinal degeneration		
- rosette-like retinal changes	√	√
- complete photoreceptors loss		√
Scar tissue between choroid and retina	√	√
Newly formed blood vessels (CNV) in RPE or BM	√	√

Ultrastructural changes		
irregular choriocapillaris	√	√
irregular CNV vessels		
- irregular endothelia	√	√
- multi-layered basal lamina	√	√
- fenestration in CNV	√	√
- finger-like filopodia into the lumen, building new lumen	√	√
- labyrinth capillaries	-	-
IHC		
- human VEGF staining	√	√
- albumin staining	√	√

Table 8 demonstrates that 81% of the eyes transduced with the HC Ad. VEGF vector show CNV in angiography. A better transduction efficacy (91%) was achieved in the AAV-VEGF vector-transduced rat model after 6 weeks' duration of VEGF overexpression. Especially, 100% of the eyes with AAV-VEGF transduction showed CNV in the latest experiment for the investigation of Avastin® treatment.

In the histological analyses, eyes with the HC Ad. VEGF vector transduction showed a more heterogeneous phenotype compared with the eyes with AAV-VEGF transduction. As shown in Table 8, the complete loss of RPE cells and photoreceptors only occurred in the eyes transduced with HC Ad. VEGF vector, due to the high retinal toxicity of the Ad. vector system. The labyrinth capillaries, an indication for leakage in human wet AMD patients (Schraermeyer et al., 2015), were not found in both rat models. CNV vessels with fenestrations were frequently observed in the rat CNV models, and the CNV vessels without fenestrations only occurred in the area away from BM. In addition, the

rosette-like retinal changes appeared more frequently in the eyes transduced with HC Ad. VEGF vector. Thickening of BM and irregular choriocapillaris were observed in both models. VEGF staining and albumin staining showed the VEGF expression and leakage of serum in the retinal tissue, respectively.

The CNV induced by the HC Ad. VEGF vector seems to be similar to the CNV induced by the AAV-VEGF vector, however, significant differences exist as well. Severe retinal degeneration like complete loss of RPE cells and photoreceptors can only be observed in the Ad. VEGF model.

4.3 Correlation of the AAV-VEGF transduced CNV rat model to the laser induced CNV model

The laser CNV animal model (normally rats and mice) is the most commonly used animal model for CNV studies (Lambert et al., 2013, Liu et al., 2017). The advantages and limitations of the laser model and the CNV model induced by overexpression of VEGF were listed in Table 9, and the details were as follows:

The laser model is easy to operate and is valid to induce several individual lesions per eye based on the number of laser burns applied. After BM is perforated by laser, inflammation lead to VEGF overexpression and infiltration of blood vessels from the choroid forms the CNV recapitulating the main features of wet AMD.

A fully grown CNV can be obtained within 1-2 weeks after the laser injury (Edelman and Castro, 2000). However, The CNV normally disappeared within 4 weeks after lasering (Kokki et al., 2018). Hoerster et al. proved that only about 8.5 % of lesions had leakage, and the regression of the CNV was began after the first week (Hoerster et al., 2012). In 2011, Giani's group demonstrated a CNV formation which reached the peak at day 5 and showed a significant reduction by day 7 (Giani et al., 2011). Additionally, the CNV in this model was induced by laser burn, an artificial stimulus, leading to scar formation within a

short time frame of several weeks (Kuroki et al., 2002). Therefore, the laser model is a fast and fertile model for late CNV and scar formation, but it is not suitable to test the long-term effect of the new treatment options.

Note that laser can be used to treat several ocular diseases, and usually do not induce neovascularisation during and after the treatment (Chhablani et al., 2018). The healthy retina is also severely damaged due to the injury of laser burn before CNV formation starts. In addition, the laser models in the previous studies used several different protocols with different laser wavelengths and applications, showing the variability of effects. Semkova et al. indicated that the neovascularisation in the laser models may origin from the retina, not the choroid (Semkova et al., 2003).

In contrast, the CNV induced by the AAV-VEGF vector can exist for a very long period of months to years (Rolling et al., 2006, Wang et al., 2003). Thus, it can be used to investigate the whole process of CNV formation, especially the early CNV that cannot properly be studied in the laser model as well as the human donor tissues.

As usually only one lesion per eye in the VEGF transduced CNV model, it is difficult to quantify the ultrastructural features. This is a limitation of this model. In contrast, the laser model has more lesions to be investigated in each eye (normally 3-5 individual lesions).

The CNV induced by overexpression of human VEGF is more similar to human CNV as compared with the laser model, because “VEGF” is the root cause of human CNV. Moreover, laser is an artificial stimulus.

Table 9: The advantages and limitations of the laser model and the CNV model induced by overexpression of VEGF.

	The CNV model induced by AAV-VEGF vector	Laser induced CNV model
Advantages	Human VEGF expression, with typical characteristics of human CNV, valid to investigate the whole process of CNV formation and to test long time effect of drugs, high success rate	Easy to operate, several lesions per eye, short waiting time to test drugs, ideal to investigate scar formation
Limitations	Subretinal injection is hard to be performed and makes trauma, maximal 1-2 lesions per eye, 6 weeks' waiting time needed to reach a full grown CNV	No human VEGF expression, only a few essential features of CNV, no long-term studies due to self-healing, retina damage due to laser injury, retinal neovascularization possible, laser can treat several ocular diseases and usually do not induce neovascularisation

4.4 Correlation of the AAV-VEGF transduced CNV rat model to the other CNV animal models

Other common CNV animal models are based on mechanical injury to the RPE or BM, subretinal injection of viral vectors (e.g. VEGF and cells) and transgenic modification (Grossniklaus et al., 2010, Pennesi et al., 2012).

In 2007, Lassota's group investigated a porcine CNV model induced by surgical techniques of RPE removal and/ or a single perforation of BM (Lassota et al., 2007). Both these surgeries have capacity to induce CNV and reduce the retinal damage as compared with laser induced CNV model. However, the surgery is expensive and hard to operation (a three port vitrectomy is needed) (Pennesi et al., 2012).

Schwesinger et al. established a transgenic mouse model with overexpression of VEGF in the RPE cells, however, it only induced intrachoroidal neovascularization (Schwesinger et al., 2001). Other transgenic mouse models (rho/VEGF mice and VMD2/VEGF mice) without subretinal surgery also did not display CNV (Ohno-Matsui et al., 2002, Oshima et al., 2004). However, C57BL/6 mice subretinal injected with cultured RPE showed CNV, even the controls (subretinal injection of PBS) developed CNV with small areas (Schmack et al., 2009). In addition, Grossniklaus et al. demonstrated that the trauma caused by the subretinal injection alone may lead to a small size CNV (Grossniklaus et al., 2010). In this study, CNV was found in one GFP control eye, might due to the rupture of BM during the subretinal injection. Its data is not quantifiable, due to its small size. Therefore, the break of BM is required to induce subretinal CNV (Schwesinger et al., 2001) and the subretinal injection of viral vectors is a good choice for the development of CNV models.

A report described a loxP-STOP-hVEGF-A165 transgenic mouse model with subretinal experiment of human VEGF-A165 by adenoviral Cre gene delivery (Kokki et al., 2018). 75% of the mice showed the maximal CNV areas in angiography at 2 weeks after subretinal injection of VEGF, however, it began to diminish at later time points. Additionally, retinal atrophy, a feature of late CNV, was observed from 2 weeks after VEGF injection. In this study, CNV induced by AAV-VEGF vector reaches a peak at 6 weeks after VEGF transduction, thus this

model has sufficient time for the investigation of early CNV and still is valid to investigate late CNV.

In another report, macrophage-rich peritoneal exudate cells were subretinal injected into C57BL/6 or MCP-1 knockout mice, to establish a subretinal fibrosis model that resembles advanced AMD. (Jo et al., 2011). The mice showed subretinal fibrosis 7 days after the subretinal injection of cells, indicating that activated macrophages lead to fibrosis. Fibrosis can be defined by the pathological deposit of extracellular matrix (mainly collagen) in the wound healing (Neary et al., 2015). In this study, macrophages/ activated microglia deposited in the CNV area as well as in the subretinal space (as shown in Figure 34), stimulating the formation of fibrosis in this model (see Figure 29).

4.5 Correlation of the rat CNV model to the human CNV with wet AMD

In the aged human eye, the choroid-retina interface undergoes age-related changes, probably leading to the pathology known as AMD if they become much more pronounced than during normal aging. The microscopic and ultrastructural changes in the CNV rat eyes and human CNV eyes with wet AMD were summarized in Table 10 and explained in more details later in this section.

Note that the structures not shown in the rat CNV eyes induced with VEGF transduction (e.g. degenerating vessels) are features of an “aged” already degenerating CNV with leakage (shown in Table 10). The early stage CNV is difficult to be investigated in the human samples, as only in the late stage the sub-macular surgery with excision of the CNV can be operated. Nevertheless, this rat model is valid to investigate the whole process of CNV, not only early phase but also late phase.

Table 10: Correlation of morphological features in human and rat CNV. The features that are typically occurred in the eyes are labelled with “√”, and “-“ refers to the

features not found yet. The features, only shown in the human CNV, are typical for late CNV with leakage, forming a retinal scar in AMD patients.

	Human CNV	**Rat CNV**
Microscopic changes		
occult CNV (sub RPE vessels)	√	√
open CNV (subretinal vessels)	√	√
pigmentary changes		
- pigmented cells in subretinal space	√	√
- multi-layered RPE	√	√
subretinal bleeding	√	√
retinal degeneration		
- rosette-like retinal changes	√	√
- degenerating photoreceptors	√	√
scar tissue between choroid and retina	√	√
calcification	√	**-**
Ultrastructural changes		
choriocapillaris loss	√	√
irregular CNV vessels		
- irregular endothelia	√	√

- multi-layered basal lamina	√	√
- fenestrations	√	√
- finger-like filopodia into the lumen, building new lumen	√	√
- labyrinth capillaries	√	-
- leaky endothelia	√	-
- incomplete lumen	√	-
- loss of perivascular cells	√	-
- irregular or multi-thrombocytes	√	-
material around CNV vessels		
- increased extracellular matrix (collagen)	√	√
- macrophages	√	√
- migrating thin cells	√	√
- fibrin	√	-
- pigmented debris	√	√

The number of pericytes in CNV vessels is higher in the human eyes with wet AMD as compared with healthy aged control eyes (Biesemeier et al., 2015). The CNV vessels with varying thicknesses of endothelial cells and associated with pericytes were seen frequently in this rat model (e.g. Figure 29). The CNV

vessels with incomplete lumen and loss of the endothelial cells and pericytes were found in the human CNV samples.

One study indicated that the proliferation of RPE could stimulate the regression of CNV in the laser induced CNV model and younger wet AMD patients (Stern and Temple, 2015). The RPE proliferation was observed in the human CNV samples, while the RPE loss and the single pigmented cells in the retinal scar were also observed frequently. In the CNV rat eyes, the multi-layered RPE was observed frequently, and the quantification of the RPE loss was shown in Figure 40 (87.38% BM was covered by RPE cells in the CNV areas).

The thickening BM with thin cells and irregular endothelial cells with finger-like projections towards the choriocapillaris vessel lumen are also observed frequently in human CNV eyes (Biesemeier et al., 2014). These changes were also found in the rat CNV model as well as the eyes with subretinal VEGF protein injection (Figure 44). However, hydroxalapatite in calcified areas in BM was observed in human AMD samples (Biesemeier et al., 2015), which was not found in the CNV rat model.

Changes of choriocapillaris (diminish in number, fewer fenestrations in CC and smaller size of lumina) in human AMD patients have already been proved in several studies (Arya et al., 2018, Biesemeier et al., 2014, Chirco et al., 2017, Moreira-Neto et al., 2018). The choriocapillaris also diminished in the CNV areas of the VEGF transduced eyes, as shown in Figure 39.

Fibrin is accumulated around leaky CNV vessels. It can be observed in human CNV by EM (as shown in Figure 46), in contrast it is not found in rat EM sections. The features, like irregular or multi-thrombocytes, labyrinth capillaries and loss of endothelia were only shown in the human CNV samples (see Figure 46). They are typical for the late CNV with leakage, forming a retinal scar in AMD patients. Therefore, it seems that the CNV vessels induced by AAV-VEGF are more stable as compare with human CNV samples.

IHC evaluation of paraffin sections of the human samples and the eyes with or without VEGF vector transduction were performed. Details is shown in the following:

VEGF expression is ubiquitous in the retina and choroid in both human and rats. VEGF overexpression has been observed in human CNV patients and the laser model of CNV animal models (Hoerster et al., 2012, Mu et al., 2018, Ryan, 1982, Yi et al., 1997). RPE cells were strongly stained with VEGF antibody in the human eyes with drusen (Figure 30). Areas with CNV were stronger stained for VEGF compared with neighbouring areas in VEGF transduced rat eyes, especially the pigmented cells within the CNV area (Figure 30). These pigmented cells in the CNV areas were also stained with RPE 65 antibody, showing that they were truly RPE cells (Figure 31). VEGF overexpression has been demonstrated in the CNV areas of this model, indicating the successful transduction of the human VEGF vector into the RPE cells of the eyes.

As the CNV vessel associated with perivascular cells was observed frequently in the CNV rat eyes by EM, the perivascular cells were stained for α-SMA and NG2 in paraffin sections. α-SMA is typical pericyte marker and NG2 is a marker for migrating nascent progenitor cells including pericytes during angiogenesis (Ozerdem et al., 2001). In general, all the blood vessels (particularly the smooth muscle cells and pericytes) in the retina, choroid and CNV are heavily stained in CNV rat eyes as well as human AMD samples. In EGFP transduced control eyes, α-SMA stained large vessels in the retina and choroid, however, CC and other smaller vessels were usually not stained. Additionally, NG2 showed a strong staining in inner segments, pigmented RPE cells and the endothelia of vessels in both CNV areas and the choroid (Figure 33). NG2 was also strong expressed in RPE and CNV areas in human eyes with CNV or drusen (not shown). According to the staining results, the perivascular cells surrounding CNV vessels are truly pericytes.

Changes of the extracellular matrix occurs in both early and late human CNV with AMD, leading to RPE proliferation, differentiation, and migration. Especially collagen type I plays a significant role in the pathogenesis of AMD (Bhutto and Lutty, 2012, Nita et al., 2014). Therefore, Masson trichrome staining was performed to investigate the component of extracellular matrix deposit in CNV lesions and choroid. In this rat model, accumulation of collagen was observed in the space between the CNV vessels and RPE cells (Figure 29) as well as in the extracellular space of the choroid (Figure 27). Fibrin and elastin were not deposited in the model, as they were not stained in the CNV areas by performing Masson trichrome staining. Only elastin in BM was visible. Accumulation of collagen was also shown in human AMD specimen by EM, similarly to the CNV rats. In general, collagen is the most abundant component of extracellular matrix deposit in CNV areas in both human and rats.

Albumin staining was performed to verify the occurrence of leakage. Individual cells and blood vessels have a strong albumin staining in the CNV rats, however, the large vacuoles with a high density of microparticles in the multi-layered RPE in EM (Figure 28) did not show positive staining for albumin. Additionally, only few rat eyes showed leakage in angiography, due to the delayed early frame angiogram (Figure 23). Therefore, foremost stable CNV vessels and few leaky vessels were observed in the CNV rat model, based on the evaluation of EM and IHC.

Taken together, the rat CNV model induced by overexpression of VEGF mimics the main features of the human CNV, including a lot of ultrastructural details, as shown in Table 10. It is a valid model to investigate the mechanism of CNV and the effect of the new treatments.

4.6 Treatment of CNV in the CNV rat using Avastin®

Anti-VEGF therapy is currently the standard treatment for CNV with wet AMD. However, it is still not an ideal treatment strategy and it has to be injected monthly. In a latest five years follow-up study (Wecker et al. 2017), a group of 1083 AMD patients treated with anti-VEGF injections showed the encouraging visual acuity results in the first treatment year which did not carry forward to the following years. Visual acuity gained or at least remained in 88.6% of patients with AMD in the first year, while only 65.7% in the fifth treatment year. Visual acuity also declined over time in the other seven-year study (Rofagha et al. 2013). A report showed that anti-VEGF therapy can lead to geographic atrophy in about 40% of patients, which is the end stage of CNV with no available treatment (Cho et al., 2015). Gemenetzi et al. supported this hypothesis based on the review of the literature on histopathologic, animal studies and clinical trials associated with geographic atrophy and anti-VEGF treatment (Gemenetzi et al., 2017). Kaynak et al. mentioned that this treatment was still indispensable compared with other treatment options, although it increased geographic atrophy (Kaynak et al., 2018). Another recent study suggested that the mortality of AMD patients who also diagnosed with acute myocardial infarct increased after anti-VEGF therapy (Hanhart et al., 2018). In addition, Avastin® can also induce retinal vein thrombosis in monkey eyes (Schraermeyer and Julien, 2013). Therefore, new treatment strategy for CNV is ongoing and a valid animal model is needed.

Avastin® is the most commonly used anti-VEGF drugs in clinic due to its extremely low price in contrast to the other drugs. Therefore, Avastin® was used in this study to verify if this CNV rat model was valid for the evaluation of treatment strategy for CNV, and it can also be used as positive control when judging the effects of new treatments.

As 6 weeks' waiting time was needed to reach a full grown CNV in this CNV rat model, Avastin® was injected into the CNV eyes at that time point. It can reduce or at least stabilize CNV within the investigated time frame of 1-3 weeks after single intravitreal injection, however, it did not show clear effect in the long-term (6 weeks after Avastin® injection), as always happens in human patients. The CNV area in FA analysis showed a slight reduction within 3 weeks after Avastin® injection, while the retinal and the CNV lesion thickness in OCT decreased significantly in treated eyes as compared to untreated eyes that showed the growth of CNV over time.

The expression of VEGF analyzed by human VEGF staining decreased in treated rat eyes, however, not statistically significant as compared with untreated eyes. One reason is that Avastin® can only inhibit the expression of VEGF in a short time term, as the plasma free-VEGF level markedly reduced within the first week after Avastin® injection in human AMD patients, but later it increased again (Avery et al., 2017). Another one is that VEGF is still overexpressing in the CNV eyes, as the untreated CNV eyes show ongoing CNV formation with significant increase of retinal and CNV lesion thickness up to 9 weeks after VEGF vector transduction.

Pachydaki et al. indicated that stable CNV vessels with pericytes support did not respond to Avastin®, and that only degenerating, leaky vessels are targeted by Avastin® (Pachydaki et al., 2012). This can also be used as an explanation for the unsignificant treatment effect of Avastin® in this CNV rat model with foremost stable CNV vessels and few or absent leaky vessels.

Additionally, Avastin® did not show significant therapeutic effect in the laser-induced rodent CNV model (Lu and Adelman, 2009), as Avastin® was unable to bind with murine VEGF with high affinity (Fuh et al., 2006, Yu et al., 2008). Non-human primate laser-induced CNV models can be used to test antiangiogenic treatments (Husain et al., 2005, Krzystolik et al., 2002, Lichtlen et

al., 2010), however, it is much more expensive and difficult to obtain permission for the use of large number of non-human primates. Therefore, the rat CNV model induced by overexpression of VEGF may be an alternative to test the anti-human VEGF therapy.

4.7 ICG patterns in CNV eyes

ICG always shows a rather spotty hyper-fluorescent pattern spreads around the CNV lesion in the CNV rat eye, which even more significant one and two weeks later without new dye injection. The spotty patterns could be caused by a pathological transport of ICG labelled proteins from CNV vessels into the surrounding tissue. Sim's group indicated that the spread of spotty hyper-fluorescent pattern in ICG was also observed in the laser-induced CNV model, and it was probably caused by the migration of macrophages after feeding ICG-labelled proteins (Sim et al., 2015). This was investigated by IHC staining in this study. Single pigmented cells (disconnected RPE cells or microphages) were found above CNV lesion in the subretinal space (e.g. Figure 32). These cells were Iba1 positively stained (Figure 34), in contrast they were not VEGF positively stained (Figure 30). Therefore, the spotty pattern in ICG is probably caused by migrating macrophages.

The spotty spread hyper-fluorescent pattern in ICG angiography is also observed in the human CNV eyes. One report described that a larger proportion of ICG-labelled cells were seen in human peripheral blood mononuclear cells, most of which were lymphocytes (Sim et al., 2015). It could be a new effective tool to follow up a single ICG injection over days or weeks, which may yield new information about the underlying pathology.

After the ICG dye fades from the retinal vessels, the hyper-fluorescent pattern in ICG angiography is still visible, indicating that the eyes transduced with VEGF-A have intense micro-vascular leakages. This is also supported by Hofman's group

(Hofman et al., 2000). In their report, the high-level VEGF could induce the leaky retinal vessels, and the leakage was pathological transported by the pinocytotic vesicles in the endothelia. The vesicles were also observed frequently in the endothelia of this CNV rat model (see Figure 27).

4.8 The early effects of VEGF overexpression in the choroid-RPE interface

VEGF is a key factor for CNV formation, promoting endothelial cells proliferation and migration (Sene et al., 2015). However, the detail ultrastructural changes of the early frame of the pathological process are still unclear. In this study, the early changes in the choroid-RPE interface were investigated 1h after VEGF protein subretinal injection. Only FA shows a slight hyper-fluorescence in the eyes, no direct effects of the VEGF protein injection were observed in angiography and OCT.

By EM, activation of RPE cells with elongated cellular processes, collagen formation around CC vessels, thickening BM with incomplete absent elastic layer and finger-like processes of endothelial cells were found in the choroid-RPE interface of the eyes injected with VEGF protein. These active endothelial cells even pointed into the lumen of the vessels in CC and sprouted into BM. A CNV vessel will be formed when the proliferating endothelial cells migrate through BM into the retina. In addition, Figure 44 shows open endothelial cell connections (a feature of leakage) in a CC vessel which will probably become a leaky CNV vessel. Thickening BM and the deposit of extracellular matrix (mainly collagen) can be frequently observed in the eyes transduced with VEGF vector in this study. Therefore, these changes are the signs for early CNV.

5 Summary

Choroidal neovascularisation (CNV) with the wet age-related macular degeneration (AMD) is a leading cause of vision loss in the developed countries. As the conventional treatment for CNV is not ideal, an efficient CNV animal model is needed to study new treatments for ocular diseases. Vascular endothelial growth factor (VEGF) is a key stimulator for CNV. The aim of this study was to develop a valid VEGF-induced CNV model and to test whether it can be used for investigation of new treatment options.

The model was first developed by subretinal injection of HC Ad. VEGF vector, however, high retinal toxicity of the vector was observed in the HC Ad. EGFP control eyes. Therefore, AAV vector system was used in the latter experiments. $2x10^9$ AAV-VEGF vector particles were subretinal injected into the eyes of female Long Evans rats. Fluorescein angiography (FA), indocyanine green angiography (ICG) and optical coherence tomography (OCT) were performed in all rats at different time points to confirm the best time point for this rat model. All the eyes were fixed for paraffin and EPON embedding and later investigated by light and electron microscopy (LM/EM) and immunohistochemistry (IHC). Additionally, 19 eyes were intravitreally injected with Avastin® (125µg / 5µl) 6 weeks after VEGF injection to test the effect of Avastin®, and 19 eyes were injected with AAV-VEGF vector simultaneously as untreated controls.

All the eyes with CNV showed hyper-fluorescent CNV areas in FA/ICG and marked subretinal edema-like changes in OCT. 91% of AAV-VEGF transduced eyes presented with a fully grown CNV observable by angiography after 6 weeks' duration of VEGF overexpression. No CNV eye showed spontaneous regression of the CNV within 9 weeks after AAV-VEGF vector injection. The retinal and CNV lesion thickness increased with time and showed a significant difference if compared between 6 and 9 weeks after VEGF transduction (ANOVA: $p < 0.05$). In the EM, newly formed blood vessels with fenestrations between Bruch's

membrane (BM) and retinal pigment epithelium (RPE) or between RPE cells, multi-layered RPE, loss of photoreceptors and collagen accumulation were observed, resembling human CNV. IHC verified VEGF overexpression (human VEGF), multi-layered RPE (RPE65), collagen accumulation (Masson trichrome staining), pericytes occurrence (alpha-smooth muscle actin (α-SMA) and neural/glial antigen 2 (NG2)), macrophages/ activated microglia (Iba1) and albumin occurrence in CNV areas.

The thickness of retinal and CNV lesion decreased significantly one week after Avastin® treatment (t-test, $P<0.05$). The decreases were no longer significant at 3 weeks after treatment, but Avastin® still has a tendency to reduce the growth of CNV. The proportion of the VEGF positive CNV area decreased 1 week after Avastin® treatment.

Based on the results, especially EM, this rat model resembles the whole process of human CNV. Avastin® tends to reduce CNV lesion thickness or at least to inhibit its growth in the short term in the rat CNV model. In conclusion, this CNV rat model developed by overexpression of AAV-VEGF vector is efficient for the investigation of new treatment options for CNV.

6 Deutsche Zusammenfassung

Die choroidale Neovaskularisation (CNV) bei feuchter altersbedingter Makuladegeneration (AMD) ist eine der Hauptursachen für Sehverlust in den Industrieländern. Da die konventionelle Behandlung von CNV nicht ideal ist, ist ein effizientes CNV-Tiermodell erforderlich, um Strategien evaluieren zu können. Der vaskuläre endotheliale Wachstumsfaktor (VEGF) ist ein Hauptstimulator für die CNV. Ziel dieser Studie war es, ein valides VEGF-induziertes CNV-Modell zu entwickeln und zu testen, ob es für die Untersuchung neuer Behandlungsoptionen verwendet werden kann.

Das Modell wurde zuerst durch subretinale Injektion von HC Ad. $VEGF^{165}$-Vektor entwickelt. Jedoch wurde eine hohe Retinatoxizität des Vektors in EGFP-Kontrollaugen beobachtet. Daher wurde in späteren Experimenten ein nicht-toxisches AAV-Vektorsystem verwendet. 2×10^{9} AAV-$VEGF^{165}$-Vektorpartikel wurden subretinell in die Augen weiblicher Long Evans-Ratten injiziert. Die Fluoreszenzangiographie (FA), die Indocyaningrünangiographie (ICG) und die optische Kohärenztomographie (OCT) wurden bei allen Ratten zu unterschiedlichen Zeitpunkten durchgeführt, um herauszufinden, wann die CNV voll entwickelt ist. Alle Augen wurden für Paraffin- und EPON-Einbettung fixiert und später mittels Licht- und Elektronenmikroskopie (LM / EM) und Immunhistochemie (IHC) untersucht. In einem weiteren Experiment wurde Avastin® (125 µg / 5 µl) sechs Wochen nach der VEGF-Injektion in 19 Augen intravitreal injiziert, um die Wirkung von Avastin® auf die CNV zu testen. Neunzehn weitere Augen wurden als unbehandelte Kontrollen mit AAV-VEGF Vektor infiziert und vergleichend untersucht.

Alle Augen mit CNV zeigten hyperfluoreszierende CNV-Bereiche im FA / ICG und ausgeprägte subretinale ödemartige Veränderungen im OCT. 91% der mit AAV-VEGF transduzierten Augen zeigten nach sechswöchiger VEGF-Überexpression eine angiographisch erkennbare, ausgewachsene CNV. Kein CNV-Auge zeigte innerhalb von neun Wochen nach der AAV-VEGF-Vektorinjektion eine spontane Regression des CNV. Die Dicke der Netzhaut- und CNV-Läsionen nahm mit der Zeit zu und zeigte einen signifikanten Unterschied im Vergleich zwischen sechs und neun Wochen nach der VEGF-Transduktion (ANOVA: $p < 0,05$). EM zeigte fenestrierte neu gebildete Blutgefäße in der Bruch'schen Membran (BM) und im vielschichtigen retinalen Pigmentepithel (RPE), Verlust von Photorezeptoren und Kollagenansammlung, die der menschlichen CNV ähnelten. IHC-verifizierte VEGF-Überexpression

(humaner VEGF), vielschichtiges RPE (RPE65), Kollagenansammlung (Masson-Trichrom-Färbung), Auftreten von Perizyten (Aktin der glatten Muskulatur (α-SMA) und neuronale / gliale Antigene 2 (NG2)), Makrophagen / Aktivierte Mikroglia (Iba1) und Albumin treten in CNV-Gebieten auf.

Die Dicke der Netzhaut- und CNV-Läsionen nahm eine Woche nach der Avastin®-Behandlung signifikant ab (t-Test, P <0,05). Die Abnahmen waren drei Wochen nach der Behandlung nicht mehr signifikant, aber Avastin® neigt immer noch dazu, das Wachstum von CNV zu verringern. Die Proportion der VEGF-positiven CNV-Fläche nahm eine Woche nach der Avastin®-Behandlung ab.

Basierend auf den Ergebnissen, insbesondere EM, ähnelt dieses Rattenmodell dem menschlichen CNV. Avastin® neigt dazu, die Dicke der CNV-Läsionen zu verringern oder zumindest deren Wachstum im Ratten-CNV-Modell kurzfristig zu hemmen. Zusammenfassend ist dieses CNV-Rattenmodell, das durch Überexpression des AAV-VEGF-Vektors entwickelt wurde, für die Untersuchung neuer Behandlungsoptionen für CNV geeignet.

7 References

ABHINAND, C. S., RAJU, R., SOUMYA, S. J., ARYA, P. S. & SUDHAKARAN, P. R. 2016. VEGF-A/VEGFR2 signaling network in endothelial cells relevant to angiogenesis. *J Cell Commun Signal,* 10**,** 347-354.

ACHEN, M. G. & STACKER, S. A. 1998. The vascular endothelial growth factor family; proteins which guide the development of the vasculature. *Int J Exp Pathol,* 79**,** 255-65.

ADAMIS, A. P., SHIMA, D. T., YEO, K. T., YEO, T. K., BROWN, L. F., BERSE, B., D'AMORE, P. A. & FOLKMAN, J. 1993. Synthesis and secretion of vascular permeability factor/vascular endothelial growth factor by human retinal pigment epithelial cells. *Biochem Biophys Res Commun,* 193**,** 631-8.

ARYA, M., SABROSA, A. S., DUKER, J. S. & WAHEED, N. K. 2018. Choriocapillaris changes in dry age-related macular degeneration and geographic atrophy: a review. *Eye Vis (Lond),* 5**,** 22.

AVERY, R. L., CASTELLARIN, A. A., STEINLE, N. C., DHOOT, D. S., PIERAMICI, D. J., SEE, R., COUVILLION, S., NASIR, M. A., RABENA, M. D., MAIA, M., VAN EVEREN, S., LE, K. & HANLEY, W. D. 2017. Systemic pharmacokinetics and pharmacodynamics of intravitreal aflibercept, bevacizumab, and ranibizumab. *Retina,* 37**,** 1847-1858.

BAFFI, J., BYRNES, G., CHAN, C. C. & CSAKY, K. G. 2000. Choroidal neovascularization in the rat induced by adenovirus mediated expression of vascular endothelial growth factor. *Invest Ophthalmol Vis Sci,* 41**,** 3582-9.

BHISITKUL, R. B. 2006. Vascular endothelial growth factor biology: clinical implications for ocular treatments. *Br J Ophthalmol,* 90**,** 1542-7.

BHUTTO, I. & LUTTY, G. 2012. Understanding age-related macular degeneration (AMD): relationships between the photoreceptor/retinal pigment epithelium/Bruch's membrane/choriocapillaris complex. *Mol Aspects Med,* 33**,** 295-317.

BIESEMEIER, A., NAN, S. & SCHRAERMEYER, U. 2015 Pericytes are more abundant in vessels of eyes affected by wet age-related macular degeneration as compared to those of agematched controls. *ARVO Meeting Abstracts.* Denver, CO, USA: Invest Ophtalmol Vis Sci.

BIESEMEIER, A., TAUBITZ, T., JULIEN, S., YOERUEK, E. & SCHRAERMEYER, U. 2014. Choriocapillaris breakdown precedes retinal degeneration in age-related macular degeneration. *Neurobiol Aging,* 35**,** 2562-2573.

BIESEMEIER, A., YOERUEK, E., EIBL, O. & SCHRAERMEYER, U. 2015. Iron accumulation in Bruch's membrane and melanosomes of donor eyes with age-related macular degeneration. *Exp Eye Res,* 137**,** 39-49.

BINDEWALD, A., SCHMITZ-VALCKENBERG, S., JORZIK, J. J., DOLAR-SZCZASNY, J., SIEBER, H., KEILHAUER, C., WEINBERGER, A. W., DITHMAR, S., PAULEIKHOFF, D., MANSMANN, U., WOLF, S. & HOLZ, F. G. 2005. Classification of abnormal fundus autofluorescence patterns in the junctional zone of geographic atrophy in patients with age related macular degeneration. *Br J Ophthalmol,* 89**,** 874-8.

CAMPOCHIARO, P. A. 2011. Gene transfer for neovascular age-related macular degeneration. *Hum Gene Ther,* 22**,** 523-9.

CAMPOCHIARO, P. A. 2013. Ocular neovascularization. *J Mol Med (Berl),* 91**,** 311-21.

CASTRO, P. R., BARBOSA, A. S., PEREIRA, J. M., RANFLEY, H., FELIPETTO, M., GONçALVES, C. A. X., PAIVA, I. R., BERG, B. B. & BARCELOS, L. S. 2018. Cellular and Molecular Heterogeneity Associated with Vessel Formation Processes. *BioMed Research International,* 2018**,** 1-32.

CHARBEL ISSA, P., BARNARD, A. R., SINGH, M. S., CARTER, E., JIANG, Z., RADU, R. A., SCHRAERMEYER, U. & MACLAREN, R. E. 2013. Fundus autofluorescence in the Abca4(-/-) mouse model of Stargardt disease--correlation with accumulation of A2E, retinal function, and histology. *Invest Ophthalmol Vis Sci,* 54**,** 5602-12.

CHHABLANI, J., ROH, Y. J., JOBLING, A. I., FLETCHER, E. L., LEK, J. J., BANSAL, P., GUYMER, R. & LUTTRULL, J. K. 2018. Restorative retinal laser therapy: Present state and future directions. *Surv Ophthalmol,* 63**,** 307-328.

CHIRCO, K. R., SOHN, E. H., STONE, E. M., TUCKER, B. A. & MULLINS, R. F. 2017. Structural and molecular changes in the aging choroid: implications for age-related macular degeneration. *Eye (Lond),* 31**,** 10-25.

CHO, H. J., LEE, T. G., HAN, S. Y., KIM, H. S., KIM, J. H., HAN, J. I., LEW, Y. J. & KIM, J. W. 2015. Long-term visual outcome and prognostic factors of Intravitreal anti-vascular endothelial growth factor treatment for retinal angiomatous proliferation. *Graefes Arch Clin Exp Ophthalmol*.

CHONG, N. H., KEONIN, J., LUTHERT, P. J., FRENNESSON, C. I., WEINGEIST, D. M., WOLF, R. L., MULLINS, R. F. & HAGEMAN, G. S. 2005. Decreased thickness and integrity of the macular elastic layer of Bruch's membrane correspond to the distribution of lesions associated with age-related macular degeneration. *Am J Pathol,* 166**,** 241-51.

CHRISTNER, S. 2017. The effects of a single intravitreal injection of the VEGF-A-inhibitors aflibercept and ranibizumab on glomeruli of monkeys. *Dissertation, University Tuebingen*.

EDELMAN, J. L. & CASTRO, M. R. 2000. Quantitative image analysis of laser-induced choroidal neovascularization in rat. *Exp Eye Res,* 71**,** 523-33.

FARAZDAGHI, M. K. & EBRAHIMI, K. B. 2019. Role of the Choroid in Age-related Macular Degeneration: A Current Review. *J Ophthalmic Vis Res,* 14**,** 78-87.

FISCHER, M. D., HUBER, G., BECK, S. C., TANIMOTO, N., MUEHLFRIEDEL, R., FAHL, E., GRIMM, C., WENZEL, A., REME, C. E., VAN DE PAVERT, S. A., WIJNHOLDS, J., PACAL, M., BREMNER, R. & SEELIGER, M. W. 2009. Noninvasive, in vivo assessment of mouse retinal structure using optical coherence tomography. *PLoS One,* 4**,** e7507.

FUH, G., WU, P., LIANG, W. C., ULTSCH, M., LEE, C. V., MOFFAT, B. & WIESMANN, C. 2006. Structure-function studies of two synthetic anti-vascular endothelial growth factor Fabs and comparison with the Avastin Fab. *J Biol Chem,* 281**,** 6625-31.

GALE, N. W., THURSTON, G., HACKETT, S. F., RENARD, R., WANG, Q., MCCLAIN, J., MARTIN, C., WITTE, C., WITTE, M. H., JACKSON, D., SURI, C., CAMPOCHIARO, P. A., WIEGAND, S. J. & YANCOPOULOS, G. D. 2002. Angiopoietin-2 is required for postnatal angiogenesis and lymphatic patterning, and only the latter role is rescued by Angiopoietin-1. *Dev Cell,* 3**,** 411-23.

GAO, Y., YU, T., ZHANG, Y. & DANG, G. 2018. Anti-VEGF Monotherapy Versus Photodynamic Therapy and Anti-VEGF Combination Treatment for Neovascular Age-Related Macular Degeneration: A Meta-Analysis. *Invest Ophthalmol Vis Sci,* 59**,** 4307-4317.

GARCIA GARRIDO, M., MUHLFRIEDEL, R. L., BECK, S. C., WALLRAPP, C. & SEELIGER, M. W. 2015. Scale Adjustments to Facilitate Two-Dimensional Measurements in OCT Images. *PLoS One,* 10**,** e0131154.

GEMENETZI, M., LOTERY, A. J. & PATEL, P. J. 2017. Risk of geographic atrophy in age-related macular degeneration patients treated with intravitreal anti-VEGF agents. *Eye (Lond),* 31**,** 1-9.

GIANI, A., THANOS, A., ROH, M. I., CONNOLLY, E., TRICHONAS, G., KIM, I., GRAGOUDAS, E., VAVVAS, D. & MILLER, J. W. 2011. In vivo evaluation of laser-induced choroidal neovascularization using spectral-domain optical coherence tomography. *Invest Ophthalmol Vis Sci,* 52**,** 3880-7.

GROSSNIKLAUS, H. E., KANG, S. J. & BERGLIN, L. 2010. Animal models of choroidal and retinal neovascularization. *Prog Retin Eye Res,* 29**,** 500-19.

GROSSNIKLAUS, H. E., LING, J. X., WALLACE, T. M., DITHMAR, S., LAWSON, D. H., COHEN, C., ELNER, V. M., ELNER, S. G. & STERNBERG, P., JR. 2002. Macrophage and retinal pigment epithelium expression of angiogenic cytokines in choroidal neovascularization. *Mol Vis,* 8**,** 119-26.

HACKETT, S. F., WIEGAND, S., YANCOPOULOS, G. & CAMPOCHIARO, P. A. 2002. Angiopoietin-2 plays an important role in retinal angiogenesis. *J Cell Physiol,* 192**,** 182-7.

HANHART, J., COMANESHTER, D. S., FREIER-DROR, Y. & VINKER, S. 2018. Mortality associated with bevacizumab intravitreal injections in age-related macular degeneration patients after acute myocardial infarct: a retrospective population-based survival analysis. *Graefes Arch Clin Exp Ophthalmol,* 256**,** 651-663.

HEE, M. R., BAUMAL, C. R., PULIAFITO, C. A., DUKER, J. S., REICHEL, E., WILKINS, J. R., COKER, J. G., SCHUMAN, J. S., SWANSON, E. A. & FUJIMOTO, J. G. 1996. Optical coherence tomography of age-related macular degeneration and choroidal neovascularization. *Ophthalmology,* 103**,** 1260-70.

HOERSTER, R., MUETHER, P. S., VIERKOTTEN, S., SCHRODER, S., KIRCHHOF, B. & FAUSER, S. 2012. In-vivo and ex-vivo characterization of laser-induced choroidal neovascularization variability in mice. *Graefes Arch Clin Exp Ophthalmol,* 250**,** 1579-86.

HOFMAN, P., BLAAUWGEERS, H. G., TOLENTINO, M. J., ADAMIS, A. P., NUNES CARDOZO, B. J., VRENSEN, G. F. & SCHLINGEMANN, R. O. 2000. VEGF-A induced hyperpermeability of blood-retinal barrier endothelium in vivo is predominantly associated with pinocytotic vesicular transport and not with formation of fenestrations. Vascular endothelial growth factor-A. *Curr Eye Res,* 21**,** 637-45.

HUBER, G., BECK, S. C., GRIMM, C., SAHABOGLU-TEKGOZ, A., PAQUET-DURAND, F., WENZEL, A., HUMPHRIES, P., REDMOND, T. M., SEELIGER, M. W. & FISCHER, M. D. 2009. Spectral domain optical coherence tomography in mouse models of retinal degeneration. *Invest Ophthalmol Vis Sci,* 50**,** 5888-95.

HUSAIN, D., KIM, I., GAUTHIER, D., LANE, A. M., TSILIMBARIS, M. K., EZRA, E., CONNOLLY, E. J., MICHAUD, N., GRAGOUDAS, E. S., O'NEILL, C. A., BEYER, J. C. & MILLER, J. W. 2005. Safety and efficacy of intravitreal injection of ranibizumab in combination with verteporfin PDT on experimental choroidal neovascularization in the monkey. *Arch Ophthalmol,* 123**,** 509-16.

JAYES, F. L., LIU, B., FENG, L., AVILES-ESPINOZA, N., LEIKIN, S. & LEPPERT, P. C. 2019. Evidence of biomechanical and collagen heterogeneity in uterine fibroids. *PLoS One,* 14**,** e0215646.

JELTSCH, M., KARPANEN, T., STRANDIN, T., AHO, K., LANKINEN, H. & ALITALO, K. 2006. Vascular endothelial growth factor (VEGF)/VEGF-C mosaic molecules reveal specificity determinants and feature novel receptor binding patterns. *J Biol Chem,* 281**,** 12187-95.

JO, Y. J., SONODA, K. H., OSHIMA, Y., TAKEDA, A., KOHNO, R., YAMADA, J., HAMURO, J., YANG, Y., NOTOMI, S., HISATOMI, T. & ISHIBASHI, T. 2011. Establishment of a new animal model of focal subretinal fibrosis that resembles disciform lesion in advanced age-related macular degeneration. *Invest Ophthalmol Vis Sci,* 52**,** 6089-95.

JOHNSON, K. E. & WILGUS, T. A. 2014. Vascular Endothelial Growth Factor and Angiogenesis in the Regulation of Cutaneous Wound Repair. *Adv Wound Care (New Rochelle),* 3**,** 647-661.

JULIEN, S., KREPPEL, F., BECK, S., HEIDUSCHKA, P., BRITO, V., SCHNICHELS, S., KOCHANEK, S. & SCHRAERMEYER, U. 2008. A reproducible and quantifiable model of choroidal neovascularization induced by VEGF A165 after subretinal adenoviral gene transfer in the rabbit. *Mol Vis,* 14**,** 1358-72.

KAYNAK, S., KAYA, M. & KAYA, D. 2018. Is There a Relationship Between Use of Anti-Vascular Endothelial Growth Factor Agents and Atrophic Changes in Age-Related Macular Degeneration Patients? *Turk J Ophthalmol,* 48**,** 81-84.

KENT, D. & SHERIDAN, C. 2003. Choroidal neovascularization: a wound healing perspective. *Mol Vis,* 9**,** 747-55.

KEYT, B. A., BERLEAU, L. T., NGUYEN, H. V., CHEN, H., HEINSOHN, H., VANDLEN, R. & FERRARA, N. 1996. The carboxyl-terminal domain (111-165) of vascular endothelial growth factor is critical for its mitogenic potency. *J Biol Chem,* 271**,** 7788-95.

KINNUNEN, K., KORPISALO, P., RISSANEN, T. T., HEIKURA, T., VIITA, H., UUSITALO, H. & YLA-HERTTUALA, S. 2006. Overexpression of VEGF-A induces neovascularization and increased vascular leakage in rabbit eye after intravitreal adenoviral gene transfer. *Acta Physiol (Oxf),* 187**,** 447-57.

KOKKI, E., KARTTUNEN, T., OLSSON, V., KINNUNEN, K. & YLA-HERTTUALA, S. 2018. Human Vascular Endothelial Growth Factor A165 Expression Induces the Mouse Model of Neovascular Age-Related Macular Degeneration. *Genes (Basel),* 9.

KRZYSTOLIK, M. G., AFSHARI, M. A., ADAMIS, A. P., GAUDREAULT, J., GRAGOUDAS, E. S., MICHAUD, N. A., LI, W., CONNOLLY, E., O'NEILL, C. A. & MILLER, J. W. 2002. Prevention of experimental choroidal neovascularization with intravitreal anti-vascular endothelial growth factor antibody fragment. *Arch Ophthalmol,* 120**,** 338-46.

KUROKI, A. M., BHUTTO, I. A., KITAOKA, T. & AMEMIYA, T. 2002. Natural course of experimental choroidal neovascularization: three-dimensional study with corrosion cast and scanning electron microscope. *Ophthalmic Res,* 34**,** 200-5.

LAMBERT, N. G., ZHANG, X., RAI, R. R., UEHARA, H., CHOI, S., CARROLL, L. S., DAS, S. K., CAHOON, J. M., KIRK, B. H., BENTLEY, B. M. & AMBATI, B. K. 2016. Subretinal AAV2.COMP-Ang1 suppresses choroidal neovascularization and vascular endothelial growth factor in a murine model of age-related macular degeneration. *Exp Eye Res,* 145**,** 248-257.

LAMBERT, V., LECOMTE, J., HANSEN, S., BLACHER, S., GONZALEZ, M. L., STRUMAN, I., SOUNNI, N. E., ROZET, E., DE TULLIO, P., FOIDART, J. M., RAKIC, J. M. & NOEL, A. 2013. Laser-induced choroidal

neovascularization model to study age-related macular degeneration in mice. *Nat Protoc,* 8**,** 2197-211.

LASSOTA, N., KIILGAARD, J. F., PRAUSE, J. U., QVORTRUP, K., SCHERFIG, E. & LA COUR, M. 2007. Surgical induction of choroidal neovascularization in a porcine model. *Graefes Arch Clin Exp Ophthalmol,* 245**,** 1189-98.

LEBHERZ, C., MAGUIRE, A. M., AURICCHIO, A., TANG, W., ALEMAN, T. S., WEI, Z., GRANT, R., CIDECIYAN, A. V., JACOBSON, S. G., WILSON, J. M. & BENNETT, J. 2005. Nonhuman primate models for diabetic ocular neovascularization using AAV2-mediated overexpression of vascular endothelial growth factor. *Diabetes,* 54**,** 1141-9.

LEESON, T. S. & LEESON, C. R. 1967. Choriocapillaris and lamina elastica (vitrea) of the rat eye. *Br J Ophthalmol,* 51**,** 599-616.

LICHTLEN, P., LAM, T. T., NORK, T. M., STREIT, T. & URECH, D. M. 2010. Relative contribution of VEGF and TNF-alpha in the cynomolgus laser-induced CNV model: comparing the efficacy of bevacizumab, adalimumab, and ESBA105. *Invest Ophthalmol Vis Sci,* 51**,** 4738-45.

LIU, C. H., WANG, Z., SUN, Y. & CHEN, J. 2017. Animal models of ocular angiogenesis: from development to pathologies. *Faseb j,* 31**,** 4665-4681.

LIU, J. T., CHEN, Y. L., CHEN, W. C., CHEN, H. Y., LIN, Y. W., WANG, S. H., MAN, K. M., WAN, H. M., YIN, W. H., LIU, P. L. & CHEN, Y. H. 2012. Role of pigment epithelium-derived factor in stem/progenitor cell-associated neovascularization. *J Biomed Biotechnol,* 2012**,** 871272.

LU, F. & ADELMAN, R. A. 2009. Are intravitreal bevacizumab and ranibizumab effective in a rat model of choroidal neovascularization? *Graefes Arch Clin Exp Ophthalmol,* 247**,** 171-7.

MOORE, N. A., BRACHA, P., HUSSAIN, R. M., MORRAL, N. & CIULLA, T. A. 2017. Gene therapy for age-related macular degeneration. *Expert Opin Biol Ther,* 17**,** 1235-1244.

MOREIRA-NETO, C. A., MOULT, E. M., FUJIMOTO, J. G., WAHEED, N. K. & FERRARA, D. 2018. Choriocapillaris Loss in Advanced Age-Related Macular Degeneration. *J Ophthalmol,* 2018**,** 8125267.

MORI, K., GEHLBACH, P., ANDO, A., DYER, G., LIPINSKY, E., CHAUDHRY, A. G., HACKETT, S. F. & CAMPOCHIARO, P. A. 2002. Retina-specific expression of PDGF-B versus PDGF-A: vascular versus nonvascular proliferative retinopathy. *Invest Ophthalmol Vis Sci,* 43**,** 2001-6.

MU, H., WANG, Y., CHU, Y., JIANG, Y., HUA, H., CHU, L., WANG, K., WANG, A., LIU, W., LI, Y., FU, F. & SUN, K. 2018. Multivesicular liposomes for sustained release of bevacizumab in treating laser-induced choroidal neovascularization. *Drug Deliv,* 25**,** 1372-1383.

NEARY, R., WATSON, C. J. & BAUGH, J. A. 2015. Epigenetics and the overhealing wound: the role of DNA methylation in fibrosis. *Fibrogenesis Tissue Repair,* 8**,** 18.

NEVE, A., CANTATORE, F. P., MARUOTTI, N., CORRADO, A. & RIBATTI, D. 2014. Extracellular matrix modulates angiogenesis in physiological and pathological conditions. *Biomed Res Int,* 2014**,** 756078.

NITA, M., STRZALKA-MROZIK, B., GRZYBOWSKI, A., MAZUREK, U. & ROMANIUK, W. 2014. Age-related macular degeneration and changes in the extracellular matrix. *Med Sci Monit,* 20**,** 1003-16.

OH, H., TAKAGI, H., TAKAGI, C., SUZUMA, K., OTANI, A., ISHIDA, K., MATSUMURA, M., OGURA, Y. & HONDA, Y. 1999. The potential angiogenic role of macrophages in the formation of choroidal neovascular membranes. *Invest Ophthalmol Vis Sci,* 40**,** 1891-8.

OHNO-MATSUI, K., HIROSE, A., YAMAMOTO, S., SAIKIA, J., OKAMOTO, N., GEHLBACH, P., DUH, E. J., HACKETT, S., CHANG, M., BOK, D., ZACK, D. J. & CAMPOCHIARO, P. A. 2002. Inducible expression of vascular endothelial growth factor in adult mice causes severe proliferative retinopathy and retinal detachment. *Am J Pathol,* 160**,** 711-9.

OSHIMA, Y., OSHIMA, S., NAMBU, H., KACHI, S., HACKETT, S. F., MELIA, M., KALEKO, M., CONNELLY, S., ESUMI, N., ZACK, D. J. & CAMPOCHIARO, P. A. 2004. Increased expression of VEGF in retinal pigmented epithelial cells is not sufficient to cause choroidal neovascularization. *J Cell Physiol,* 201**,** 393-400.

OZERDEM, U., GRAKO, K. A., DAHLIN-HUPPE, K., MONOSOV, E. & STALLCUP, W. B. 2001. NG2 proteoglycan is expressed exclusively by mural cells during vascular morphogenesis. *Dev Dyn,* 222**,** 218-27.

PACHYDAKI, S. I., JAKOBIEC, F. A., BHAT, P., SOBRIN, L., MICHAUD, N. A., SESHAN, S. V. & D'AMICO, D. J. 2012. Surgical management and ultrastructural study of choroidal neovascularization in punctate inner choroidopathy after bevacizumab. *J Ophthalmic Inflamm Infect,* 2**,** 29-37.

PENNESI, M. E., NEURINGER, M. & COURTNEY, R. J. 2012. Animal models of age related macular degeneration. *Mol Aspects Med,* 33**,** 487-509.

RAUNIYAR, K., JHA, S. K. & JELTSCH, M. 2018. Biology of Vascular Endothelial Growth Factor C in the Morphogenesis of Lymphatic Vessels. *Front Bioeng Biotechnol,* 6**,** 7.

ROLLING, F., LE MEUR, G., STIEGER, K., SMITH, A. J., WEBER, M., DESCHAMPS, J. Y., NIVARD, D., MENDES-MADEIRA, A., PROVOST, N., PEREON, Y., CHEREL, Y., ALI, R. R., HAMEL, C., MOULLIER, P. & ROLLING, F. 2006. Gene therapeutic prospects in early onset of severe retinal dystrophy: restoration of vision in RPE65 Briard dogs using an AAV serotype 4 vector that specifically targets the retinal pigmented epithelium. *Bull Mem Acad R Med Belg,* 161**,** 497-508; discussion 508-9.

ROY, K., STEIN, L. & KAUSHAL, S. 2010. Ocular gene therapy: an evaluation of recombinant adeno-associated virus-mediated gene therapy interventions for the treatment of ocular disease. *Hum Gene Ther,* 21**,** 915-27.

RYAN, S. J. 1982. Subretinal neovascularization. Natural history of an experimental model. *Arch Ophthalmol,* 100**,** 1804-9.

SCHLINGEMANN, R. O. 2004. Role of growth factors and the wound healing response in age-related macular degeneration. *Graefes Arch Clin Exp Ophthalmol,* 242**,** 91-101.

SCHMACK, I., BERGLIN, L., NIE, X., WEN, J., KANG, S. J., MARCUS, A. I., YANG, H., LYNN, M. J., KAPP, J. A. & GROSSNIKLAUS, H. E. 2009. Modulation of choroidal neovascularization by subretinal injection of retinal pigment epithelium and polystyrene microbeads. *Mol Vis,* 15**,** 146-61.

SCHMID, M. K., BACHMANN, L. M., FAS, L., KESSELS, A. G., JOB, O. M. & THIEL, M. A. 2015. Efficacy and adverse events of aflibercept, ranibizumab and bevacizumab in age-related macular degeneration: a trade-off analysis. *Br J Ophthalmol,* 99**,** 141-6.

SCHRAERMEYER, U. & JULIEN, S. 2013. Effects of bevacizumab in retina and choroid after intravitreal injection into monkey eyes. *Expert Opin Biol Ther,* 13**,** 157-67.

SCHRAERMEYER, U., JULIEN, S., BIESEMEIER, A., BARTZ-SCHMIDT, K. U. & WOLBURG, H. 2015. A new kind of labyrinth-like capillary is responsible for leakage from human choroidal neovascular endothelium, as investigated by high-resolution electron microscopy. *Graefes Arch Clin Exp Ophthalmol,* 253**,** 681-9.

SCHWESINGER, C., YEE, C., ROHAN, R., JOUSSEN, A., FERNANDEZ, A., MEYER, T., POULAKI, V., MA, J., REDMOND, T., LIU, S., ADAMIS, A. & D'AMATO, R. 2001. Intrachoroidal Neovascularization in Transgenic Mice Overexpressing Vascular Endothelial Growth Factor in the Retinal Pigment Epithelium. *Am J Pathol,* 158**,** 1161-72.

SEMKOVA, I., PETERS, S., WELSANDT, G., JANICKI, H., JORDAN, J. & SCHRAERMEYER, U. 2003. Investigation of laser-induced choroidal neovascularization in the rat. *Invest Ophthalmol Vis Sci,* 44**,** 5349-54.

SENE, A., CHIN-YEE, D. & APTE, R. S. 2015. Seeing through VEGF: innate and adaptive immunity in pathological angiogenesis in the eye. *Trends Mol Med,* 21**,** 43-51.

SHIBUYA, M. 2011. Vascular Endothelial Growth Factor (VEGF) and Its Receptor (VEGFR) Signaling in Angiogenesis: A Crucial Target for Anti- and Pro-Angiogenic Therapies. *Genes Cancer,* 2**,** 1097-105.

SIM, D. A., CHU, C. J., SELVAM, S., POWNER, M. B., LIYANAGE, S., COPLAND, D. A., KEANE, P. A., TUFAIL, A., EGAN, C. A., BAINBRIDGE, J. W., LEE, R. W., DICK, A. D. & FRUTTIGER, M. 2015. A simple method for in vivo labelling of infiltrating leukocytes in the mouse retina using indocyanine green dye. *Dis Model Mech,* 8**,** 1479-87.

SPILSBURY, K., GARRETT, K. L., SHEN, W. Y., CONSTABLE, I. J. & RAKOCZY, P. E. 2000. Overexpression of vascular endothelial growth

factor (VEGF) in the retinal pigment epithelium leads to the development of choroidal neovascularization. *Am J Pathol,* 157**,** 135-44.

STERN, J. & TEMPLE, S. 2015. Retinal pigment epithelial cell proliferation. *Exp Biol Med (Maywood),* 240**,** 1079-86.

TAHIRI, H., OMRI, S., YANG, C., DUHAMEL, F., SAMARANI, S., AHMAD, A., VEZINA, M., BUSSIERES, M., VAUCHER, E., SAPIEHA, P., HICKSON, G., HAMMAMJI, K., LAPOINTE, R., RODIER, F., TREMBLAY, S., ROYAL, I., CAILHIER, J. F., CHEMTOB, S. & HARDY, P. 2016. Lymphocytic Microparticles Modulate Angiogenic Properties of Macrophages in Laser-induced Choroidal Neovascularization. *Sci Rep,* 6**,** 37391.

VAN BERGEN, T., ETIENNE, I., CUNNINGHAM, F., MOONS, L., SCHLINGEMANN, R. O., FEYEN, J. H. M. & STITT, A. W. 2019. The role of placental growth factor (PlGF) and its receptor system in retinal vascular diseases. *Prog Retin Eye Res,* 69**,** 116-136.

WANG, F., RENDAHL, K. G., MANNING, W. C., QUIROZ, D., COYNE, M. & MILLER, S. S. 2003. AAV-mediated expression of vascular endothelial growth factor induces choroidal neovascularization in rat. *Invest Ophthalmol Vis Sci,* 44**,** 781-90.

WANG, X., MA, W., HAN, S., MENG, Z., ZHAO, L., YIN, Y., WANG, Y. & LI, J. 2017. TGF-beta participates choroid neovascularization through Smad2/3-VEGF/TNF-alpha signaling in mice with Laser-induced wet age-related macular degeneration. *Sci Rep,* 7**,** 9672.

WOOLARD, J., BEVAN, H. S., HARPER, S. J. & BATES, D. O. 2009. Molecular diversity of VEGF-A as a regulator of its biological activity. *Microcirculation,* 16**,** 572-92.

YI, X., OGATA, N., KOMADA, M., YAMAMOTO, C., TAKAHASHI, K., OMORI, K. & UYAMA, M. 1997. Vascular endothelial growth factor expression in choroidal neovascularization in rats. *Graefes Arch Clin Exp Ophthalmol,* 235**,** 313-9.

YU, L., WU, X., CHENG, Z., LEE, C. V., LECOUTER, J., CAMPA, C., FUH, G., LOWMAN, H. & FERRARA, N. 2008. Interaction between bevacizumab and murine VEGF-A: a reassessment. *Invest Ophthalmol Vis Sci,* 49**,** 522-7.

YU, M. J., SHEN, W. Y., LAI, M. C., CONSTABLE, I. J. & RAKOCZY, P. E. 1999. Generation and characterization of a recombinant adenovirus expressing vascular endothelial growth factor for studies of neovascularization in the eye. *Aust N Z J Ophthalmol,* 27**,** 250-3.

ZHANG, S., WU, J., WU, X., XU, P., TIAN, Y., YI, M., LIU, X., DONG, X., WOLF, F., LI, C. & HUANG, Q. 2012. Enhancement of rAAV2-mediated transgene expression in retina cells in vitro and in vivo by coadministration of low-dose chemotherapeutic drugs. *Invest Ophthalmol Vis Sci,* 53**,** 2675-84.

8 Declaration of Contributions to the Dissertation

The dissertation work was carried out at the division for experimental vitreoretinal surgery, center for ophthalmology, University of Tuebingen under the supervision of Prof. Dr. rer. nat. Ulrich Schraermeyer.

The study was designed by Prof. Dr. rer. nat. Ulrich Schraermeyer.

After training by laboratory member Dr. rer. nat. Antje Biesemeier, I analysed the rat CNV model by light and electron microscopy. In vivo imaging was carried out by me with the assistance of Dr. rer. nat. Alexander Tschulakow. Immunohistochemistry was carried out by me with the assistance of Antonina Burda. Statistical analysis was carried out independently by me.

I confirm that I wrote the thesis myself under the supervision of Prof. Dr. rer. nat. Ulrich Schraermeyer and that any additional sources of information have been duly cited.

Signed_____

on _____ in Tuebingen

9 Acknowledgments

First and foremost, I would like to express my deepest appreciation to my supervisor, Prof. Dr. rer. nat. Ulrich Schraermeyer for providing the topic for this research work, the excellent working conditions and the valuable guidance. His keen and vigorous academic observation enlightens me not only in this project but also in my future research work.

Special thanks should be given to Dr. rer. nat. Antje Biesemeier, for her professional training, unreserved support, impressive kindness and patience. She helped me work out the problems during the difficult course of the thesis.

I shall extend my thanks to Dr. rer. nat. Alexander Tschulakow for his valuable help in this research work.

My sincere appreciation also goes to the other members at the division for experimental vitreoretinal surgery of center for ophthalmology: PD Dr. rer. nat. Sylvie Julien-Schraermeyer, Dr. rer. nat. Barbara Illing, Yuan Fang, Tatjana Taubitz, Antonina Burda, Judith Birch, Harsh Thakkar, Monika Rittgarn, Sigrid Schultheiß and Lei Xi, for their valuable support, useful advice and their encouragements. They really helped me a lot in the past five years.

Finally, I'd like to thank my family for their continued support, love and encouragements throughout the entire research work.